(12) INTERNATIONAL APPLICATION PUBLISHED UNDER THE PATENT COOPERATION TREATY (PCT)

(19) World Intellectual Property Organization
International Bureau

(43) International Publication Date
24 April 2025 (24.04.2025)

WIPO | PCT

(10) International Publication Number
WO 2025/085275 A1

(51) International Patent Classification:
A61K 33/00 (2006.01) *A61P 31/00* (2006.01)
A61K 33/04 (2006.01) *A61P 39/06* (2006.01)
A61K 47/52 (2017.01) *B82Y 5/00* (2011.01)
A61K 9/70 (2006.01) *A61K 31/765* (2006.01)
A61P 3/00 (2006.01)

(21) International Application Number:
PCT/US2024/050330

(22) International Filing Date:
08 October 2024 (08.10.2024)

(25) Filing Language: English

(26) Publication Language: English

(30) Priority Data:
63/590,673 16 October 2023 (16.10.2023) US

(71) Applicant: **THE TEXAS A&M UNIVERSITY SYSTEM** [US/US]; 3369 Tamu, College Station, TX 77843-3369 (US).

(72) Inventors: **GAHARWAR, Akhilesh**; 3369 Tamu, College Station, TX 77843-3369 (US). **SINGH, Kanwar, Abhay**; 3369 Tamu, College Station, TX 77843-3369 (US). **SINGH, Irtisha**; 3369 Tamu, College Station, TX 77843-3369 (US). **GOHIL, Vishal**; 3369 Tamu, College Station, TX 77843-3369 (US).

(74) Agent: **WILSON, Kristi, D.**; Dentons US LLP, P.O. Box 1302, Chicago, IL 60606 (US).

(81) Designated States *(unless otherwise indicated, for every kind of national protection available)*: AE, AG, AL, AM, AO, AT, AU, AZ, BA, BB, BG, BH, BN, BR, BW, BY, BZ, CA, CH, CL, CN, CO, CR, CU, CV, CZ, DE, DJ, DK, DM, DO, DZ, EC, EE, EG, ES, FI, GB, GD, GE, GH, GM, GT, HN, HR, HU, ID, IL, IN, IQ, IR, IS, IT, JM, JO, JP, KE, KG, KH, KN, KP, KR, KW, KZ, LA, LC, LK, LR, LS, LU, LY, MA, MD, MG, MK, MN, MU, MW, MX, MY, MZ, NA, NG, NI, NO, NZ, OM, PA, PE, PG, PH, PL, PT, QA, RO, RS, RU, RW, SA, SC, SD, SE, SG, SK, SL, ST, SV, SY, TH, TJ, TM, TN, TR, TT, TZ, UA, UG, US, UZ, VC, VN, WS, ZA, ZM, ZW.

(84) Designated States *(unless otherwise indicated, for every kind of regional protection available)*: ARIPO (BW, CV, GH, GM, KE, LR, LS, MW, MZ, NA, RW, SC, SD, SL, ST, SZ, TZ, UG, ZM, ZW), Eurasian (AM, AZ, BY, KG, KZ, RU, TJ, TM), European (AL, AT, BE, BG, CH, CY, CZ, DE, DK, EE, ES, FI, FR, GB, GR, HR, HU, IE, IS, IT, LT, LU, LV, MC, ME, MK, MT, NL, NO, PL, PT, RO, RS, SE, SI, SK, SM, TR), OAPI (BF, BJ, CF, CG, CI, CM, GA, GN, GQ, GW, KM, ML, MR, NE, SN, TD, TG).

Published:
— *with international search report (Art. 21(3))*
— *with sequence listing part of description (Rule 5.2(a))*

(54) Title: SYNTHESIS, FABRICATION AND USE OF NANOPARTICLES WITH ATOMIC VACANCIES FOR MITOCHONDRIAL THERAPIES

(57) Abstract: The present disclosure provides compositions and methods for increasing mitochondrial function or decreasing cellular oxidative stress. The present disclosure further provides nanomaterial structures comprising high atomic vacancy concentrations. Aspects of the disclosure further relate to methods for treating diseases or disorders associated with decreased mitochondrial function or increased cellular oxidative stress.

WO 2025/085275 A1

TITLE OF THE INVENTION

SYNTHESIS, FABRICATION AND USE OF NANOPARTICLES WITH ATOMIC VACANCIES FOR MITOCHONDRIAL THERAPIES

CROSS-REFERENCE TO RELATED APPLICATIONS

[0001] This application claims the priority of U.S. Provisional Appl. Ser. No. 63/590,673, filed October 16, 2023, the entire disclosure of which is incorporated herein by reference.

STATEMENT OF GOVERNMENT RIGHTS

[0002] This invention was made with government support under DP2-EB026265, R21NS121945, R01GM143630, and R01GM111672 awarded by the National Institutes of Health and under W81XWH2210932 awarded by the Department of Defense. The government has certain rights in the invention.

INCORPORATION OF SEQUENCE LISTING

[0003] A sequence listing containing the file named "TAMC080WO_ST26.xml" which is 7.8 kilobytes (measured in MS-Windows®) and created on October 1, 2024, and comprises 8 sequences, is incorporated herein by reference in its entirety.

FIELD OF THE INVENTION

[0004] This present disclosure relates to the field of diseases or conditions associated with decreased mitochondrial function or increased cellular oxidative stress.

BACKGROUND OF THE INVENTION

[0005] Mitochondria generate cellular energy in the form of adenosine triphosphate (ATP) *via* oxidative phosphorylation (OXPHOS), which is carried out by the mitochondrial respiratory chain (MRC) and ATP synthase. The mitochondrion is the only organelle with an independent genome, and its replication and function relying on the transcription of genes within both the nuclear and mitochondrial genomes. Given its central role in cellular metabolism, defects in mitochondrial function are associated with a number of rare inheritable disorders of energy metabolism as well as common age-related diseases including cancer, type 2 diabetes,

osteoporosis and neurodegenerative disorders such as Parkinson's and Alzheimer's. Although several mitochondria-targeting therapeutics have been developed, they suffer from limited efficacy, high toxicity, and inadequate bioavailability.

[0006] The present disclosure describes atomic scale modification of two dimensional (2D) nanomaterials to boost mitochondrial biogenesis. Ultrathin 2D nanomaterials have an extremely high surface-to-volume ratio compared to other nanomaterials, resulting in high surface energy. The increase in surface energy of nanomaterials has been shown to enhance the catalytic activity, which can be leveraged in biological systems to modulate cellular metabolism. In many cases the basal plane of the nanomaterials remains chemically inert, while the edges act as active sites for catalytic activity. By incorporating empty sites within the atomic lattice of 2D nanomaterials (i.e., atomic vacancies), it is possible to create structural defects that can result in an increase of active sites for catalysis. For this, the present disclosure describes selection of transition metal dichalcogenide (TMD), which is an emerging class of ultrathin 2D nanomaterials with a high degree of anisotropy and chemical functionality. Transition metals play a crucial role in cellular homeostasis and serve as cofactors in enzymatic reactions, as they can readily transition between oxidized and reduced states. Transition metals such as molybdenum (Mo) are essential for nearly all organisms and form the catalytic centers of several metalloenzymes. Mo shuttles between three versatile oxidation states (+4, +5, and +6) and is crucial for catalyzing redox reactions. These characteristics provide a strong basis for synthesizing TMD nanoparticles for the purpose of modulating mitochondrial function.

[0007] Molybdenum disulfide (MoS_2) is a promising 2D nanomaterial and has attracted significant interest in biomedicine due to its superior electrochemical characteristics. MoS_2 comprises of one layer of molybdenum (Mo) oriented between two sulfur (S) layers with a strong covalent bond. MoS_2 can boost electrocatalytic performance by enhancing electrochemical kinetics and low-loss electrical transport.

SUMMARY OF THE INVENTION

[0008] In one aspect, the present disclosure provides a method of increasing mitochondrial function in a subject in need thereof, the method comprising administering to the subject an effective amount of a nanomaterial structure comprising a transition metal and a chalcogen to increase mitochondrial function in the subject, wherein the nanomaterial structure comprises a high atomic vacancy concentration. In certain embodiments, the transition metal is a transition metal dichalcogenide. In one embodiment, the transition metal is selected from the group

consisting of: titanium, vanadium, zirconium, niobium, molybdenum, hafnium, tantalum, and tungsten. In another embodiment, the chalcogen is selected from the group consisting of sulfur, selenium, and tellurium. In yet another embodiment, the nanomaterial structure comprises molybdenum disulfide. The high atomic vacancy concentration, in one embodiment, is greater than about 0.50×10^2 μM g^{-1}. The high atomic vacancy concentration, in another embodiment, is about 0.50×10^2 μM g^{-1} to about 10.0×10^2 μM g^{-1}. The nanomaterial structure, in yet another embodiment, is about 5 nm to about 400 nm in diameter. In some embodiments, the increased mitochondrial function comprises increased mitochondrial biogenesis, mitochondrial encoded gene expression, increased nuclear encoded mitochondrial gene expression, increased mitochondrial protein expression, increased mitochondrial respiratory capacity, or increased adenosine triphosphate production.

[0009] In another aspect, the present disclosure provides a method of decreasing cellular oxidative stress in a subject in need thereof, the method comprising administering to the subject an effective amount of a nanomaterial structure comprising a sulfur moiety active site, wherein the sulfur moiety active site acts as an active site of reaction to reduce cellular oxidative stress. In one embodiment, the nanomaterial structure comprises a transition metal selected from the group consisting of: titanium, vanadium, zirconium, niobium, molybdenum, hafnium, tantalum, and tungsten. In another embodiment, the nanomaterial structure comprises molybdenum disulfide. In yet another embodiment, the nanomaterial structure comprises a plurality of sulfur moiety active sites. The concentration of the plurality of sulfur moiety active sites, in one embodiment, is greater than about 0.50×10^2 μM g^{-1} of nanomaterial structure. The concentration of the plurality of sulfur moiety active sites, in another embodiment, is about 0.50×10^2 μM g^{-1} to about 10.0×10^2 μM g^{-1} of nanomaterial structure, The nanomaterial structure, in yet another embodiment, is about 5 nm to about 400 nm in diameter.

[0010] In certain embodiments, the nanomaterial structure further comprises a targeting molecule. In one embodiment, the targeting molecule is cell-specific or tissue-specific. In another embodiment, the nanomaterial structure further comprises a therapeutic agent or a detectable label. In another embodiment, the therapeutic agent is a chemotherapeutic agent, an immunotherapeutic agent, a mitochondrial therapeutic agent, a neurotherapeutic agent, a metabolic therapeutic agent, an ophthalmic therapeutic agent, a cardio therapeutic agent, or a radiotherapeutic agent, or the detectable label is a paramagnetic ion, a radioactive isotope, a fluorochrome, an NMR-detectable agent, or an X-ray imaging agent. In yet another embodiment, the mitochondrial therapeutic agent is selected from the group consisting of

CoQ10 (ubiquinone), idebenone, riboflavin, dichloroacetate, thiamine, creatine, lipoic acid, glutathione, N-acetylcysteine, cysteamine, EPI-743 (para-benzoquinone analog), arginine, citrulline, cardiolipin, elamipretide, bezafibrate, resveratrol, AICAR (aminoimidazole carboxamide ribonucleoside), epicatechin, RTA 408 (synthetic isoprenoid), decanoic acid, a therapeutic peptide, and a therapeutic polynucleotide molecule.

[0011] In particular embodiments, the subject is afflicted with or at risk of developing a disease or condition associated with decreased mitochondrial function or increased cellular oxidative stress. Non-limiting examples of diseases or conditions associated with decreased mitochondrial function or increased cellular oxidative stress include Barth syndrome, mitochondrial encephalopathy, lactic acidosis, stroke-like episodes (MELAS), Myoclonus epilepsy with ragged-red fibers (MERRF), neuropathy, ataxia, and retinitis pigmentosa (NARP), Leber's hereditary optic neuropathy (LHON), Kearns–Sayre syndrome (KSS), Pearson syndrome (PS), progressive external ophthalmoplegia (PEO), autosomal-dominant/ recessive PEO (ad/ar PEO), mtDNA depletion syndrome (MDDS), mitochondrial neurogastrointestinal encephalopathy (MNGIE), mitochondrial recessive ataxia syndrome (MIRAS), Alpers syndrome (AS), Leigh syndrome (LS), optic nerve atrophy, subacute necrotizing encephalopathy, early-onset hepatocerebral disorder, juvenile catastrophic epilepsy, adult-onset ataxia-neuropathy syndrome, cardiomyopathy, cerebral white matter disease, ovarian dysfunction, hearing loss, cancer, diabetes mellitus, osteoporosis, and neurodegenerative disease. In one embodiment, the administering comprises injection, microneedle administration, oral administration, buccal administration, vaginal administration, inhalation, intraosseous administration, trans nasal application, topical administration, transdermal application, or rectal administration. Non-limiting types of injection include intravenous injection, intramuscular injection, intraarticular injection, subcutaneous injection, and intraarterial injection.

[0012] In some embodiments, the methods of the present disclosure may further comprise administering a second therapy to the subject. In one embodiment, the second therapy is a therapeutic agent or surgery. In another embodiment, the methods of the present disclosure may further comprise administering a pharmaceutical composition comprising the effective amount of the nanomaterial structure to the subject.

[0013] In another aspect, the present disclosure provides a pharmaceutical composition comprising a) a nanomaterial structure comprising sulfur active sites or comprising a transition metal and a chalcogen, wherein the nanomaterial structure comprises a high atomic vacancy

concentration; and b) a second mitochondrial therapeutic agent. In some embodiments, the transition metal is a transition metal dichalcogenide. In one embodiment, the transition metal is selected from the group consisting of: titanium, vanadium, zirconium, niobium, molybdenum, hafnium, tantalum, and tungsten. In another embodiment, the chalcogen is selected from the group consisting of sulfur, selenium, and tellurium. In yet another embodiment, the transition metal is molybdenum, and the chalcogen is sulfur. In yet another embodiment, the second mitochondrial therapeutic agent is selected from the group consisting of CoQ10 (ubiquinone), idebenone, riboflavin, dichloroacetate, thiamine, creatine, lipoic acid, glutathione, N-acetylcysteine, cysteamine, EPI-743 (para-benzoquinone analog), arginine, citrulline, cardiolipin, elamipretide, bezafibrate, resveratrol, AICAR (aminoimidazole carboxamide ribonucleoside), epicatechin, RTA 408 (synthetic isoprenoid), decanoic acid, a therapeutic peptide, and a therapeutic polynucleotide molecule.

[0014] In some embodiments, the high atomic vacancy concentration is greater than about 0.50×10^2 μM g^{-1}. The high atomic vacancy concentration, in one embodiment, is about 0.50×10^2 μM g^{-1} to about 10.0×10^2 μM g^{-1}. The nanomaterial structure, in another embodiment, is about 5 nm to about 400 nm in diameter. The nanomaterial structure, in yet another embodiment, further comprises a targeting molecule. In still yet another embodiment, the targeting molecule is cell-specific or tissue-specific. In one embodiment, the nanomaterial structure is modified with or conjugated to a peptide, a protein, a colloidal molecule, or a polymer to facilitate delivery or adsorption. In another embodiment, the composition is serum-free, endotoxin-free, or sterile.

[0015] In yet another aspect, the present disclosure provides a pharmaceutical composition comprising a) a nanomaterial structure comprising a sulfur moiety active site, wherein the sulfur moiety active site acts as an active site of reaction to reduce cellular oxidative stress; and b) a second mitochondrial therapeutic agent. In one embodiment, the nanomaterial structure comprises molybdenum disulfide. In another embodiment, the nanomaterial structure comprises a plurality of sulfur moiety active sites. The concentration of the plurality of sulfur moiety active sites, in yet another embodiment, is greater than about 0.50×10^2 μM g^{-1} of nanomaterial structure. The concentration of the plurality of sulfur moiety active sites, in still yet another embodiment, is about 0.50×10^2 μM g^{-1} to about 10.0×10^2 μM g^{-1} of nanomaterial structure. In one embodiment, the nanomaterial structure is about 5 nm to about 400 nm in diameter. The nanomaterial structure, in another embodiment, further comprises a targeting molecule. In yet another embodiment, the targeting molecule is cell-specific or tissue-specific.

The nanomaterial structure, in still yet another embodiment, is modified with or conjugated to a peptide, a protein, a colloidal molecule, lipid molecule, phospholipid molecule, or a polymer to facilitate delivery or adsorption. In one embodiment, the pharmaceutical composition is serum-free, endotoxin-free, or sterile. The second mitochondrial therapeutic agent, in another embodiment, is selected from the group consisting of CoQ10 (ubiquinone), idebenone, riboflavin, dichloroacetate, thiamine, creatine, lipoic acid, glutathione, N-acetylcysteine, cysteamine, EPI-743 (para-benzoquinone analog), arginine, citrulline, cardiolipin, elamipretide, bezafibrate, resveratrol, AICAR (aminoimidazole carboxamide ribonucleoside), epicatechin, RTA 408 (synthetic isoprenoid), decanoic acid, a therapeutic peptide, and a therapeutic polynucleotide molecule.

BRIEF DESCRIPTION OF THE DRAWINGS

[0016] The following drawings form part of the present specification and are included to further demonstrate certain aspects of the present invention. The invention may be better understood by reference to one or more of these drawings in combination with the detailed description of specific embodiments presented herein.

[0017] FIG. 1 demonstrates the synthesis and characterization of MoS_2 nanoflowers with predefined atomic vacancies. FIG. 1, Panel A - Atomic arrangement of Mo and S in 2D MoS_2. Changing molybdenum:sulfur precursor ratio leads to the formation of MoS2 with different degrees of atomic vacancies. Transmission electron microscopy (TEM) images show MoS_2 nanoflower assembly consisting of multiple individual MoS_2 nanosheets. X-ray diffraction (XRD) peaks of MoS_2 nanoflowers (002, 100, 110) show the presence of hexagonal crystal structure. FIG. 1, Panel B - X-ray photoelectron spectra (XPS) show the binding energies (BE) for Mo and S within MoS_2 nanoflowers. 1T (trigonal prismatic) and 2H phase (hexagonal symmetry) within the trigonal prismatic MoS_2 crystal. FIG. 1, Panel C - Cyclic voltagrams for a MoS_2 coated electrode in comparison with a standard uncoated electrode. The density of active sites calculated from these voltagrams are presented in the table in moles/g. The density of active sites increases with increasing sulfur precursor ratio. FIG. 1, Panel D - The effect of MoS_2 nanoflowers concentration (with differing degree of atomic vacancies) on cell viability in hMSCs following 24h of exposure. MoS_2 nanoflowers exhibit a half-inhibitory concentration (IC_{50}) of ~400 μg/mL. FIG. 1, Panel E - Cell membrane integrity in presence of MoS_2 nanoflowers was determined by monitoring release of LDH in media following 24h of exposure. No significant effect of atomic defect is observed at lower concentration (<IC50) of

MoS_2 nanoflowers. FIG. 1, Panel F - Effect of atomic defect of MoS_2 nanoflowers (1:6) on cell cycle is determined after 72h. FIG. 1, Panel G - Internalization of MoS_2 nanoflower (1:6) is evident from fluorescence images of cells after 24h. FIG. 1, Panel H - Cellular internalization of MoS_2 nanoflowers was determined using ICP-MS– elemental analysis following 18h of exposure to nanoflowers. The levels of Mo are plotted for hMSCs treated with and without MoS_2 nanoflowers.

[0018] FIG. 2 demonstrates the effect of atomic scale vacancies on catalytic activity. FIG. 2, Panel A - Amperometric analysis to evaluate H_2O_2 reduction. The analysis was performed at a voltage of -0.6 V, and the output currents of the MoS_2 formulations with varying degree of vacancies were observed. The increase in output reduction current density of high atomic vacancy MoS_2 (1:6) formulations indicates this formulation exhibits enhanced H_2O_2 reduction capability. FIG. 2, Panel B - Biochemical determination of H_2O_2 reduction by direct comparison with catalase enzyme. All formulations demonstrated some degree of catalytic activity, however, high atomic vacancy MoS_2 nanoflowers showed significantly enhanced catalytic activity (n=3, *$p<0.05$; **$p<0.01$).

[0019] FIG. 3 demonstrates the interaction of MoS_2 nanoflowers with serum proteins using SDS-PAGE. The surface charge before and after protein corona formation was determined using zeta potential measurements.

[0020] FIG. 4 demonstrates the effect of vacancy rich MoS_2 (1:6) nanoflowers on cell proliferation and intracellular ROS production. FIG. 4, Panel A - The effect of vacancy rich MoS_2 (1:6) nanoflowers on hMSC proliferation across multiple days. MoS_2 (25 µg/mL) exposure appears to cause no significant change in long-term cell proliferation compared to untreated hMSCs (n=4, for each time point). FIG. 4, Panel B - The amount of intracellular ROS was determined before and after treatment with MoS_2 nanoflowers (1:6) across multiple time points (n=3, for each time point). (n.s. $p>0.05$; *$p<0.05$; **$p<0.01$, ****$p<0.001$).

[0021] FIG. 5 demonstrates the sub-cellular localization of MoS_2 (1:6) nanoflowers by TEM. Monolayers of cells were treated with nanoflowers for 24h, then embedded in resin and sectioned. Sections were stained with uranyl acetate and Venable lead citrate prior to imaging.

[0022] FIG. 6 demonstrates the role of atomic vacancies of MoS_2 on transcriptomic profile of human mesenchymal stem cells. FIG. 6, Panel A - Principal component analysis (PCA) of hMSC samples treated with MoS_2 nanoflower with predefined atomic vacancies (1:1 and 1:6 based on mRNA expression obtained from RNA-seq (n = 2, technical replicates). Untreated

hMSCs are used as control. The PCA was done on the mRNA expression (Log_2FPKM) of 20% of the most variable genes across all samples (n = 2214). FIG. 6, Panel B - MA plot showing differences in gene expression [Log_2(fold change)] between hMSC samples treated with MoS_2 nanoflower (1:1 and 1:6). FIG. 6, Panel C - Hierarchical clustering of hMSC samples treated with MoS_2 nanoflower (1:1 and 1:6) based on mRNA expression obtained from RNA-seq. The heatmap shows the DEGs (Log_2FPKM of DEGs; P-adj < 0.05) across all treatment groups compared with control hMSC samples. The total number of distinct DEGs across all samples is 2214. FIG. 6, Panel D - Semantic comparisons of GO annotations for hMSC samples treated with MoS_2 nanoflower (1:6), resulting in seven broad clusters of GO terms: morphogenesis, extracellular matrix, cell–matrix regulation, cellular locomotion component, mitochondrial electron chain transport, triphosphate metabolic, and protein catabolic targeting membrane.

[0023] FIG. 7 shows the correlation of gene expression profiles between hMSCs, MoS_2 (1:1) and MoS_2 (1:6) replicates. All three experimental groups showed high correlation (r > 0.98) of gene expression profiles between replicates. Correlation was determined using Pearson correlation coefficient (r).

[0024] FIG. 8 shows key GO terms associated generated from the DEGs in hMSCs treated with low atomic vacancy and high atomic vacancy MoS_2 respectively ($p<0.05$). GO terms associated with mitochondrial activity and respiration are uniquely activated in high atomic vacancy MoS_2 treated cells. Circle size correlates to the gene ratio, i.e., the DEGs associated with a GO term divided by the total number of genes mapped to the GO term. Color intensity is associated with increasing - log(p-adj) (dark: greater significance, light: less significance).

[0025] FIG. 9 shows compiled GO biological processes and cellular components generated from DEGs from MoS_2 (1:6) treated cells. P-adjust values are reported using -log10 transformation with Padj. < 0.05 threshold. Highlighted terms correspond to processes relating to mitochondrial function.

[0026] FIG. 10 demonstrates the effect of atomic vacancies in MoS_2 nanoflowers on nuclear-encoded mitochondrial genes. FIG. 10, Panel A - Heatmap showing the DEGs (Log_2FPKM of DEGs; P-adj < 0.01) known to encode mitochondrial proteins. Samples treated with high atomic vacancy MoS_2 show consistent upregulation of mitochondrial genes as compared to untreated hMSC samples. FIG. 10, Panel B - Volcano plot highlighting genes involved in mitochondrial ATP synthesis coupled proton transport (GO:0042776) and mitochondrial

electron transport cytochrome *c* to oxygen (GO:0006123) for high vacancies MoS_2 nanoflowers (1:6) is shown. MoS_2 nanoflowers with high atomic vacancies enhance the transcription of key MRC genes, including those in the adenosine triphosphate (ATP) and mitochondrial cytochrome *c* oxidase (COX) families. FIG. 10, Panel C - RNA-seq tracks showing normalized mRNA expression (aligned reads normalized by total library size—transcript per million (TPM)) at the genomic locus of ATP5E and COX5A. FIG. 10, Panel D - GSEA shows positive enrichment of MRC related terms. Positive NES indicates a significant number of genes belonging to these processes are upregulated. FIG. 10, Panel E - GSEA enrichment results showing NES for *Hallmark: Reactive oxygen species, Hallmark: OXPHOS and Hallmark: Fatty acid metabolism* for MoS_2 (1:6) treatment. The vertical black lines ("bar code") represent the projection onto the ranked gene list of individual genes of the gene set. The horizontal bar in graded color represents the gene list ranked from up-regulated on the left to down-regulated on the right. FIG. 10, Panel F - Sub-cellular localization of MoS_2 nanoflowers was determined by co-staining of mitochondria and MoS_2 nanoflowers. The nucleus and mitochondria were stained using DAPI and Mito tracker red, respectively. The arrow points toward the MoS_2 nanoparticles that were visualized using reflective light imaging. FIG. 10, Panel G -Mitochondrial morphology analysis using the Mito hacker pipeline was performed to determine the effect of MoS_2 nanoflowers on the mitochondrial morphology. No significant change in mitochondrial network parameters, such as mitochondrial branch length, mitochondrial area, and mitochondrial form factor following MoS_2 nanoflower treatment was observed.

[0027] FIG. 11 shows DEGs from cells treated with atomic vacancy rich MoS_2 (1:6) corresponding to the MRC complexes and mitochondrial protein translation. Log_2 transformed fold changes are represented nominally on the x-axis (*P-adj* <0.01).

[0028] FIG. 12 demonstrates that treatment with MoS_2 nanoflowers stimulates mitochondrial biogenesis. FIG. 12, Panel A - Schematic showing mitochondrial genome (mt-DNA), indicating mitochondrial encoded proteins. FIG. 12, Panel B - Visualization of mitochondrial gene expression in cells with and without MoS_2(1:6) treatment. Data indicates enhanced expression of the entire mitochondrial genome in cells treated with MoS_2 (1:6). FIG. 12, Panel C - The effect of high atomic vacancies MoS_2 on mitochondrial biogenesis. A significant increase in mt-DNA encoded transcript (ND2) as well as copy number (mitochondrial DNA / nuclear DNA) shows that the MoS_2 (1:6) treatment results in a significant increase in mitochondrial biogenesis. (n=3, *p<0.05; **p<0.01, ***p<0.001). FIG. 12, Panel D - Western

blotting is used to determine the relative expression of key mitochondrial proteins. MoS_2 (1:6) treatment results in significant upregulation of ATP5B, SDHB, UQCRC2, VDAC1 (n=4, *p<0.05; **p<0.01, ***p<0.001). FIG. 12, Panel E - GSEA enrichment of *C3: Regulatory Target (TFT: Transcription Factor Targets)* for cells following treatment with MoS_2 (1:6). FIG. 12, Panel F - Relative protein levels of PGC-1α in cells following treatment with MoS_2 (1:6) were evaluated using Western blotting. MoS_2 treated cells show increased expression of PGC-1 α at both 3- and 7-days following treatment. (n=4, *p<0.05; **p<0.01). FIG. 12, Panel G - Temporal expression of TFAM was monitored at the 7-day time period. TFAM and showed a 6-fold increase in peak expression due to treatment with MoS_2 (1:6) (n=3, ****p<0.0001).

[0029] FIG. 13 shows the effect of atomic vacancy rich MoS_2 (1:6) on mitochondrial biogenesis. A significant increase in relative mitochondrial copy number (determined as a ratio of mitochondrial DNA / nuclear DNA abundance) indicates MoS_2 (1:6) treatment significantly increases mitochondrial biogenesis. (n=3, ***p<0.001, ****p<0.0001).

[0030] FIG. 14 demonstrates that high atomic vacancy MoS_2 decreases oxidative stress and enhances mitochondrial bioenergetics. FIG. 14, Panel A - The effect of MoS_2 on OCR was determined. C2C12 Cells were treated with different concentrations of MoS_2 (0, 10 and 25 μg/mL). A concentration-dependent increase in spare respiratory capacity was observed, indicating the strong ability of MoS_2 to trigger mitochondrial respiration machinery. Data points are shown as mean ± SEM, n = 3. FIG. 14, Panel B - Evaluation of ATP levels in cells treated with MoS_2 (1:6). MoS_2 (1:6) treatment resulted in a marked increase in ATP levels compared to control hMSCs. FIG. 14, Panel C - Effect of MoS_2 on mitochondrial membrane potential was evaluated using the JC-1 dye. Cells treated with MoS_2 (1:6) showed no significant changes in mitochondrial membrane potential as compared to untreated cells. Cell number variation was normalized using nuclear stain (DAPI) (n=4, ***p<0.001). FIG. 14, Panel D - The amount of intracellular ROS was determined before and after treatment with MoS_2 nanoflowers (1:6). MoS_2 treatment significantly suppressed ROS production (n=3, ****p<0.0001). FIG. 14, Panel E - The amount of mitochondrial ROS is determined using MitoSox before and after treatment with MoS_2 nanoflowers (1:6). MoS_2 treatment significantly suppressed mitochondrial ROS production (n=3, ***p<0.001). FIG. 14, Panel F - RNA-seq data demonstrates the upregulation of multiple genes related to antioxidant activity (GO: 0016209). FIG. 14, Panel G – RT-PCR-based detection of PGC-1α expression in C2C12 cells transduced with either empty vector (pLKO) or shRNA targeting PGC-1α. FIG. 14, Panel

H - Evaluation of relative mitochondrial copy number in transduced cells following treatment with MoS_2 (1:6) for 72h. Cells transduced with empty vector show a significant increase in mitochondrial copy number and PGC-1α knocked cells showed no significant change in mitochondrial copy number, following treatment with vacancy-rich MoS_2. FIG. 14, Panel I - Increase mitochondrial copy number in hMSCs following treatment with N-acetyl cysteine (NAC), resveratrol, and vacancy-rich MoS_2. Cells were treated with either NAC (3 mM), resveratrol (25 μm), or MoS_2 (1:6) (25 μg/mL) for 72h prior to harvesting of DNA and subsequent quantification of mitochondrial copy number. FIG. 14, Panel J - Mechanism of action of MoS_2 with high atomic vacancies on triggering mitochondrial biogenesis. It is expected that atomic vacancies of MoS_2 exhibit free radical scavenging activity through rapid reactions with reactive oxygen species (ROS), including hydrogen peroxide (H_2O_2), superoxide anions (O_2^-), and hydroxyl radicals ($^{\bullet}OH$). Reduction in intracellular ROS due to the presence of atomic vacancies on MoS_2 is expected to trigger the SIRT1/PGC1α/NRF2 pathway.

[0031] FIG. 15 shows the OCR of bone marrow-derived macrophages (BDMS) cells treated with or without atomic vacancy rich MoS_2 for 18h. Oligomycin, CCCP, and antimycin were used to measure ATP-coupled respiration, maximum respiratory capacity, and mitochondria-specific respiration. MoS_2 (1:6) treated cells showed enhanced cellular respiration in cells irrespective of polarization. Data were normalized to Draq5 DNA staining and are shown as mean ± SEM, n = 4.

[0032] FIG. 16 shows Western blot analysis of key mitochondrial proteins in H9c2 cells following treatment with MoS_2(1:6). MoS_2 treated cells showed an increase in the expression of key mitochondrial proteins as compared to control cells. (n=3, *p<0.05; **p<0.01, ***p<0.001, ****p<0.0001).

[0033] FIG. 17 shows the effect of atomic vacancy rich MoS_2 on mitochondrial membrane potential evaluated using the JC-1 dye. Cells (H9c2 and MCF-7) treated with MoS_2 (1:6) showed no significant changes in mitochondrial membrane potential as compared to untreated cells. Cell number variation was normalized using nuclear stain (DAPI) (n=4, ***p<0.01, ***p<0.001).

[0034] FIG. 18 demonstrates that vacancy rich nanoflowers mediate mitochondrial biogenesis primarily via PGC-1α activation. FIG. 18, Panel A - RT-PCR-based detection of TFAM expression in C2C12 transduced with either empty vector (pLKO) or shRNA targeting TFAM.

FIG. 18, Panel B - Evaluation of relative mitochondrial copy number in transduced cells following treatment with MoS_2 (1:6) for 72h. Control cells show a significant increase in mitochondrial copy number, whereas TFAM-knockdown cells showed a small increase in mitochondrial copy number, following treatment with vacancy rich MoS_2.

BRIEF DESCRIPTION OF THE SEQUENCES

[0001] SEQ ID NO:1 – A representative forward primer sequence for amplification of *PGC- 1α.*

[0002] SEQ ID NO:2 – A representative reverse primer sequence for amplification of *PGC- 1α.*

[0003] SEQ ID NO:3 – A representative forward primer sequence for amplification of *TFAM.*

[0004] SEQ ID NO:4 – A representative reverse primer sequence for amplification of *TFAM.*

[0005] SEQ ID NO:5 – A representative forward primer sequence for amplification of *GAPDH.*

[0006] SEQ ID NO:6 – A representative reverse primer sequence for amplification of *GAPDH.*

[0007] SEQ ID NO:7 – A representative forward primer sequence for amplification of *mt-ND2.*

[0008] SEQ ID NO:8 – A representative reverse primer sequence for amplification of *mt-ND2.*

DETAILED DESCRIPTION OF THE INVENTION

[0035] The present disclosure provides compositions and method for increasing mitochondrial function or decreasing cellular oxidate stress. The present disclosure provides a significant advance in the art by providing high efficacy, low toxicity mitochondria-targeted therapeutics demonstrating adequate bioavailability.

A. High Atomic Vacancy Nanomaterial Structures

[0036] The present disclosure provides nanomaterial structures with high atomic vacancy. These vacancies, embedded within the layered architecture of the nanomaterial structures, serve to increase the number of active catalysis sites in the structures. As used herein the term "high atomic vacancy" refers to a nanomaterial comprising an atomic vacancy concentration of at least about $0.72 \times 10^2\ \mu M\ g^{-1}$. Methods for calculating high atomic vacancy concentration are known in the art and any such method may be used according to the embodiments of the present disclosure. In one embodiment, methods for determining high atomic vacancy

concentration may include those described in Jaiswal *et al.*, Chem. Commun. 55: 8772-8775, 2019. In some embodiments, a high atomic vacancy concentration as described herein may be at least about 0.50×10^2 μM g^{-1}, at least about 0.60×10^2 μM g^{-1}, at least about 0.70×10^2 μM g^{-1}, at least about 0.80×10^2 μM g^{-1}, at least about 0.90×10^2 μM g^{-1}, at least about 1.00×10^2 μM g^{-1}, at least about 1.10×10^2 μM g^{-1}, at least about 1.20×10^2 μM g^{-1}, at least about 1.30×10^2 μM g^{-1}, at least about 1.40×10^2 μM g^{-1}, at least about 1.50×10^2 μM g^{-1}, at least about 1.60×10^2 μM g^{-1}, at least about 1.70×10^2 μM g^{-1}, at least about 1.80×10^2 μM g^{-1}, at least about 1.90×10^2 μM g^{-1}, at least about 2.00×10^2 μM g^{-1}, or at least about 2.10×10^2 μM g^{-1}, including all ranges and values derivable therebetween. In certain embodiments, a high atomic vacancy concentration may be about 0.50×10^2 μM g^{-1} to about 10.0×10^2 μM g^{-1}, about 0.60×10^2 μM g^{-1} to about 10.0×10^2 μM g^{-1}, about 0.70×10^2 μM g^{-1} to about 10.0×10^2 μM g^{-1}, about 0.80×10^2 μM g^{-1} to about 10.0×10^2 μM g^{-1}, about 0.90×10^2 μM g^{-1} to about 10.0×10^2 μM g^{-1}, about 1.00×10^2 μM g^{-1} to about 10.0×10^2 μM g^{-1}, about 1.10×10^2 μM g^{-1} to about 10.0×10^2 μM g^{-1}, about 1.20×10^2 μM g^{-1} to about 10.0×10^2 μM g^{-1}, about 1.30×10^2 μM g^{-1} to about 10.0×10^2 μM g^{-1}, about 1.40×10^2 μM g^{-1} to about 10.0×10^2 μM g^{-1}, about 1.50×10^2 μM g^{-1} to about 10.0×10^2 μM g^{-1}, about 1.60×10^2 μM g^{-1} to about 10.0×10^2 μM g^{-1}, about 1.70×10^2 μM g^{-1} to about 10.0×10^2 μM g^{-1}, about 1.80×10^2 μM g^{-1} to about 10.0×10^2 μM g^{-1}, about 1.90×10^2 μM g^{-1} to about 10.0×10^2 μM g^{-1}, about 2.00×10^2 μM g^{-1} to about 10.0×10^2 μM g^{-1}, or about 2.10×10^2 μM g^{-1} to about 10.0×10^2 μM g^{-1}, including all ranges and values derivable therebetween. In certain embodiments of the present disclosure a high vacancy nanomaterial structure may be referred to as a high atomic vacancy nanoflower.

[0037] The present disclosure describes atomic scale modification of two dimensional (2D) nanomaterials to boost mitochondrial biogenesis. Ultrathin 2D nanomaterials have an extremely high surface-to-volume ratio compared to other nanomaterials, resulting in high surface energy. The increase in surface energy of nanomaterials has been shown to enhance the catalytic activity, which can be leveraged in biological systems to modulate cellular metabolism. In many cases the basal plane of the nanomaterials remains chemically inert, while the edges act as active sites for catalytic activity. By incorporating empty sites within the atomic lattice of 2D nanomaterials (i.e., atomic vacancies), it is possible to create structural defects that can result in an increase of active sites for catalysis. For this, the present disclosure describes selection of transition metal dichalcogenide (TMD), which is an emerging class of ultrathin 2D nanomaterials with a high degree of anisotropy and chemical functionality.

Transition metals play a crucial role in cellular homeostasis and serve as cofactors in enzymatic reactions, as they can readily transition between oxidized and reduced states. Transition metals such as molybdenum (Mo) are essential for nearly all organisms and form the catalytic centers of several metalloenzymes. Mo shuttles between three versatile oxidation states (+4, +5, and +6) and is crucial in catalyzing redox reactions. These characteristics provide a strong basis for synthesizing TMD nanoparticles for the purpose of enhancing mitochondrial function.

[0038] The nanomaterial structures of the present disclosure can boost electrocatalytic performance by enhancing electrode kinetics and low-loss electrical transport. The present disclosure further provides data demonstrating significantly increased ATP production, elevated cellular respiration, and increased relative expression of OXPHOS Complexes II, III, and V subunits, as well as VDAC1, a mitochondrial outer membrane protein following treatment with high vacancy nanomaterial structures. This upsurge in mitochondrial activity stems from the activation of the SIRT1/PGC-1α pathway, leading to mitochondrial biogenesis, initiated by the reduction of cellular ROS by nanomaterial structures with high atomic vacancies. Existing mitochondrial therapeutics predominantly operate by modulating mitochondrial bioenergetics or enhancing mitochondrial biogenesis. However, these strategies demonstrate limited efficacy and bioavailability, and the issue of targeted delivery further complicates their implementation. *See*, for example, Almannai *et al.*, Molecular Genetics and Metabolism 131, 1-13, 2020. In contrast, the compositions and methods of the present disclosure demonstrate that high vacancy nanomaterial structures, as described herein, are promising novel mitochondrial therapeutics. Nanomaterial-based approaches provide numerous advantages, including improved therapeutic targeting and efficacy through surface modification and addition of cell or tissue-specific targeting moieties. The high surface area and photo-responsive nature of these high vacancy nanomaterial structures make them an ideal platform for combinatorial therapies.

[0039] In some embodiments of the present disclosure a high atomic vacancy nanomaterial structure, as described herein, may comprise a transition metal and a chalcogen. In certain embodiments, the transition metal may be a transition metal dichalcogenide. Non-limiting example of transition metals that may be included in a high atomic vacancy nanomaterial structure of the present disclosure include titanium, vanadium, zirconium, niobium, molybdenum, hafnium, tantalum, and tungsten. Non-limiting examples of chalcogens that may be used according to the present disclosure include sulfur, selenium, and tellurium. In one

embodiment, the high atomic vacancy nanomaterial of the present disclosure may include a sulfur moiety active site.

[0040] In particular embodiments, a high atomic vacancy nanomaterial structure of the present disclosure is about 5 nm to about 400 nm, about 50 nm to about 400 nm, about 50 nm to about 350 nm, about 50 nm to about 300 nm, about 50 nm to about 250 nm, about 50 nm to about 200 nm, about 50 nm to about 150 nm, or about 50 nm to about 100 nm in diameter, including all ranges and values derivable therebetween. In one embodiment, the high atomic vacancy nanomaterial structure of the present disclosure is about 5 nm, about 10 nm, about 20 nm, about 30 nm, about 40 nm, about 50 nm, about 60 nm, about 70 nm, about 80 nm, about 90 nm, about 100 nm, about 110 nm, about 120 nm, about 130 nm, about 140 nm, about 150 nm, about 160 nm, about 170 nm, about 180 nm, about 190 nm, about 200 nm, about 210 nm, about 220 nm, about 230 nm, about 240 nm, about 250 nm, about 260 nm, about 270 nm, about 280 nm, about 290 nm, about 300 nm, about 310 nm, about 320 nm, about 330 nm, about 340 nm, about 350 nm, about 360 nm, about 370 nm, about 380 nm, about 390 nm, or about 400 nm in length, width, depth, or diameter, including all ranges and values derivable therebetween.

[0041] The high atomic vacancy nanomaterial structures of the present disclosure may be produced using any method known in the art. In particular embodiments, the high atomic vacancy nanomaterial structures may be produced by altering the molecular precursor ratio of the transition metal and the chalcogen used to produce the nanomaterial structure. A person of ordinary skill in the art would understand appropriate precursor ratios for use according to the methods of the present disclosure based on the oxidation states, molar concentration of the transition metal and chalcogen in the precursors. In some embodiments, the molecular precursor ratio of the transition metal and the chalcogen may be about 0.5:1, about 1:1, about 1:2, about 1:3, about 1:4, about 1:5, about 1:6, about 1:7, about 1:8, about 1:9, about 1:10, about 1:15, about 1:20, about 1:25, about 1:30, about 1:35, or about 1:40, including all ranges and values derivable therebetween.

B. High Atomic Vacancy Nanomaterial Compositions

[0042] In certain aspects, the present disclosure provides pharmaceutical and therapeutic compositions comprising the high atomic vacancy nanomaterial structures of the present disclosure. In some embodiments, the high atomic vacancy nanomaterial structures of the present disclosure may be combined with a pharmaceutically acceptable carrier. As used herein, a "pharmaceutically acceptable carrier," "pharmaceutically acceptable adjuvant," or

"adjuvant" refers to reagents, cells, compounds, materials, compositions, and/or dosage forms that are not only compatible with the nanomaterial structures or other agents to be administered therapeutically, but also are, within the scope of sound medical judgment, suitable for use in contact with the tissues of human beings and animals without excessive toxicity, irritation, allergic response, or other complication commensurate with a reasonable benefit/risk ratio. Also included may be an agent that modifies the effect of other agents and is useful in preparing a therapeutic compound or composition that is generally safe, non-toxic, and neither biologically nor otherwise undesirable. Such an agent may be added to a therapeutic composition or pharmaceutical composition to modify for example the cellular target, cellular localization, or cellular uptake of a nanomaterial structure as described herein. Such an agent may include any excipient, diluent, carrier, or adjuvant that is acceptable for pharmaceutical use. Such an agent may be non-naturally occurring, or may be naturally occurring, but not naturally found in combination with other agents in the therapeutic or pharmaceutical composition.

[0043] As used herein, a "therapeutic compound" or "therapeutic composition" refers to a composition comprising a high atomic vacancy nanomaterial structure of the present disclosure. In some embodiments, a therapeutic composition has the activity of increasing mitochondrial function in a subject or decreasing cellular oxidative stress in a subject as described herein. In one embodiment, the composition is capable of increasing mitochondrial biogenesis, mitochondrial encoded gene expression, nuclear encoded mitochondrial gene expression, mitochondrial protein expression, mitochondrial respiratory capacity, or adenosine triphosphate production. In another embodiment, the therapeutic composition has the activity of decreasing ROS in a subject. Non-limiting examples of ROS that may be reduced by a therapeutic composition of the present disclosure include hydrogen peroxide (H_2O_2), superoxide anions (O_2^-), and hydroxyl radicals ($^{\bullet}OH$). Such a compound or composition is meant to encompass a composition suitable for administration to a subject, such as a mammal, particularly a human subject. In general, a therapeutic composition is sterile, and preferably free of contaminants that are capable of eliciting an undesirable response within the subject (e.g., the compound(s) in the composition are pharmaceutical grade). Therapeutic compositions may be designed for administration to subjects in need thereof via a number of different routes of administration including oral, intravenous, intraarticular, intraarterial, buccal, rectal, parenteral, intraperitoneal, intradermal, intratracheal, intramuscular, subcutaneous, inhalation, vaginal, intraosseous, trans nasal,

injection, microneedle, topical, and transdermal. The appropriate dosage of a composition, as described herein, may be determined based on the type of disease to be treated, the severity and course of the disease, the clinical condition of the individual, clinical history, response to the treatment, and the discretion of the attending physician. In some embodiments, therapeutic compositions provided by the present disclosure may include various "unit doses." A unit dose is defined as containing a predetermined quantity of the therapeutic composition. The quantity to be administered, and the particular route and formulation, is within the skill of determination of those in the clinical arts. A unit dose need not be administered as a single injection but may comprise continuous infusion over a set period of time. In some aspects, a unit dose comprises a single administrable dose.

[0044] Precise amounts of the therapeutic composition also depend on the judgment of the practitioner and are peculiar to each individual. Factors affecting dose include physical and clinical state of the patient, the route of administration, the intended goal of treatment (alleviation of symptoms versus cure) and the potency, stability and toxicity of the particular therapeutic substance or other therapies a subject may be undergoing.

[0045] As used herein, "subject" or "patient" refers to animals, including humans, who are treated with the therapeutic compounds or compositions or in accordance with the methods described herein. For diagnostic or research applications, a wide variety of mammals may be suitable subjects, including rodents (e.g., mice, rats, hamsters), rabbits, primates, and swine, such as inbred pigs and the like. In particular embodiments, a subject in need of therapy may be any subject who comprises a cell that which exhibits decreased mitochondrial function or increased cellular oxidative stress as described herein. In another embodiment, the subject may be afflicted with or at risk of developing a disease or condition associated with decreased mitochondrial function or increased cellular oxidate stress. Non-limiting examples of such diseases or conditions include Barth syndrome, mitochondrial encephalopathy, lactic acidosis, stroke-like episodes (MELAS), Myoclonus epilepsy with ragged-red fibers (MERRF), neuropathy, ataxia, and retinitis pigmentosa (NARP), Leber's hereditary optic neuropathy (LHON), Kearns–Sayre syndrome (KSS), Pearson syndrome (PS), progressive external ophthalmoplegia (PEO), autosomal-dominant/ recessive PEO (ad/ar PEO), mtDNA depletion syndrome (MDDS), mitochondrial neurogastrointestinal encephalopathy (MNGIE), mitochondrial recessive ataxia syndrome (MIRAS), Alpers syndrome (AS), Leigh syndrome (LS), optic nerve atrophy, subacute necrotizing encephalopathy, early-onset hepatocerebral disorder, juvenile catastrophic epilepsy, adult-onset ataxia-neuropathy syndrome,

cardiomyopathy, cerebral white matter disease, ovarian dysfunction, hearing loss, cancer, diabetes mellitus, osteoporosis, and neurodegenerative disease.

[0046] A composition, as described herein, may include, in particular embodiments, a combination of therapeutic agents. In some embodiments, a composition as described here may be administered as a single composition or as more than one composition. Different compositions as provided herein, in certain embodiments, may be administered by the same route of administration or by different routes of administration.

[0047] A pharmaceutical composition of the present disclosure may comprise, in certain embodiments, a) a nanomaterial structure comprising sulfur active sites or comprising a transition metal and a chalcogen, wherein the nanomaterial structure comprises a high atomic vacancy concentration; and b) a second mitochondrial therapeutic agent. In certain embodiments the transition metal may be a transition metal dichalcogenide. Any mitochondrial therapeutic agent known in the art may be used in a pharmaceutical composition of the present disclosure. Non-limiting examples of such mitochondrial therapeutic agents include CoQ10 (ubiquinone), idebenone, riboflavin, dichloroacetate, thiamine, creatine, lipoic acid, glutathione, *N*-acetylcysteine, cysteamine, EPI-743 (*para*-benzoquinone analog), arginine, citrulline, cardiolipin, elamipretide, bezafibrate, resveratrol, AICAR (aminoimidazole carboxamide ribonucleoside), epicatechin, RTA 408 (synthetic isoprenoid), decanoic acid, a therapeutic peptide, and a therapeutic polynucleotide molecule. A therapeutic peptide or nucleic acid used according to the present disclosure may be any therapeutic peptide or nucleic acid known in the art to increase mitochondrial function or decrease cellular oxidate stress. In particular embodiments, the therapeutic peptide or therapeutic nucleic acid may function in or encode a protein associated with cellular metabolism and respiration. A pharmaceutical composition of the present disclosure may comprise, in some embodiments, a targeting molecule. In one embodiment, the targeting molecule may be cell-specific or tissue-specific. Numerous such targeting molecules are known in the art and any such targeting molecule may be used according to the present disclosure. In certain embodiments, a nanomaterial structure of the present disclosure may be modified with or conjugated to a peptide, a protein, a colloidal molecule, or a polymer to facilitate delivery or adsorption. The pharmaceutical composition of the present disclosure, in some embodiments, may be serum-free, endotoxin-free, or sterile.

[0048] A peptide or polynucleotide molecule for use according to the compositions of the present disclosure may, in some embodiments, be a recombinant peptide or nucleic acid. As

used herein, the term "recombinant" refers to a polynucleotide molecule, protein, or cell that is not naturally present, or is not naturally present in the same form or structure and was created by human intervention. In one embodiment, a recombinant polynucleotide may be a DNA molecule or may be an RNA molecule. A recombinant polynucleotide molecule or a recombinant polypeptide molecule or protein may comprise, in certain embodiments, a combination of two or more polynucleotide or polypeptide sequences that do not naturally occur together in the same manner, such as a polynucleotide molecule or protein that comprises at least two polynucleotide or protein sequences that are operably linked but heterologous with respect to each other. As used herein the term "heterologous" refers to a polynucleotide molecule or protein that is not naturally present or is not naturally present in the same form or structure and was created by human intervention. For example, a heterologous polynucleotide molecule or protein may not naturally occur in the cell being transformed or may be expressed in a manner or genomic context that differs from the natural expression pattern or genomic context found in the cell being transformed. The heterologous polynucleotide molecule or protein, in some embodiments, may be overexpressed in the cell being transformed. In certain embodiments, a recombinant polynucleotide molecule, protein, construct, or vector may comprise any combination of two or more polynucleotide or protein sequences in the same molecule which are heterologous to one another, such that the combination is man-made and not normally found in nature. As used herein, the phrase "not normally found in nature" means not found in nature without human intervention. A recombinant polynucleotide or protein molecule, may comprise, for example, polynucleotide or protein sequences that are separated from other polynucleotide or protein sequences that exist in proximity to each other in nature. A recombinant polynucleotide or protein molecule may also comprise, for example, polynucleotide or protein sequences that are adjacent to or contiguous with other polynucleotide or protein sequences that are not naturally in proximity with each other. Such a recombinant polynucleotide molecule, protein, or expression construct may also refer to a polynucleotide or protein molecule or sequence that has been genetically engineered or constructed outside of a cell. For example, a recombinant polynucleotide molecule may comprise any engineered or man-made plasmid, vector, or expression construct, and may include a linear or circular DNA molecule. Such plasmids, vectors, and expression constructs may comprise, for example, various maintenance elements including, but not limited to, a heterologous promoter sequence, a prokaryotic origin of replication, or a selectable marker.

[0049] In certain aspects, a therapeutic composition of the present disclosure may comprise a nanomaterial structure of the present disclosure and a therapeutic agent or a detectable label. Non-limiting example of therapeutic agents that may be used according to the present disclosure include a chemotherapeutic agent, an immunotherapeutic agent, a mitochondrial therapeutic agent, a neurotherapeutic agent, a metabolic therapeutic agent, an ophthalmic therapeutic agent, a cardio therapeutic agent, and a radiotherapeutic agent. Non-limiting examples of detectable labels that may used according to embodiments of the present disclosure include a paramagnetic ion, a radioactive isotope, a fluorochrome, an NMR-detectable agent, and an X-ray imaging agent.

[0050] In certain embodiments, the compositions and methods for treating an individual described herein may be combined with any other composition or method of treatment known in the art. The compositions and methods may be administered in any suitable manner known in the art. For example, a first and a second mitochondrial treatment may be administered sequentially (at different times) or concurrently (at the same time). In some aspects, a first and a second mitochondrial treatment may be administered in separate compositions. In certain embodiments, a first and a second treatment may be administered in the same composition.

[0051] Non-limiting examples of additional treatment modalities that may be included in combination with the compositions and methods provided herein include a therapeutic agent or surgery. In specific embodiments, the methods and compositions of the present disclosure may be combined with other therapies directed towards increasing mitochondrial function or decreasing cellular oxidate stress as described herein.

C. Detection and Therapeutic Agents

[0052] In some aspects, the present disclosure provided methods and compositions for detection and therapeutic labeling of the high atomic vacancy nanomaterial structures of the present disclosure. Methods for labeling and detection of such structures are well-known in the art, and any such method known in the art may be used to label or detect the nanomaterial structures described herein. As a non-limiting example, nanomaterial structures may be labeled with a detectable moiety, such as a radioactive atom, a chromophore, a fluorophore, or the like, and then detected using methods known in the art. Such labeled nanomaterial structures may be used, in some embodiments, for *in vivo* or *in vitro* diagnostic techniques.

[0053] As used herein, the term "label" refers to a directly or indirectly detectable compound or composition that is conjugated directly or indirectly to the composition to be detected. In certain embodiments, a nanomaterial structure, a polynucleotide molecule, protein, or cell may be labeled to generate a labeled composition. In particular embodiments, labeled compositions also include sequences which are conjugated a polynucleotide molecule that will provide a signal upon expression of the inserted sequences, such as green fluorescent protein (GFP) and the like. The label may be detectable by itself (e.g., radioisotope labels or fluorescent labels) or, in the case of an enzymatic label, may catalyze chemical alteration of a substrate compound or composition that is detectable. Labels may be suitable for small scale detection or for high-throughput screening. As such, suitable labels include, but are not limited to radioisotopes, fluorochromes, chemiluminescent compounds, dyes, and proteins, including enzymes. Labels may be simply detected or may be quantified. In certain embodiments, labels that may be quantified provide numerically reportable value. In luminescence or fluorescence assays, the detectable response may be generated directly using a luminophore or fluorophore associated with an assay component involved in binding, or indirectly using a luminophore or fluorophore associated with another (e.g., reporter or indicator) component.

[0054] The term "about" is used to indicate that a value includes the standard deviation of the mean for the device or method being employed to determine the value. The use of the term "or" in the claims is used to mean "and/or" unless explicitly indicated to refer to alternatives only or the alternatives are mutually exclusive. When used in conjunction with the word "comprising" or other open language in the claims, the words "a" and "an" denote "one or more," unless specifically noted otherwise. The terms "comprise," "have," and "include" are open-ended linking verbs. Any forms or tenses of one or more of these verbs, such as "comprises," "comprising," "has," "having," "includes," and "including," are also open-ended. For example, any method that "comprises," "has," or "includes" one or more steps is not limited to possessing only those one or more steps and also covers other unlisted steps. Similarly, any system or method that "comprises," "has," or "includes" one or more components is not limited to possessing only those components and covers other unlisted components.

[0055] Other objects, features, and advantages of the present disclosure are apparent from detailed description provided herein. It should be understood, however, that the detailed description and any specific examples provided, while indicating specific embodiments of the disclosure, are given by way of illustration only, since various changes and modifications

within the spirit and scope of the disclosure will become apparent to those skilled in the art from this detailed description. Any embodiment of the present disclosure may be used in combination with any other embodiment described herein.

[0056] All references herein are incorporated herein by reference in their entirety.

EXAMPLES

[0057] The following examples are included to illustrate embodiments of the present disclosure. It should be appreciated by those of skill in the art that the techniques disclosed in the examples that follow represent techniques discovered by the inventor to function well in the practice of the invention. However, those of skill in the art should, in light of the present disclosure, appreciate that many changes can be made in the specific embodiments which are disclosed and still obtain a like or similar result without departing from the concept, spirit and scope of the invention. More specifically, it will be apparent that certain agents which are both chemically and physiologically related may be substituted for the agents described herein while the same or similar results would be achieved. All such similar substitutes and modifications apparent to those skilled in the art are deemed to be within the spirit, scope and concept of the invention as defined by the appended claims.

Example 1: Synthesis and Characterization of MoS_2 Nanoflowers with Predefined Atomic Vacancies

[0058] To synthesize MoS_2 nanomaterials, molecular precursors of molybdenum (hexaammonium heptamolybdate tetrahydrate) and sulfur (thiourea) are used in a stoichiometric ratio of 1:2. After hydrothermal synthesis and removal of unreacted precursor and impurities, MoS_2 nanoflowers were obtained, which are composed of MoS_2 nanosheets. The individual MoS_2 nanosheets consist of a hexagonal lattice structure, where each layer is made of a covalently linked S–Mo–S nanosheet. These nanosheets are held together by short-range *van der Waals* interactions resulting in their flower-like morphology. Due to the planar MoS_2 lattice, it is possible to introduce atomic vacancies by altering the precursor ratio (Mo:S). In this example, a Mo:S ratio of 1:1 was used to incorporate a relatively low degree of atomic vacancies and a Mo:S ratio of 1:6 was used to incorporate a relatively high degree of atomic vacancies (or vacancy rich) compared to a typical synthesis with a precursor ration of 1:2. The morphology of the MoS_2 nanoflowers was characterized by transmission electron microscopy (TEM). The individual nanosheets were stacked together due to Ostwald ripening to form concentric, hierarchical flower-like structures ~ 200 nm in diameter (FIG. 1, Panel

A). Thus, the introduction of atomic vacancy did not affect the morphology of the MoS_2 nanoflowers.

[0059] The crystallographic arrangement of the Mo and S atoms within the nanoflowers and the effect of atomic vacancies on the crystalline structure was determined by X-ray diffraction (XRD) spectroscopy. The diffraction peaks (002, 100, 110) of the MoS_2 nanoflowers indicate the presence of a hexagonal crystal structure, similar to hexagonal MoS_2 (JCPDS card No. 73-1508) (FIG. 1, Panel A). The crystallite size of the nanoflowers was calculated using the Scherrer equation (using the 002 peak), nanoflowers with a typical degree of atomic vacancies (1:2) and a relativity low degree of atomic vacancies (1:1) had a crystallite size of 6.13 nm, while nanoflowers with a relatively high degree of atomic vacancies (1:6) had a larger crystallite size of 7.59 nm.

[0060] X-ray photoelectron spectra (XPS) analysis of the binding energies (BE) for Mo and S core-level electrons indicated the presence of Mo^{4+} ($3d^{5/2}$ ~ 228 eV and $3d^{3/2}$ ~231 eV) and S^{2-} ($2p^{3/2}$ ~161 eV and $2p^{1/2}$~ 162 eV) within MoS_2 nanoflowers with predefined atomic vacancies (FIG. 1, Panel B). Further deconvolution of the XPS spectra indicated the presence of predominantly 2H phase (hexagonal symmetry) within the trigonal prismatic MoS_2 crystal (1T phase). This demonstrates that the incorporation of atomic vacancies did not cause appreciable changes in the morphology or crystal structure of the MoS_2 nanoflowers. The increased density of active centers (sites of atomic vacancy) within the nanoflowers was verified using cyclic voltammetry. The density of active sites in the high degree of atomic vacancies nanoflowers (1:6) was determined to be 5.59×10^{-4} moles g^{-1} (FIG. 1, Panel C). The increase in active sites also results in enhanced catalytic decomposition of hydrogen peroxide (H_2O_2) by the nanoflowers. This was evaluated using electrochemical (amperometric evaluation of H_2O_2 reduction) and biochemical (catalase enzyme activity) assays, respectively. Both assays demonstrate that nanoflowers with high atomic vacancies (MoS_2 (1:6)) exhibit enhanced catalytic activity as compared to the other formulations (FIG. 2).

[0061] To determine the effect of atomic vacancies on aqueous stability and the zeta potential, MoS_2 nanoflowers were evaluated in deionized water (DI) and cell culture media containing fetal bovine serum (FBS) (FIG. 3). In DI water, MoS_2 nanoflowers exhibited a strong negative zeta potential of -33.58 ± 0.39 mV. The introduction of atomic vacancies resulted in a slight increase in zeta potential to -29.32 ± 0.511 mV for (1:1) and -30.5 ± 2 mV for (1:6) MoS_2 nanoflowers, respectively. However, in cell culture media the zeta-potential of all three types

of nanoflowers showed an increase (-11.5 ± 0.5 mV). This change is attributed to the adsorption of proteins onto the surface of the nanoflowers and resultant charge shielding. The adsorbed proteins on the MoS_2 nanoflowers were evaluated by Sodium Dodecyl Sulfate – Polyacrylamide Gel Electrophoresis (SDS-PAGE). Analysis of the protein bands indicated that the degree of atomic vacancies within the nanoflowers does not impact the type of proteins absorbed (FIG. 3).

[0062] Cellular compatibility of the MoS_2 nanoflowers was determined by measuring cellular DNA content in human mesenchymal stem cells (hMSCs) post 24h of exposure (FIG. 1, Panel D). The concentration of MoS_2 nanoflowers at which the cell viability is reduced by 50%, was regarded as the half-maximal inhibitory concentration (IC_{50}) as determined by fitting a logarithmic dose-response curve. All variations of MoS_2 were highly cytocompatible, as evident from a high IC_{50} value (~400 µg/mL), with no significant effect of degree of atomic vacancies on cytocompatibility observed. The cellular compatibility of MoS_2 nanoflowers were similar to other biocompatible nanoparticles such as graphene, hydroxyapatite, bioglass, and gold nanoparticles. The integrity of the cell membrane was evaluated by measuring the release of the cytosolic enzyme, lactate dehydrogenase (LDH), in the cell culture media. No significant release of LDH was observed from cells treated with concentrations up to 200 µg/mL of MoS_2, indicating the presence of an intact plasma membrane (FIG. 1, Panel E).

[0063] The effect of MoS_2 nanoflowers on various cell cycle stages was evaluated by treating hMSCs with 25-100 µg/mL of MoS_2 nanoflowers for 72h (FIG. 1, Panel F). While a MoS_2 concentration of 25 µg/mL produced no significant cell cycle alteration, an observable reduction in the S and G2/M phase was noted at doses exceeding 50 µg/mL, demonstrating that higher concentrations of MoS_2 inhibit cell proliferation over time. Exposure of hMSCs to atomic vacancy rich nanoflowers at a concentration of 25 µg/mL showed no significant changes in long term cell proliferation (FIG. 4, Panel A). The internalization process of MoS_2 nanoflowers by cells was assessed using F-actin and nuclear fluorescence staining, and the MoS_2 nanoflowers were visualized *via* reflective light. (FIG. 1, Panel G). Additionally, TEM was used to visualize the nanoflower uptake, and the TEM micrographs of internalized nanoflowers demonstrate that the nanoflowers are localized within endosomal vesicles (FIG. 5). The extent of cellular internalization of MoS_2 nanoflowers was further quantified by inductively coupled plasma mass spectroscopy-based elemental analysis. After 18h of incubation with MoS_2 nanoflowers (25 µg/mL), there was a pronounced increase in intracellular Mo, which was unaffected by the degree of vacancy (FIG. 1, Panel H). Following

these *in vitro* observations, all subsequent cellular studies with MoS_2 nanoflowers were conducted at a concentration of 25 µg/mL unless otherwise mentioned.

Example 2: Atomic Vacancies Alter the Cellular Transcriptomic Profile

[0064] To investigate the effect of atomic vacancies on transcriptome dynamics, whole transcriptome sequencing (RNA-seq) of human mesenchymal stem cells (hMSCs) treated with MoS_2 (1:1 and 1:6) at a concentration of 25 µg/mL for 7 days was performed. The cells treated with MoS_2 nanoflowers showed substantial differences in their transcriptome profiles as evident from principal component analysis (PCA) of differentially expressed genes (DEGs) (FIG. 6, Panel A). PCA of the 20% most variable genes (assessed by median absolute deviation) from the study group revealed a pronounced distinction (represented by PC1, accounting for 59.90% of the total variance) between hMSCs treated with and without MoS_2 having different atomic vacancies. PC2 further accounted for 26.02% of the variance, adding to the interpretability of the data. In addition, the PCA and linear correlation analysis showed limited variation within the control and treatment group replicates (FIG. 7). DEGs between treated and untreated hMSCs were also identified as described in Carrow *et al.* Proceedings of the National Academy of Sciences 117, 13329-13338 (2020). The results demonstrate that the treatment of hMSCs with low atomic vacancies MoS_2 (1:1) significantly ($P\text{-}adj < 0.01$) affected the expression of 1,047 genes (454 upregulated and 593 downregulated, FIG. 6, Panel B). For cells treated with MoS_2 with high atomic vacancies (1:6), the expression profile of 1,959 genes changed significantly (916 upregulated and 1,043 downregulated genes respectively (FIG. 6, Panel B, FIG. 6, Panel C).

[0065] The key biological processes that were affected by MoS_2 treatment were identified *via* Gene Ontology (GO) enrichment analysis. GO enrichment analysis hierarchically classifies gene and gene products, utilizing statistical tests (hypergeometric test) to identify modulated cellular processes across samples. For cells exposed to high atomic vacancy MoS_2 (1:6), the significant GO terms ($P<0.05$) were refined using semantic similarity as a criterion. This process, which prioritizes GO terms with shared meaning, facilitated the formation of seven comprehensive clusters: "morphogenesis," "extracellular matrix," "cell-matrix regulation," "cellular locomotion component," "mitochondrial electron chain transport," "triphosphate metabolism," and "protein catabolic targeting membrane" (FIG. 6, Panel D). Similarly, for cells treated with low atomic vacancy MoS_2 (1:1) GO terms such as "extracellular matrix", "cell–matrix regulation", and "cellular locomotion component" were enriched (FIG. 8). Notably, two of the broader GO term clusters relating to biological processes primarily

involved in cellular metabolism and respiration, were observed only in cells treated with MoS_2 having high atomic vacancies (1:6). Some of these uniquely regulated GO terms pointed to genes encoding OXPHOS proteins, including mitochondrial respiratory chain complex assembly (GO:0033108), mitochondrial respiratory chain complex I assembly (GO:0032981), mitochondrial electron transport (GO:0006120), and ATP synthesis coupled electron transport (GO:0042773) (FIG. 9).

Example 3: High Atomic Vacancies of MoS_2 Upregulate Transcription of Nuclear-Encoded Mitochondrial Genes

[0066] In order to understand the effect of atomic vacancies of MoS_2 on nuclear-encoded mitochondrial genes, a selective inspection of the DEGs was performed using the MitoCarta 3.0 dataset, which is a curated repository of 1,136 mitochondrial proteins. hMSCs treated with high atomic vacancy MoS_2 showed consistent upregulation of mitochondrial genes as compared to untreated cells (FIG. 10, Panel A). Treatment with high atomic vacancy MoS_2 also resulted in the stimulation of biological processes such as Mitochondrial ATP synthesis coupled proton transport (GO:004277) and Mitochondrial electron transport (GO:0006123) (FIG. 10, Panel B). Within these processes, a significant upregulation of OXPHOS genes such as *ATP5E* (fold change = 2^1.31, *Padj* <0.01) and *COX5A* (fold change = 2^1.39, *Padj* < 0.01) (FIG. 10, Panel C) was observed. Analysis of DEGs in cells treated with high atomic vacancy MoS_2 indicated a global upregulation of genes involved in OXPHOS complexes I, IV, V and mitochondrial protein synthesis, respectively (FIG. 11). This data indicates that treatment with high atomic vacancy MoS_2 results in an enhanced expression of genes involved in mitochondrial biogenesis.

[0067] To ensure the robustness of our RNA-Seq analysis, Gene Set Enrichment Analysis (GSEA) was employed. GSEA of cells exposed to MoS_2 with high atomic vacancies indicated a significant upregulation (normalized enrichment score (NES) >1) of processes relating to OXPHOS, which correlated well with our GO enrichment analysis (FIG. 10, Panel D). Particularly, the *Hallmark* gene sets *Oxidative Phosphorylation (NES= 2.67, P-adj<0.05), Fatty Acid Metabolism (NES= 1.4, P-adj <0.1)*, and *Reactive Oxygen Species Pathways* (*NES= 1.6, P*-adj<0.05) showed a positive correlation (FIG. 10, Panel E), indicating mitochondrial energy metabolism and cellular reactive oxygen species (ROS) homeostasis as key cellular processes affected by the treatment with high atomic vacancy MoS_2. The subcellular localization of MoS_2 nanoflowers was evaluated using confocal microscopy and no colocalization between the nanoflowers and mitochondria was observed (FIG. 10, Panel

F), demonstrating their influence extends to cytoplasmic targets to boost mitochondrial function and reduce cellular ROS. Additionally, these confocal images were used to perform mitochondrial morphology analysis using the Mito hacker pipeline to determine the effect of MoS_2 nanoflowers on the mitochondrial morphology. The data generated indicated no significant change in mitochondrial network parameters, such as mitochondrial branch length, mitochondrial area, and mitochondrial form factor following MoS_2 nanoflower treatment (FIG. 10, Panel G).

Example 4: High Atomic Vacancies of MoS_2 Stimulate Mitochondrial Biogenesis

[0068] The human mitochondrial genome is 16.6 kbp of circular double-stranded DNA, which encodes for 13 polypeptides that form essential components of the OXPHOS machinery as well as RNA molecules required for the translation of the mitochondrial DNA (mt-DNA) (FIG. 12, Panel A). Thus, to evaluate the effect of MoS_2 with high atomic vacancies on mitochondrial function the RNA-seq dataset was examined, which showed an enhanced expression of all 13 mt-DNA encoded genes (FIG. 12, Panel B). Next, mt-DNA copy number was assessed in hMSCs by qRT-PCR analysis, which revealed a two-fold increase in relative mt-DNA levels in cells treated with high atomic vacancy MoS_2 (1:6) (FIG. 12, Panel C). Additionally, a similar increase was observed in mRNA expression of mt-DNA-encoded genes, such as *NADH:Ubiquinone Oxidoreductase Core Subunit 2 (mt-ND2)* (FIG. 12, Panel C). To ensure the effect of MoS_2 (1:6) treatment is not cell type specific, the relative abundance of mt-DNA in MCF-7 and H9c2 cells treated with MoS_2 (1:6) nanoflowers was evaluated. A similar trend was observed in both cell lines when treated with MoS_2 (1:6), each exhibiting a nearly 2-fold increase of mt-DNA content compared to untreated cells (FIG. 13). To investigate whether an increased expression of mt-DNA encoded genes translates into an increased abundance of their respective proteins, SDS-PAGE/Western blot analysis was conducted. Cells exposed to MoS_2 with high atomic vacancies (MoS_2 (1:6)) showed an increased abundance of multiple OXPHOS subunits including, succinate dehydrogenase subunit B (SDHB, Complex II), ubiquinol-cytochrome *c* reductase core protein 2 (UQCRC2, Complex III), ATP synthase alpha-subunit (ATP5A, Complex V) and mitochondrial membrane proteins such as voltage dependent anion channel 1 (VDAC1, mitochondrial porin) (FIG. 12, Panel D).

[0069] To better understand the molecular mechanism by which MoS_2 with high atomic vacancies activates mitochondrial biogenesis, the role of the master regulators of mitochondrial biogenesis, proliferator-activated receptor gamma coactivator 1 alpha (PGC-

1α) and mitochondrial transcription factor A (*TFAM*) was explored. PGC-1α activates transcription factors NRF1 and NRF2 to induce expression of TFAM. TFAM traffics to mitochondria, where it is required for mt-DNA maintenance and replication. GSEA was performed for targets of PGC-1α using the ENCODE *Transcription Factor Targets* dataset. The GSEA data showed a statistically significant enrichment of PGC-1α associated genes (*P-adj* <0.01, NES = 1.92) (FIG. 12, Panel E).

[0070] Importantly, an increased expression of PGC-1α following exposure to MoS_2 with high atomic vacancies was observed for 3 and 7 days, respectively (FIG. 12, Panel F). While PGC-1α is primarily responsible for governing the expression of nuclear-encoded mitochondrial genes, the expression of mitochondria-encoded genes is regulated by TFAM. A spike in the expression levels of *TFAM* was observed as early as day 3 after treatment with MoS_2 with high atomic vacancies (FIG. 12, Panel G). This demonstrates the activation of mitochondrial biogenesis as a result of MoS_2 treatment occurs as early as 72h post treatment with the nanoparticle. Concordant with these findings, treated cells exhibited increased expression of genes required for the maintenance of mt-DNA copy number, such as DNA binding protein *SSBP1* (fold change = 2^1.39, *Padj* <0.01), *DGUOK* (fold change = 2^1.03, *Padj* <0.01), and *MPV17* (fold change = 2^0.75, *Padj* <0.01). Taken together, these results demonstrate that MoS_2 treatment triggers mitochondrial biogenesis by inducing the expression of PGC-1α and subsequent mitochondrial biogenesis.

Example 5: High Atomic Vacancy Increases Mitochondrial Bioenergetics While Decreasing Oxidative Stress

[0071] Increased mitochondrial biogenesis is expected to increase mitochondrial respiration and ATP production. Oxygen consumption rate (OCR) measurement by Seahorse XF24 assay, in C2C12 cells treated with or without high atomic vacancy MoS_2, showed that MoS_2 treatment increased the spare respiratory capacity (FIG. 14, Panel A). Similarly, in mouse bone marrow derived monocytes exposed to MoS_2 with high atomic vacancies for 18h increased both basal and spare respiratory capacity, irrespective of monocyte polarization (FIG. 15). In addition, enhanced total ATP production in hMSCs treated with MoS_2 as compared to untreated cells was observed (FIG. 14, Panel B). This increase in respiratory capacity and total cellular ATP production can be attributed to increased mitochondrial biogenesis, as observed by the higher mt-DNA copy number and increased abundance of OXPHOS proteins in cells exposed to MoS_2 with high atomic vacancies (FIG. 13 and FIG. 16). Further, no significant disruption of mitochondrial membrane potential in treated cells

was observed, indicating that treatment with MoS_2 does not disrupt mitochondrial membrane integrity and likely results in more newly synthesized mitochondria capable of maintaining a mitochondrial membrane potential comparable to that of untreated cells (FIG. 14, Panel C and FIG. 17).

[0072] To determine whether nanomaterial treatment resulted in altered cellular ROS levels, hMSCs were treated with vacancy rich MoS_2 for 24h and measured total cellular ROS. A decrease in cellular ROS was observed in cells treated with MoS_2, when compared to untreated cells (FIG. 14, Panel D; FIG. 4, Panel B). A similar decrease in mitochondria-specific ROS was also observed, as determined using mitochondrial superoxide indicator MitoSOX (FIG. 14, Panel E). This corroborates with the RNA-Seq data showing cells treated with high atomic vacancy MoS_2 exhibited an increased expression of antioxidant genes such as *superoxide dismutase type 1* (*SOD1*, fold change= 2^0.89, *Padj* < 0.01), and members of the glutathione *S*-transferase (*GST*) family *Glutathione S-transferase omega-2 (GST02,* fold change= 2^1.50, *Padj* < 0.01), *Glutathione S-Transferase Zeta 1* (*GSTZ1,* fold change= 2^1.37, *Padj* < 0.01) (FIG. 14, Panel F). Together these results demonstrate that MoS_2 nanoflowers with high atomic vacancies scavenge cellular ROS, reducing oxidative stress in treated cells. The reduction in ROS levels at early (24h) and the enhanced expression of antioxidant genes at later (7 day) time points may be attributed to a combination of catalytic reduction by MoS_2 with high atomic vacancies and the activation of antioxidant genes by PGC-1α, respectively.

[0073] PGC-1α acts as the primary conduit through which signaling cascades modulate mitochondrial biogenesis. The post-transcriptional activation of PGC-1α can occur *via* pathways such as SIRTs or AMP-activated protein kinase (AMPK). SIRT1 directly responds to levels of oxidative stress within cells, acts as a ROS-suppressor, and exhibits antioxidative effects. SIRT1 has been shown to be directly responsible for the activation of PGC-1α through deacetylation of inactive PGC-1α in the cytosol. The ability of vacancy-rich MoS_2 to enhance mitochondrial biogenesis *via* PGC-1α activation was further validated using PGC-1α knockdown cells (FIG. 14, Panel G). PGC-1α knockdown cells showed no significant increase in mt-DNA copy number following exposure to vacancy rich MoS_2, this was in stark contrast to cells transfected with empty pLKO vector (FIG. 14, Panel H). In TFAM knockdown cells (FIG. 18, Panel A), MoS_2 treatment led to a minor increase in mt-DNA copy number (FIG. 18, Panel B), which can be attributed to the activity of residual TFAM. In

summary, these results demonstrate that vacancy rich nanoflowers mediate mitochondrial biogenesis primarily via PGC-1α activation.

[0074] It is interesting to note that a reduction in oxidative stress resulting in SIRT1/PGC-1α activation and subsequent mitochondrial biogenesis has been observed in other therapeutic compounds, such as Resveratrol. However, compared to vacancy rich MoS_2, single dose treatment with Resveratrol or the antioxidant N-acetyl cysteine induces a less robust increase in mitochondrial biogenesis (FIG. 14, Panel I). Based on the above results, which demonstrate a reduction in cellular ROS production and an enhancement of mitochondrial biogenesis, vacancy rich MoS_2 may mitigate cellular ROS. This reduction would then trigger the SIRT1/PGC-1α cascade, one of the principal activators of mitochondrial biogenesis, leading to increased mitochondrial function and formation (FIG. 14, Panel J).

Example 6: Materials and Methods

[0075] ***Nanoparticle synthesis:*** To synthesize MoS_2 nanoflowers with atomic scale defects, varying ratios of molecular precursors of molybdenum and sulfur (hexaammonium heptamolybdate tetrahydrate and thiourea respectively) were added to 15 mL of water. This solution was then transferred to a hydrothermal device and placed at 220 °C for 18h. The solution obtained was subsequently washed with water and ethanol multiple times to remove any unreacted precursors and impurities. In this manner, three different formulations of MoS_2 nanoflowers were synthesized: nanoflowers with a typical degree of atomic vacancies (Mo:S ratio of 1:2), nanoflowers with a relatively low degree of atomic vacancies (Mo:S ratio of 1:1), and nanoflowers with high degree of atomic vacancies (Mo:S ratio of 1:6).

[0076] ***Nanoparticle characterization:*** Transmission electron microscopy (TEM) was performed on a carbon grid at an accelerating voltage of 200 kV using a JEOL-JEM 1200 (Japan). For sample preparation, an aqueous dispersion of MoS_2 samples was drop-casted and air-dried on a copper grid (procured from Ted Pella Inc.). The zeta potential and hydrodynamic size of MoS_2-albumin solutions were measured with a Zetasizer Nano ZS (Malvern Instrument, U.K.) furnished with a He–Ne laser at 25°C. The crystallographic phase of monolayer MoS_2 sheets together with bulk counterpart was confirmed by X-ray powder diffraction (Bruker D8 advanced) using copper Kα source (wavelength, 1.54 Å). The data was recorded from 5 to 70 degrees and the obtained peaks were indexed using JCPDS card No. 73-1508. The characteristic peak (002) was used to calculate crystallite size (D) using the Scherrer equation given as follows: $D = (K\lambda)/(\beta \cos \theta)$. Where K is the shape factor

(approx. 0.94), λ is X-ray wavelength, β is line broadening at full width half maxima (FWHM), and θ is the Bragg angle. The crystallographic arrangement of Mo-S atoms within the nanoflowers following the synthesis was determined using X-ray photoelectron spectroscopy (XPS, Omicron Inc.). The binding energies (B.E.) for Mo (3d) and S (2p) for MoS_2 samples along with that of adventitious carbon (C1s) for both bulk and monolayer counterparts were recorded. The raw data was further processed and deconvoluted by CasaXPS multiple peak fit software version 2.3.15 and indexed using the standard library.

[0077] ***Cyclic voltammetry (CV):*** CV analysis was conducted to determine the active sites in the samples, following the procedure described in Jaiswal *et al.*, Advanced Materials 29, 1702037 (2017). All the measurements were done on CH Instruments (model number CHI-660D) electrochemical workstation. A three-electrode screen printed electrode (SPE) (TE100, CH Instruments) with a diameter of φ = 3 mm was used as the working electrode, a conducting carbon as the counter electrode, and an Ag/AgCl electrode as the reference electrode. All the CV measurements were carried out in 1x phosphate buffer solution (PBS) of 7 pH at a scan rate of 50 mV/s. Before conducting experiments, the screen-printed electrodes underwent a cleaning process. This involved running 10 cyclic voltammetry (CV) cycles at a scan rate of 100 mV/s within a voltage window of -0.3 to 1.3 V in a 0.5 M H_2SO_4 solution. Following the cleaning procedure, a 2-microliter volume of a dispersed MoS_2 solution (labeled 1:1, 1:2, and 1:6) at a concentration of 10 mg/mL was drop-casted onto the working electrode of the cleaned SPEs. Subsequently, all the coated electrodes were air-dried at room temperature for 60 minutes and then used for further electrochemical characterizations. Active sites were calculated by extracting the absolute values of voltametric charges (both cathodic and anodic) obtained from the cyclic voltammetry scanning from -0.2 to 0.6 V (versus Ag/AgCl) using a scan rate of 50 mV/s in PBS with a pH of 7.0. Considering a one-electron redox process that occurred during the reaction, the total charges were divided into two. The number of active sites (n) for the sample deposited on the electrode was determined using the following equation: $n = Q/2F$ (mol/g), where Q: Voltametric charges; F: Faraday constant (C mol-1).

[0078] ***Amperometric analysis:*** Amperometry was performed at the H_2O_2 reduction voltage of -0.6 V in order to compare the output currents of all the MoS_2 samples. All amperometric measurements are carried out in N_2-saturated 5 mM H_2O_2 in 1xPBS of 7 pH. The output reduction current density of samples was used to determine their H_2O_2 reduction capability.

[0079] ***Catalase Activity*****:** The catalytic activity of MoS_2 nanoflowers was determined by comparing the reduction of hydrogen peroxide by nanoflowers to the reduction caused by the bovine catalase enzyme. The assay was performed using the Catalase Colorimetric Activity Kit (Invitrogen, catalog no: EIACATC), with the nanoflowers dispersed in PBS at a concentration of 25 µg/mL.

[0080] ***Cell culture:*** Human mesenchymal stem cells (hMSCs) (RoosterBio and Lonza) were cultured under normal media conditions consisting of α-minimal essential media (alpha-MEM, Hyclone, GE Sciences) with 16.5% fetal bovine serum (Atlanta Biologicals, USA) and 1% penicillin/streptomycin (100 U/100 µg/mL, Gibco). Every 2-3 days, half of the culture media was exchanged for fresh media. Cells were passaged with 0.5% trypsin-EDTA upon reaching a confluency of ~70% and seeded at ~2500 cells/cm^2. All experiments were completed with cell populations under passage 5. H9c2 and C2C12: Cells were cultured in high-glucose Dulbecco's Modified Eagle Medium (DMEM) media supplemented with 10% fetal bovine serum (FBS) (Sigma), 1 mM sodium pyruvate, and Pen/Strep (Life Technologies). Cells were passaged with 0.5% trypsin-EDTA upon reaching a confluency of ~70% and seeded at ~2500 cells/cm^2. Cells were cultured under 5% CO_2 at 37°C. BMDM: Bone marrow derived macrophages (WT) were isolated from mice as described in Keeney *et al.*, The Journal of Immunology, ji2200596, 2023. BMDM cells were cultured in Dulbecco's Modified Eagle Medium (DMEM) (Life Technologies) supplemented with 10% fetal bovine serum (FBS) (VWR). LPS (200ng/mL) and IL-4 (20 ng/mL) treatments were performed 5h after treatment with nanoparticles.

[0081] ***Protein corona formation:*** The composition of the protein corona formed around the nanosheet was investigated by an SDS-PAGE gel electrophoresis. Briefly the nanosheets were incubated with serum supplemented alpha MEM media for 2h at 37°C. The samples were then centrifuged at 10,000g and washed 3 times with PBS. The nanosheets were then suspended in LDS loading buffer (Thermo Fisher), followed by incubation at 90°C for 15 minutes and subsequent gel electrophoresis was performed. The gels were then stained using Imperial Blue stain (Thermo Fisher).

[0082] ***In vitro assays:*** For cytotoxicity assays hMSCs were seeded in 96 well plates at a seeding density of 5,000 cells per well. The cells were exposed to varying concertation of MoS_2 nanosheets for a pre-defined time 24h for cytotoxicity followed by measurement of toxicity using Cyquant and LDH assay (Thermo Scientific), respectively as per the manufacturer's protocols. For assessing cell proliferation, hMSCs were seeded in different

96 wells (corresponding to each time point) plates at 5,000 cells per well, and then treated with MoS_2 (1:6) at a concertation of 25 µg/mL. Following each time point, DNA content and total cell number were assessed in cells, with and without MoS_2 exposure, using the Cyquant assay (Thermo Scientific) per the manufacturer's protocols. For cell cycle analysis hMSCs were cultured in 6 well plates. After reaching 50% confluency hMSCs were serum starved (only 1% FBS in media) for 12h to synchronize cell populations, followed by treatment with MoS_2 nanosheets (25µg/mL). After 72h of exposure the cells are trypsinized and fixed in ice cold 70% ethanol. The cells were then centrifuged and washed with PBS three times, followed by incubation with PI (40 µg/mL) and Rnase (100 µg/mL) at 37°C for 1 h. Cells were stored at 4 °C until flow cytometry analysis was performed using the BD Accuri C6 flow cytometer. ATP production was measured using a bioluminescence assay. For this assay hMSCs, were seeded in a 96 well plate at a density of 5000 cells per well. Following this, the hMSCs were treated with varying concentrations of vacancy rich MoS_2 nanoflowers for 72h, after which ATP levels were measured using an ATP determination kit (Thermo Fisher) as per the manufacturer's protocol. Fluorescence imaging of hMSCs treated with MoS_2 nanoflowers was performed using a confocal microscope (Leica Sp8). Cells were cultured in chambered coverslips followed by exposure to nanoflowers for 24h, after which cells were washed three times with PBS and fixed by incubation of samples with 4% paraformaldehyde (PFA) for 20 minutes at room temperature. If needed, cells were permeabilized with 0.1 % Triton X-100 for 10 minutes at room temperature. MoS_2 nanoflowers were imaged using reflective light, with the nucleus, f-actin, and mitochondria stained using DAPI (Biotium), Acti-Stain 670 Phalloidin (Cytockeleton, Inc) and Mito tracker red (Thermo Fisher), respectively.

[0083] ***TEM imaging of internalized nanoflowers:*** hMSCs were cultured in chambered slides (Nunc, Lab-Tek Chamber Slide, Thermo Scientific) overnight, followed by treatment with MoS_2 (1:6) nanoflowers for 24h. Cells were then fixed using Trump's universal fixative for 2h at room temperature. Following this, samples were subjected to sequential dehydration in varying concentrations of ethanol (50%, 70%, and 100%) and infiltration with and polymerization of epoxy resins. The polymerized epoxy resin blocks were separated from the glass slide to expose the embedded cell monolayer. Ultra-thin sections (60-80nm) were cut parallel with the surface on a Leica UC7 ultramicrotome using a diamond knife, collected on 300-mesh copper grids with carbon support film and stained with uranyl acetate and Venable lead citrate, 5 minutes each. Transmission electron microscopy (TEM) of the stained grids was performed using a JEOL-JEM 1200 (Japan) at an accelerating voltage of 200 kV.

[0084] ***Transcriptome sequencing (RNA-seq):*** hMSCs were treated with low atomic vacancy and high atomic vacancy MoS_2 nanoflowers respectively, at a concentration of 25 µg/mL for 7 days with untreated cells acting as a control group. Following 48h of initial treatment, the excess nanoflowers were then removed during routine media exchange and the cells were cultured for an additional 5 days under normal media conditions. On the 7^{th} day of treatment, cells were harvested, and total RNA was extracted using the Zymogen Quick RNA Miniprep kit. mRNA concentration and quality were assessed using NanoDrop®, with an absorbance ratio threshold A260/A280 > 2 for samples used for sequencing. Sequencing was performed using a Nova seq platform (Illumina Nova sEq. 6000), using a Truseq RNA preparation and 75 paired-end read length. Following sequencing, reads were aligned in reference to the human genome (hg38, GRCh37 Genome Reference Consortium Human Reference 37, obtained from University of California, Santa Cruz) using the R-Bioconductor package Spliced Transcripts Aligned to a Reference (STAR) (Dobin *et al.*, Bioinformatics 29, 15-21, 2013. mRNA levels of nanomaterials treated hMSC samples were compared to untreated hMSC samples to determine nanomaterial exposure induced differential expression of genes. For untreated hMSCs 30672868 (22477324 uniquely mapped) and 26167130 (19300764 uniquely mapped) reads were aligned to the genome for the 2 replicates. Similarly, for hMSCs treated with low atomic vacancy MoS_2 24580412 (17841369 uniquely mapped) and 29456043 (22339102 uniquely mapped) reads were aligned to the genome for the 2 replicates. In the case of hMSCs treated with high atomic vacancy MoS_2 24852928 (18123996 uniquely mapped) and 23488937 (17814934 uniquely mapped) reads were aligned to the genome for the 2 replicates.

[0085] Only uniquely mapped reads were utilized for further analysis. RefSeq gene models were retrieved from UCSC, and expression was quantified to read counts using the uniquely mapped reads of the coding exons, normalized by gene length using reads per kilobase of transcript per million mapped reads (RPKM) factor. Genes expressed with RPKM > 1 in at least half of the samples of any condition were considered expressed and genes with RPKM <1 were considered to have minimal to no expression. Bioconductor package DESeq2 was utilized for genes expressed in treatment conditions (i.e., differentially expressed genes) via negative binomial distribution as described in Gentleman *et al.,* Genome biology 5, 1-16, 2004 and Anders & Huber, Nature Precedings, 1-1, 2010. Following this, Log_2-adjusted RPKM was used to perform high dimensional clustering (HDC). Differentially expressed genes (DEGs) were sorted with a statistical threshold (Benjamin-Hochberg false discovery rate

(FDR) adjust) *Padj* <0.01. Statistically significant DEGs were used to determine functional annotation enrichment of gene ontology terms belonging to Biological Processes (BP), Molecular Functions and Cellular Components. Enrichment analysis was performed using the Bioconductor package GoStats (Falcon & Gentleman, Bioinformatics 23, 257-258, 2007). (using conditional hyperGTest of overrepresentation) and Metascape (Zhou *et al.,* Nature communications 10, 1523, 2019). Gene tracks for key target genes were generated using the Gviz package (Hahne & Ivanek. Statistical genomics: methods and protocols, 335-351, 2016).

[0086] Gene set enrichment analysis (GSEA) was performed using the GSEA java desktop application against the current Molecular Signatures Database (v7.4 MsigDB). DEG rank lists were constructed according to the following function: Rank = Log_{10}(P value)*sign(Fold Change). Ranked lists were uploaded to the GSEA desktop application and used in performing GSEA Preranked analysis with default test parameters (which included "collapse" to collapse dataset to gene symbols before analysis and excluded gene set sizes of greater than 500 and less than 15) where the ranked list was compared to a priori sets of genes in the curated collection of the Molecular Signatures Database (v7.4 MsigDB). The chip platform used for analysis was "Human_ENSEMBL_Gene_ID_MsigDB.v7.5.chip". Probed databases included current releases of curated Hallmarks (h.all.v7.5.symbols.gmt), Reactome (c2.cp.reactome.v7.5.symbols.gmt), Wikipathways (c2.cp.wikipathways.v7.5.symbols.gmt), and GO (c5.all.v7.5.symbols.gmt). Enriched GSEA terms are represented using Log_{10} transformation of FDR-adjusted P value (i.e., Q value) and normalized enrichment score (NES). Gene sets with an FDR of less than 10% (FDR < 0.1) were considered significant.

[0087] ***Gene expression analysis and mt-DNA copy number:*** To measure the mt-DNA encoded transcripts, hMSCs were treated with or without MoS_2 (1:6) for 1, 3, 5 and 7 days, respectively, followed by RNA extraction using RNA extraction Kit (Zymo research). The RNA was converted into cDNA using a first strand cDNA synthesis kit (Qunatbio) following the manufacturer recommended protocol. cDNA generated was then stored at -20 °C until further use.

[0088] Quantitative real-time polymerase chain reaction (qRT-PCR) experiments were performed using TaqMan assays for target genes (*mt-ND2* assay ID: Hs02596874_g1; *ACTB* assay ID: Hs03023943_g1; *TFAM* assay ID: Hs00273372_s1; *GAPDH* assay ID: Hs02758991_g1) and TaqMan Fast Advanced Master Mix (Thermo Fisher), with an initial cDNA mass of 1 ng per reaction. Changes in the expression levels of target genes as a result

of MoS_2 exposure were determined using Comparative CT ($^{\Delta\Delta}$CT) analysis, with β-actin (*ACTB*) acting as an endogenous control.

[0089] The relative mt-DNA copy number was determined by using DNA extracted from the control and MoS_2 treated cells via a DNA extraction Kit (Zymo research). By comparing the expression levels of a mitochondrial encoded gene (*mt-ND2*) and nuclear DNA encoded gene (*GAPDH*), the relative change in mt-DNA expression was determined by comparing MoS_2 treated cells to untreated (control) cells. qRT-PCR assays were performed in a manner similar to those described above, with total cellular DNA being utilized in place of mRNA derived cDNA. All qRT-PCR experiments were performed using a QuantStudio™ 3 System (Applied Biosystems). For mouse cell lines, RT-PCR experiments were performed using SYBR chemistry for the following targets:

PGC-1α F:GAATCAAGCCACTACAGACACCG (SEQ ID NO:1);

PGC-1α R:CATCCCTCTTGAGCCTTTCGTG (SEQ ID NO:2);

TFAM F:GAGGCAAAGGATGATTCGGCTC (SEQ ID NO:3);

TFAM R: CGAATCCTATCATCTTTAGCAAGC (SEQ ID NO:4);

GAPDH F: CATCACTGCCACCCAGAAGACTG (SEQ ID NO:5);

GAPDH R: ATGCCAGTGAGCTTCCCGTTCAG (SEQ ID NO:6);

mt-ND2 F: AGGGATCCCACTGCACATAG (SEQ ID NO:7);

mt-ND2 R: TGAGGGATGGGTTGTAAGGA (SEQ ID NO:8).

RT-PCR was performed using 5 ng of cDNA/genomic DNA template, with the default SYBR cycling condition of the QuantStudio.

[0090] ***Seahorse assay:*** The OCR was measured using the Seahorse XF24 Extracellular Flux Analyzer as described in Gohil *et al.*, Nature biotechnology 28, 249-255, 2010, with minor modifications. Briefly, the cells were then seeded in XF24-well cell culture microplates (Agilent Technologies) at 10,000 cells/well in 200-μL growth media and incubated at 37 °C in a 5% CO_2 incubator for ~20h. Following this, cells were treated with high atomic vacancy MoS_2 for varying periods depending on the cell type (48h for C2C12 cells and 18h for BMDM cells). Before measurements, 575 μL of the pre-warmed growth medium was added to each well, and cells were further incubated at 37 °C for 30 min in a non-CO_2 incubator. OCR measurements were carried out in intact cells using Seahorse XF24 Extracellular Flux Analyzer (Agilent Technologies). Mix, wait, and measure durations were set to 2, 2, and 2 min, respectively. For the mitochondrial stress test, oligomycin, carbonyl cyanide 3-

cholorophenylhydrazone (CCCP), and antimycin A were sequentially injected to achieve final concentrations of 2, 20, and 2 μM, respectively. Immediately after the assay, cells were washed thrice with 500 μL PBS, and protein was extracted using 25 μL RIPA lysis buffer. Protein concentration in each well was measured by the bicinchronic acid (BCA) assay (Pierce) and was used to normalize OCR values. For BMBD cells, post assay cell normalization was performed by evaluating quantifying cellular DNA content using the DRAQ5™.

[0091] ***Reactive oxygen species (ROS):*** Untreated hMSCs (negative control) and MoS_2 (1:6) treated cells were seeded in a 6-well plate at 40% confluency. After 24h of growth, media was replaced by PBS and samples incubated with 1-2 μM DCFDA (for cellular ROS) for 10-15 min in the dark. The cells were then harvested, and fluorescence was measured using flow cytometry (BD Accuri C6). Cells exposed to 1% DMSO for 10 minutes or 100 μm H_2O_2 for 15 minutes at 37°C were used as a positive control. Similarly, to determine mitochondria specific ROS production, mitoSOX (Thermo Fisher) was used according to the manufacturer's protocol. In the case of mitochondrial ROS generation, cells exposed to 100 μm H_2O_2 for 15 minutes at 37°C, were used as a positive control. Samples were analyzed using flow cytometry (BD Accuri C6) with appropriate gating and fluorescent channels.

[0092] ***shRNA lentiviral infection and knockdown generation:*** The gene-specific shRNA plasmids (PGC-1α: TRCN0000234017, TFAM: TRCN0000311846, Empty pLKO vector: SHC001V) were purchased from the Mission shRNA collection (Sigma). Lentiviral particle production and infection were performed as described in Gohil *et al.*, Journal of Biological Chemistry 285, 13742-13747 (2010). For constructing stable knockdown cell lines, 100,000 C2C12 cells were seeded in a six-well dish, and 100 μl of viral supernatant was added to cells to a final volume of 2 ml of medium containing 8 μg/ml polybrene. The plates were spun at 805g for 30 min at 30°C, returned to a 37°C incubator, and selected for infection after 24h with 2 μg/ml puromycin-containing medium for 72h. Knockdown efficiency was determined using RT-PCR using C2C12 cells transfected with empty pLKO vectors as controls.

[0093] ***Western blot analysis:*** Cells were harvested, washed with phosphate-buffered saline (PBS), and lysed on ice in radioimmunoprecipitation assay (RIPA) extraction buffer (Boston BioProducts, BP-115), supplemented with a 1× complete protease inhibitor cocktail (Roche), for 30 min and centrifuged at 14,000 × g for 15 min at 4 °C. Clear supernatants were collected, and protein concentration was determined using the BCA assay (Pierce). Proteins were separated in 12% NuPAGE Bis-Tris gel (Life Technologies) followed by transfer (Invitrogen,

iBlot 2) to a polyvinylidene fluoride PVDF membrane as per manufacturer's instructions. Membranes were blocked with 5% milk in TBST (1X TBS with 0.1% Tween20) for 60 minutes prior to antibody staining. Primary antibody incubation was performed overnight at 4 °C, while secondary antibody incubation was performed at room temperature for 1h. Membranes were washed three times for 5 minutes with TBST after both the primary and secondary antibody incubation, following which they were developed (SuperSignal™ West Pico PLUS Chemiluminescent Substrate, Thermo Fisher) and imaged using LI-COR® 3600 C-Digit Blot Scanner. Restoration and re-blocking with 5% milk in TBST of the membranes were then performed for further protein analysis. Quantification of bands was performed using ImageJ.

[0094] ***Mitochondrial membrane potential:*** Mitochondrial membrane potential in cells was evaluated using the JC-1 assay (Cayman). JC-1 dye exhibits different fluorescence in response to membrane potential (under high membrane potential JC-1 for aggregates with red fluorescence, while at low membrane potential the dye remains in monomeric form giving a green fluorescence signal). The ratio of these signals indicates a change in mitochondrial membrane potential in response to treatment conditions. Cells treated with 100 µm CCCP for 5 minutes at 37 °C were used as positive control. Cell numbers across different treatments were normalized using Hoechst nuclear staining. Fluorescence was measured on a Cytation 5 (Agilent) using appropriate filters.

[0095] ***Inductively coupled plasma-mass spectrometry (ICP-MS)***: Cellular levels of Mo were measured by ICP-MS using a NexION 300D, PerkinElmer, Inc. Briefly, 2 x10^5 cells from each treatment group (low atomic vacancy MoS_2, high atomic vacancy MoS_2, no vacancy MoS_2 and untreated hMSCs) were harvested after 18h of exposure to treatment conditions. Cells were washed twice with 1 mL of PBS, followed by two more washes with 0.9% NaCl prepared in ultrapure water. Following this the samples were digested with 40% (w/v) nitric acid (TraceSELECT; Sigma-Aldrich) at 90 °C for 18h, after which samples were subjected to a 6h digestion with 0.75% H_2O_2 (Sigma-Supelco), and then serially diluted in ultrapure water. A calibration curve was generated by serially diluting ammonium molybdate in 1.5% nitric acid.

[0096] ***Statistical analysis:*** Determination of statistical significance when directly comparing untreated cells and MoS_2 treated cells was determined using the student t-test. Similarly, the determination of statistical significance between multiple groups was achieved via ANOVA

with the post hoc Tukey method. Significant P values were considered <0.05 unless otherwise noted. All analysis was completed in GraphPad Prism 9.0.

* * *

[0097] All of the methods disclosed and claimed herein can be made and executed without undue experimentation in light of the present disclosure. While the compositions and methods of this invention have been described in terms of preferred embodiments or aspects, it will be apparent to those of skill in the art that variations may be applied to the methods and in the steps or in the sequence of steps of the method described herein without departing from the concept, spirit and scope of the invention. More specifically, it will be apparent that certain agents which are both chemically and physiologically related may be substituted for the agents described herein while the same or similar results would be achieved. All such similar substitutes and modifications apparent to those skilled in the art are deemed to be within the spirit, scope and concept of the invention as defined by the appended claims.

CLAIMS

What is claimed is:

1. A method of increasing mitochondrial function in a subject in need thereof, the method comprising administering to the subject an effective amount of a nanomaterial structure comprising a transition metal and a chalcogen to increase mitochondrial function in the subject, wherein the nanomaterial structure comprises a high atomic vacancy concentration.

2. The method of claim 1, wherein the transition metal is selected from the group consisting of: titanium, vanadium, zirconium, niobium, molybdenum, hafnium, tantalum, and tungsten.

3. The method of claim 1, wherein the chalcogen is selected from the group consisting of sulfur, selenium, and tellurium.

4. The method of claim 1, wherein the nanomaterial structure comprises molybdenum disulfide.

5. The method of claim 1, wherein the high atomic vacancy concentration is greater than about 0.50×10^2 μM g^{-1}.

6. The method of claim 1, wherein the high atomic vacancy concentration is about 0.50×10^2 μM g^{-1} to about 10.0×10^2 μM g^{-1}.

7. The method of claim 1, wherein the nanomaterial structure is about 5 nm to about 400 nm in diameter.

8. The method of claim 1, wherein said increased mitochondrial function comprises increased mitochondrial biogenesis, increased mitochondrial encoded gene expression, increased nuclear encoded mitochondrial gene expression, increased mitochondrial protein expression, increased mitochondrial respiratory capacity, or increased adenosine triphosphate production.

9. The method of claim 1, wherein the nanomaterial structure further comprises a targeting molecule.

10. The method of claim 9, wherein the targeting molecule is cell-specific or tissue-specific.

11. The method of claim 1, wherein the nanomaterial structure further comprises a therapeutic agent or a detectable label.

12. The method of claim 11, wherein the therapeutic agent is a chemotherapeutic agent, an immunotherapeutic agent, a mitochondrial therapeutic agent, a neurotherapeutic agent, a metabolic therapeutic agent, an ophthalmic therapeutic agent, a cardio therapeutic agent, or a radiotherapeutic agent, or wherein the detectable label is a paramagnetic ion, a radioactive isotope, a fluorochrome, an NMR-detectable agent, or an X-ray imaging agent.

13. The method of claim 12, wherein the mitochondrial therapeutic agent is selected from the group consisting of CoQ10 (ubiquinone), idebenone, riboflavin, dichloroacetate, thiamine, creatine, lipoic acid, glutathione, *N*-acetylcysteine, cysteamine, EPI-743 (*para*-benzoquinone analog), arginine, citrulline, cardiolipin, elamipretide, bezafibrate, resveratrol, AICAR (aminoimidazole carboxamide ribonucleoside), epicatechin, RTA 408 (synthetic isoprenoid), decanoic acid, a therapeutic peptide, and a therapeutic polynucleotide molecule.

14. The method of claim 1, wherein the subject is afflicted with or at risk of developing a disease or condition associated with decreased mitochondrial function.

15. The method of claim 14, wherein the disease or condition associated with decreased mitochondrial function is selected from the group consisting of: Barth syndrome, mitochondrial encephalopathy, lactic acidosis, stroke-like episodes (MELAS), Myoclonus epilepsy with ragged-red fibers (MERRF), neuropathy, ataxia, and retinitis pigmentosa (NARP), Leber's hereditary optic neuropathy (LHON), Kearns–Sayre syndrome (KSS), Pearson syndrome (PS), progressive external ophthalmoplegia (PEO), autosomal-dominant/ recessive PEO (ad/ar PEO), mtDNA depletion syndrome (MDDS), mitochondrial neurogastrointestinal encephalopathy (MNGIE), mitochondrial recessive ataxia syndrome (MIRAS), Alpers syndrome (AS), Leigh syndrome (LS), optic nerve atrophy, subacute necrotizing encephalopathy, early-onset hepatocerebral disorder, juvenile catastrophic epilepsy, adult-onset ataxia-neuropathy syndrome, cardiomyopathy, cerebral white matter disease, ovarian dysfunction, hearing loss, cancer, diabetes mellitus, osteoporosis, dyskeratosis congenita (DC), bone marrow failure, idiopathic pulmonary fibrosis, cryptogenic liver cirrhosis, telomere biology disorders, and neurodegenerative disease.

16. The method of claim 1, wherein said administering comprises injection, microneedle administration, oral administration, buccal administration, vaginal administration, inhalation, intraosseous administration, trans nasal application, topical administration, transdermal application, or rectal administration.

17. The method of claim 1, further comprising administering a second therapy to said subject.

18. The method of claim 17, wherein the second therapy is a therapeutic agent or surgery.

19. The method of claim 1, the method comprising administering a pharmaceutical composition comprising the effective amount of the nanomaterial structure to the subject.

20. A pharmaceutical composition comprising a) a nanomaterial structure comprising sulfur active sites or comprising a transition metal and a chalcogen, wherein the nanomaterial structure comprises a high atomic vacancy concentration; and b) a second mitochondrial therapeutic agent.

21. The pharmaceutical composition of claim 20, wherein the transition metal is selected from the group consisting of: titanium, vanadium, zirconium, niobium, molybdenum, hafnium, tantalum, and tungsten.

22. The pharmaceutical composition of claim 20, wherein the chalcogen is selected from the group consisting of sulfur, selenium, and tellurium.

23. The pharmaceutical composition of claim 20, wherein the transition metal is molybdenum, and wherein the chalcogen is sulfur.

24. The pharmaceutical composition of claim 20, wherein the second mitochondrial therapeutic agent is selected from the group consisting of CoQ10 (ubiquinone), idebenone, riboflavin, dichloroacetate, thiamine, creatine, lipoic acid, glutathione, *N*-acetylcysteine, cysteamine, EPI-743 (*para*-benzoquinone analog), arginine, citrulline, cardiolipin, elamipretide, bezafibrate, resveratrol, AICAR (aminoimidazole carboxamide ribonucleoside), epicatechin, RTA 408 (synthetic isoprenoid), decanoic acid, a therapeutic peptide, and a therapeutic polynucleotide molecule.

25. The pharmaceutical composition of claim 20, wherein the high atomic vacancy concentration is greater than about 0.50×10^2 μM g^{-1}.

26. The pharmaceutical composition of claim 20, wherein the high atomic vacancy concentration is about 0.50×10^2 μM g^{-1} to about 10.0×10^2 μM g^{-1}.

27. The pharmaceutical composition of claim 20, wherein the nanomaterial structure is about 5 nm to about 400 nm in diameter.

28. The pharmaceutical composition of claim 20, wherein the nanomaterial structure further comprises a targeting molecule.

29. The pharmaceutical composition of claim 28, wherein the targeting molecule is cell-specific or tissue-specific.

30. The pharmaceutical composition of claim 20, wherein the nanomaterial structure is modified with or conjugated to a peptide, a protein, a colloidal molecule, lipid molecule, phospholipid molecule, or a polymer to facilitate delivery or adsorption.

31. The pharmaceutical composition of claim 20, wherein said pharmaceutical composition is serum-free, endotoxin-free, or sterile.

32. A method of decreasing cellular oxidative stress in a subject in need thereof, the method comprising administering to the subject an effective amount of a nanomaterial structure comprising a sulfur moiety active site, wherein said sulfur moiety active site acts as an active site of reaction to reduce cellular oxidative stress.

33. The method of claim 32, wherein the nanomaterial structure comprises a transition metal selected from the group consisting of: titanium, vanadium, zirconium, niobium, molybdenum, hafnium, tantalum, and tungsten.

34. The method of claim 32, wherein the nanomaterial structure comprises molybdenum disulfide.

35. The method of claim 32, wherein the nanomaterial structure comprises a plurality of sulfur moiety active sites.

36. The method of claim 35, wherein the concentration of the plurality of sulfur moiety active sites is greater than about 0.50×10^2 μM g^{-1} of nanomaterial structure.

37. The method of claim 35, wherein the concentration of the plurality of sulfur moiety active sites is about 0.50×10^2 μM g^{-1} to about 10.0×10^2 μM g^{-1} of nanomaterial structure.

38. The method of claim 32, wherein the nanomaterial structure is about 5 nm to about 400 nm in diameter.

39. The method of claim 32, wherein the nanomaterial structure further comprises a targeting molecule.

40. The method of claim 39, wherein the targeting molecule is cell-specific or tissue-specific.

41. The method of claim 32, wherein the nanomaterial structure further comprises a therapeutic agent or a detectable label.

42. The method of claim 41, wherein the therapeutic agent is a chemotherapeutic agent, an immunotherapeutic agent, a mitochondrial therapeutic agent, a neurotherapeutic agent, a metabolic therapeutic agent, an ophthalmic therapeutic agent, a cardio therapeutic agent, or a radiotherapeutic agent, or wherein the detectable label is a paramagnetic ion, a radioactive isotope, a fluorochrome, an NMR-detectable agent, or an X-ray imaging agent.

43. The method of claim 42, wherein the mitochondrial therapeutic agent is selected from the group consisting of CoQ10 (ubiquinone), idebenone, riboflavin, dichloroacetate, thiamine, creatine, lipoic acid, glutathione, *N*-acetylcysteine, cysteamine, EPI-743 (*para*-benzoquinone analog), arginine, citrulline, cardiolipin, elamipretide, bezafibrate, resveratrol, AICAR (aminoimidazole carboxamide ribonucleoside), epicatechin, RTA 408 (synthetic isoprenoid), decanoic acid, a therapeutic peptide, and a therapeutic polynucleotide molecule.

44. The method of claim 32, wherein the subject is afflicted with or at risk of developing a disease or condition associated with increased cellular oxidative stress.

45. The method of claim 44, wherein the disease or condition associated with increased cellular oxidative stress is selected from the group consisting of: Barth syndrome, mitochondrial encephalopathy, lactic acidosis, stroke-like episodes (MELAS), Myoclonus epilepsy with ragged-red fibers (MERRF), neuropathy, ataxia, and retinitis pigmentosa (NARP), Leber's hereditary optic neuropathy (LHON), Kearns–Sayre syndrome (KSS), Pearson syndrome (PS), progressive external ophthalmoplegia (PEO), autosomal-dominant/ recessive PEO (ad/ar PEO), mtDNA depletion syndrome (MDDS), mitochondrial neurogastrointestinal encephalopathy (MNGIE), mitochondrial recessive ataxia syndrome (MIRAS), Alpers syndrome (AS), Leigh

syndrome (LS), optic nerve atrophy, subacute necrotizing encephalopathy, early-onset hepatocerebral disorder, juvenile catastrophic epilepsy, adult-onset ataxia-neuropathy syndrome, cardiomyopathy, cerebral white matter disease, ovarian dysfunction, hearing loss, cancer, diabetes mellitus, osteoporosis, dyskeratosis congenita (DC), bone marrow failure, idiopathic pulmonary fibrosis, cryptogenic liver cirrhosis, telomere biology disorders, and neurodegenerative disease.

46. The method of claim 32, wherein said administering comprises injection, microneedle administration, oral administration, buccal administration, vaginal administration, inhalation, intraosseous administration, trans nasal application, topical administration, transdermal application, or rectal administration.

47. The method of claim 32, further comprising administering a second therapy to said subject.

48. The method of claim 47, wherein the second therapy is a therapeutic agent or surgery.

49. The method of claim 32, the method comprising administering a pharmaceutical composition comprising the effective amount of the nanomaterial structure to the subject.

50. A pharmaceutical composition comprising a) a nanomaterial structure comprising a sulfur moiety active site, wherein said sulfur moiety active site acts as an active site of reaction to reduce cellular oxidative stress; and b) a second mitochondrial therapeutic agent.

51. The pharmaceutical composition of claim 50, wherein the nanomaterial structure comprises molybdenum disulfide.

52. The pharmaceutical composition of claim 50, wherein the nanomaterial structure comprises a plurality of sulfur moiety active sites.

53. The pharmaceutical composition of claim 52, wherein the concentration of the plurality of sulfur moiety active sites is greater than about 0.50×10^2 μM g^{-1} of nanomaterial structure.

54. The composition of claim 52, wherein the concentration of the plurality of sulfur moiety active sites is about 0.50×10^2 μM g^{-1} to about 10.0×10^2 μM g^{-1} of nanomaterial structure.

55. The pharmaceutical composition of claim 50, wherein the nanomaterial structure is about 5 nm to about 400 nm in diameter.

56. The pharmaceutical composition of claim 50, wherein the nanomaterial structure further comprises a targeting molecule.

57. The pharmaceutical composition of claim 50, wherein the targeting molecule is cell-specific or tissue-specific.

58. The pharmaceutical composition of claim 50, wherein the nanomaterial structure is modified with or conjugated to a peptide, a protein, a colloidal molecule, lipid molecule, phospholipid molecule, or a polymer to facilitate delivery or adsorption.

59. The pharmaceutical composition of claim 50, wherein said pharmaceutical composition is serum-free, endotoxin-free, or sterile.

60. The pharmaceutical composition of claim 50, wherein the second mitochondrial therapeutic agent is selected from the group consisting of CoQ10 (ubiquinone), idebenone, riboflavin, dichloroacetate, thiamine, creatine, lipoic acid, glutathione, *N*-acetylcysteine, cysteamine, EPI-743 (*para*-benzoquinone analog), arginine, citrulline, cardiolipin, elamipretide, bezafibrate, resveratrol, AICAR (aminoimidazole carboxamide ribonucleoside), epicatechin, RTA 408 (synthetic isoprenoid), decanoic acid, a therapeutic peptide, and a therapeutic polynucleotide molecule.

FIG. 1

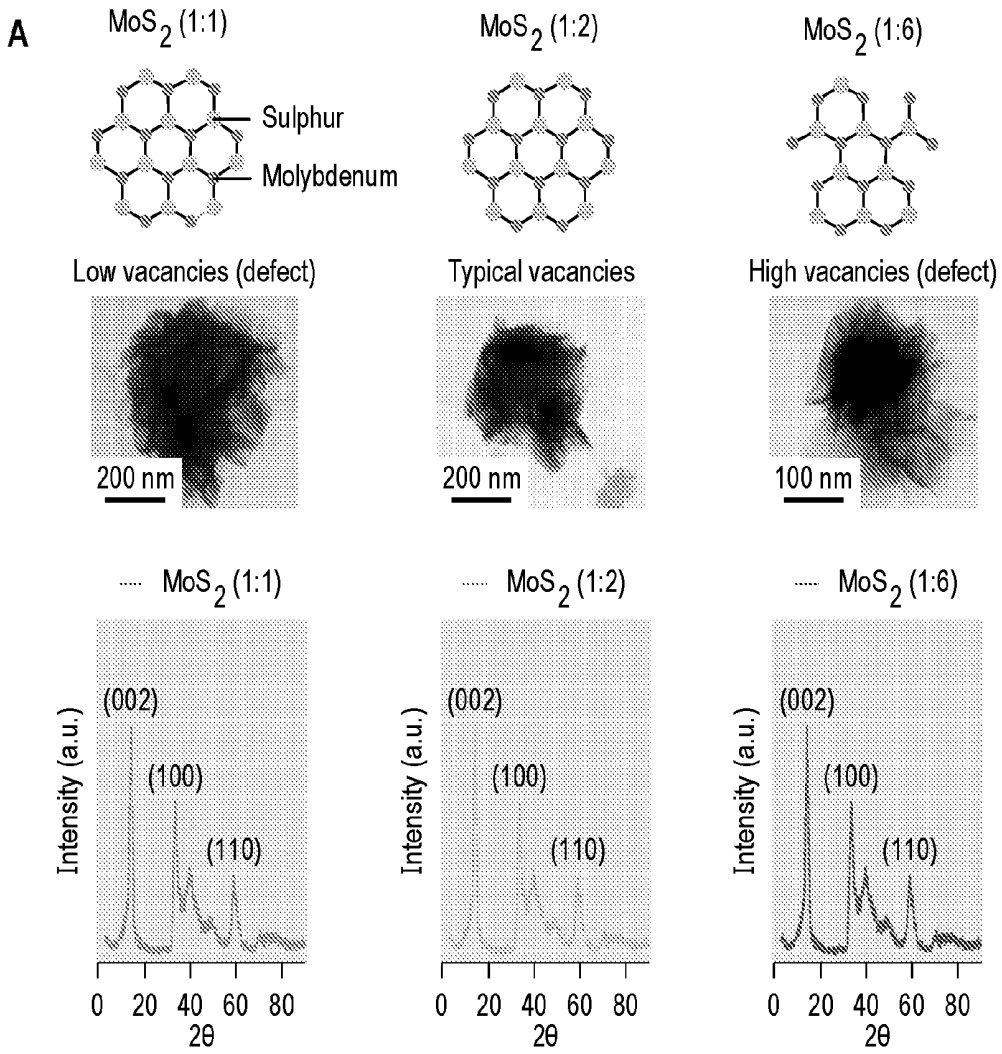
A
MoS2 (1:1)
MoS2 (1:2)
MoS2 (1:6)
Sulphur
Molybdenum
Low vacancies (defect)
Typical vacancies
High vacancies (defect)
200 nm
200 nm
100 nm
MoS2 (1:1)
MoS2 (1:2)
MoS2 (1:6)
(002)
(100)
(110)
Intensity (a.u.)
0 20 40 60 80
2θ

FIG. 1
(CONTINUED)

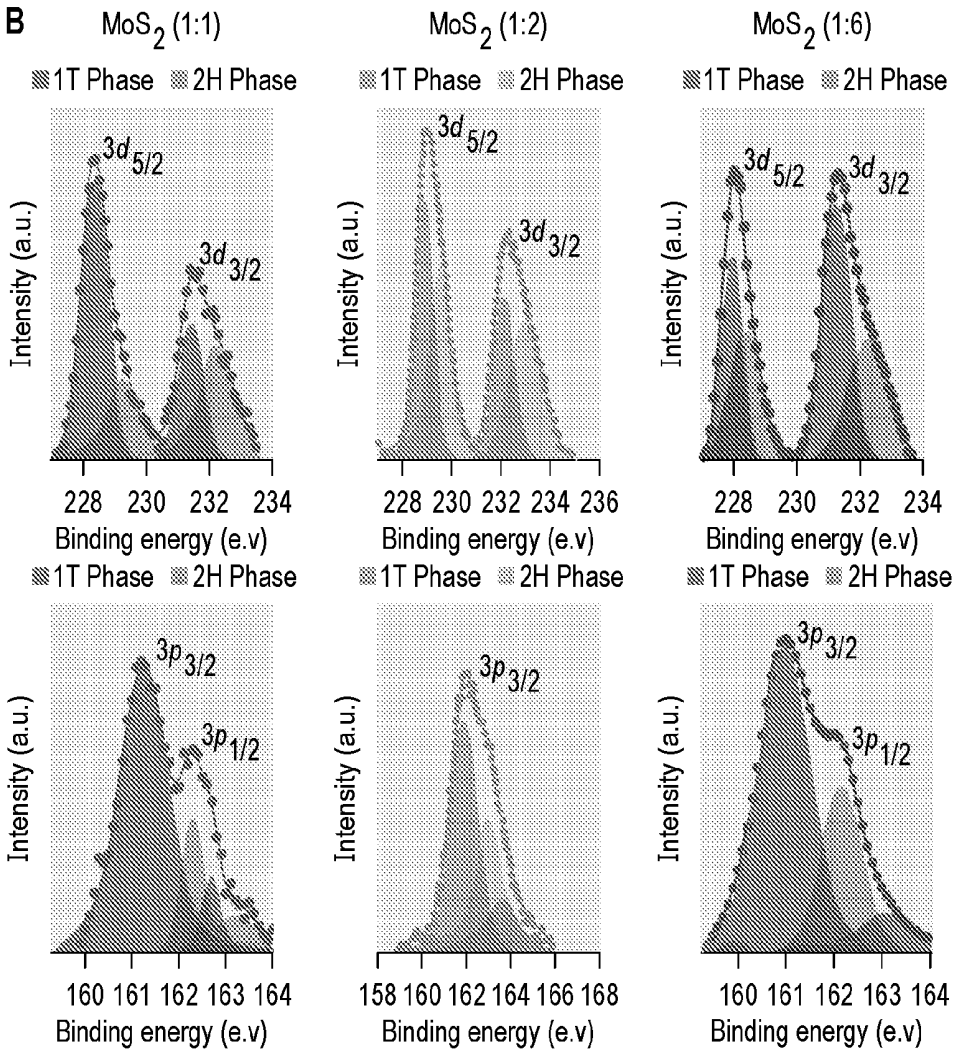

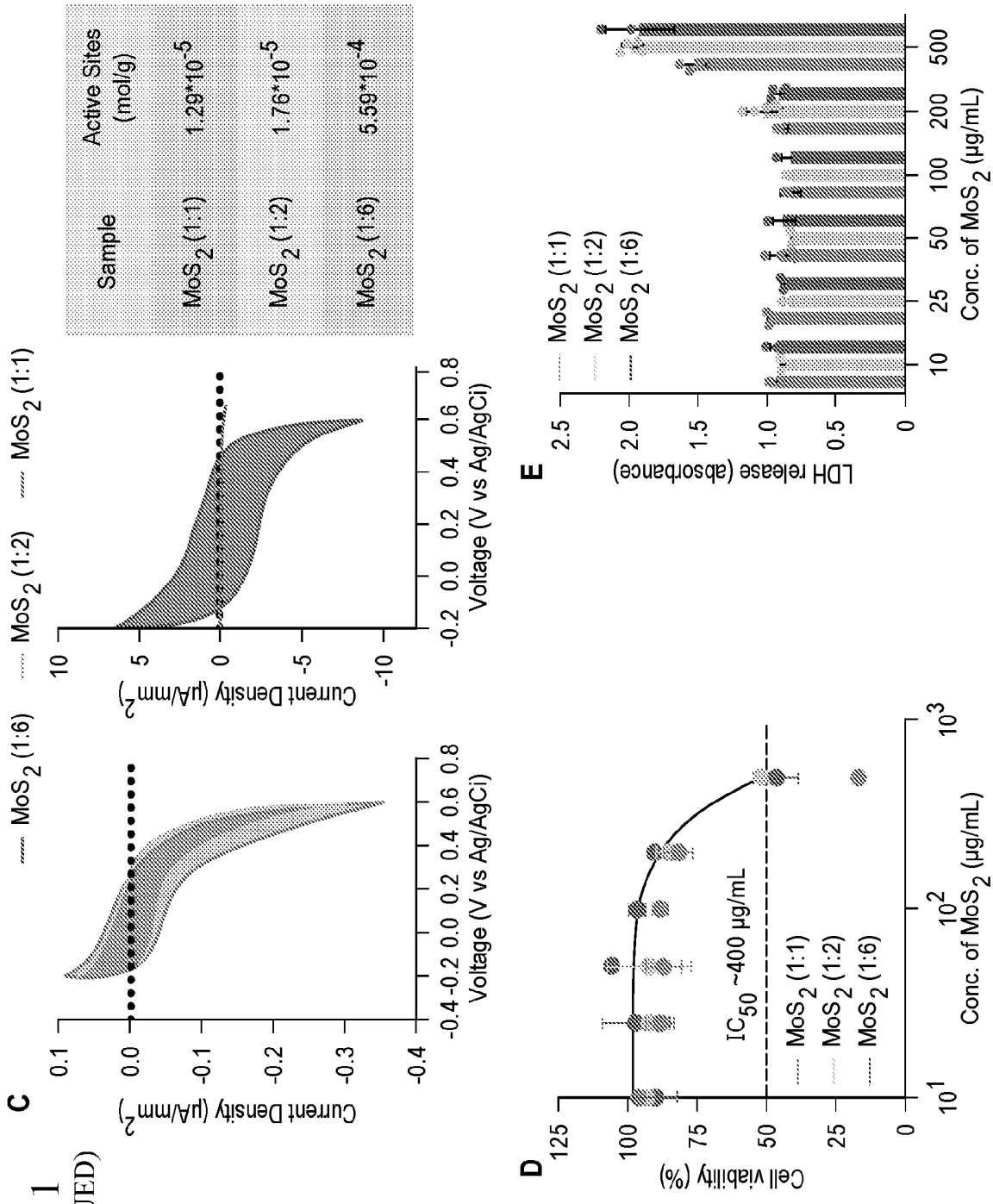

FIG. 1
(CONTINUED)

FIG. 1
(CONTINUED)

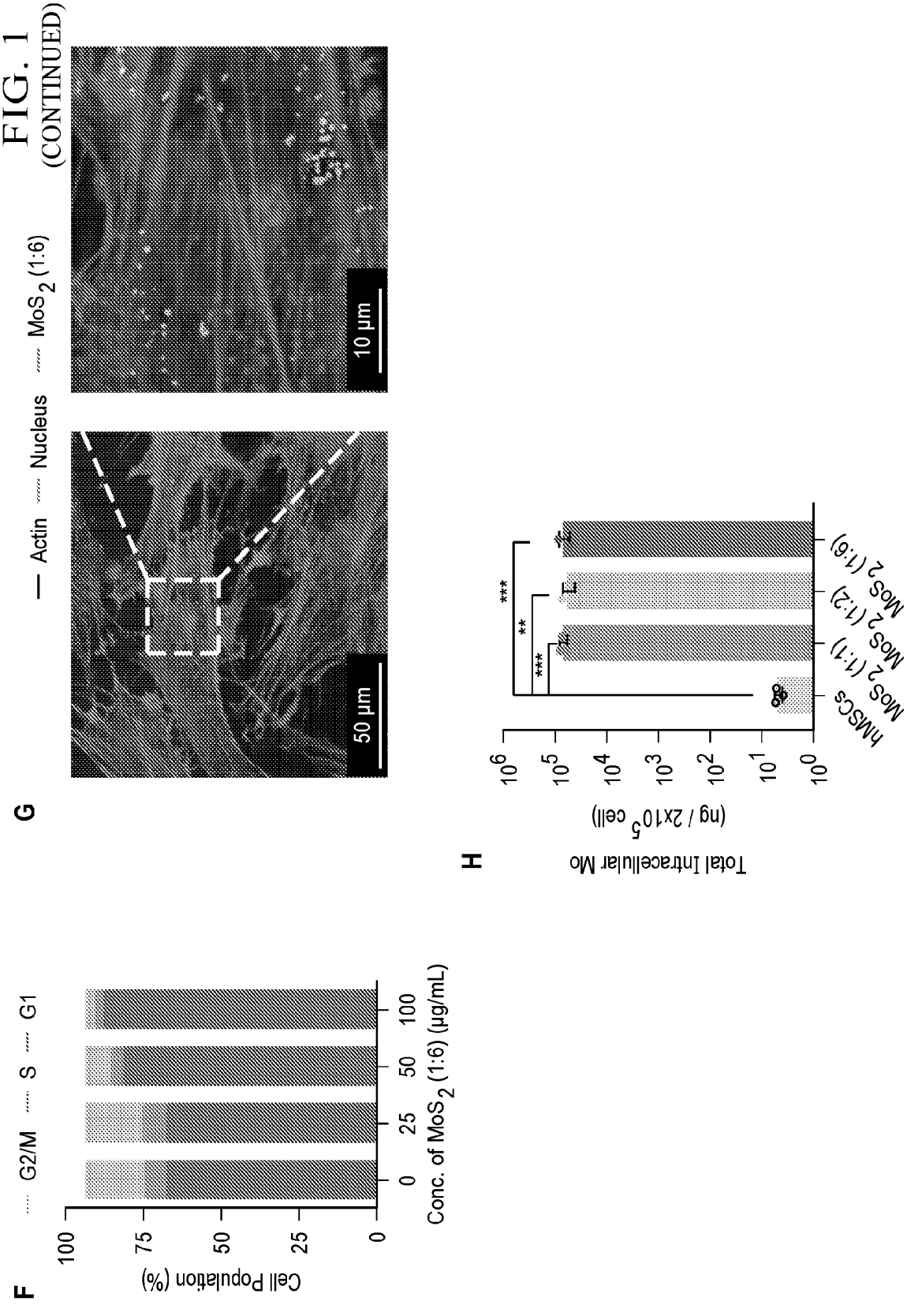

FIG. 2

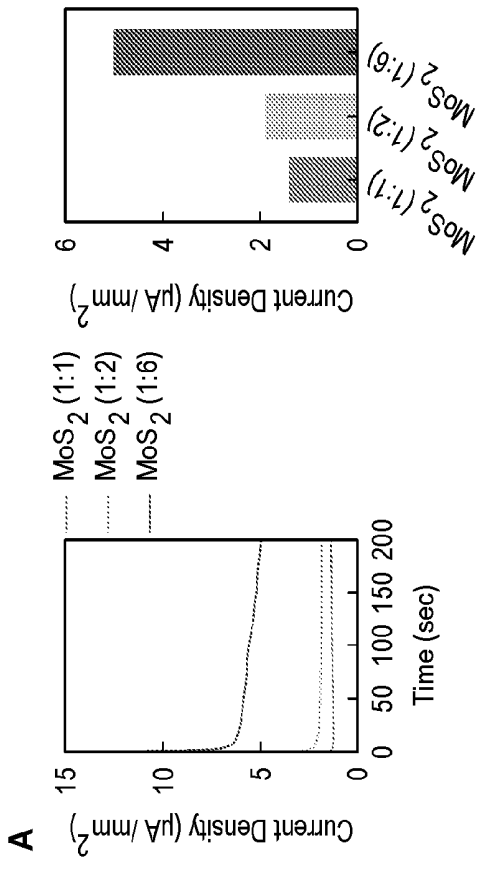
A
Current Density (μA /mm²)
15
10
5
0
0 50 100 150 200
Time (sec)
MoS2 (1:1)
MoS2 (1:2)
MoS2 (1:6)
Current Density (μA /mm²)
6
4
2
0
MoS2 (1:1)
MoS2 (1:2)
MoS2 (1:6)
B
Equilvalent Catalase Activity
(U/mL)
0.20
0.15
0.10
0.05
0.00
**
MoS2 (1:1)
MoS2 (1:2)
MoS2 (1:6)

FIG. 3

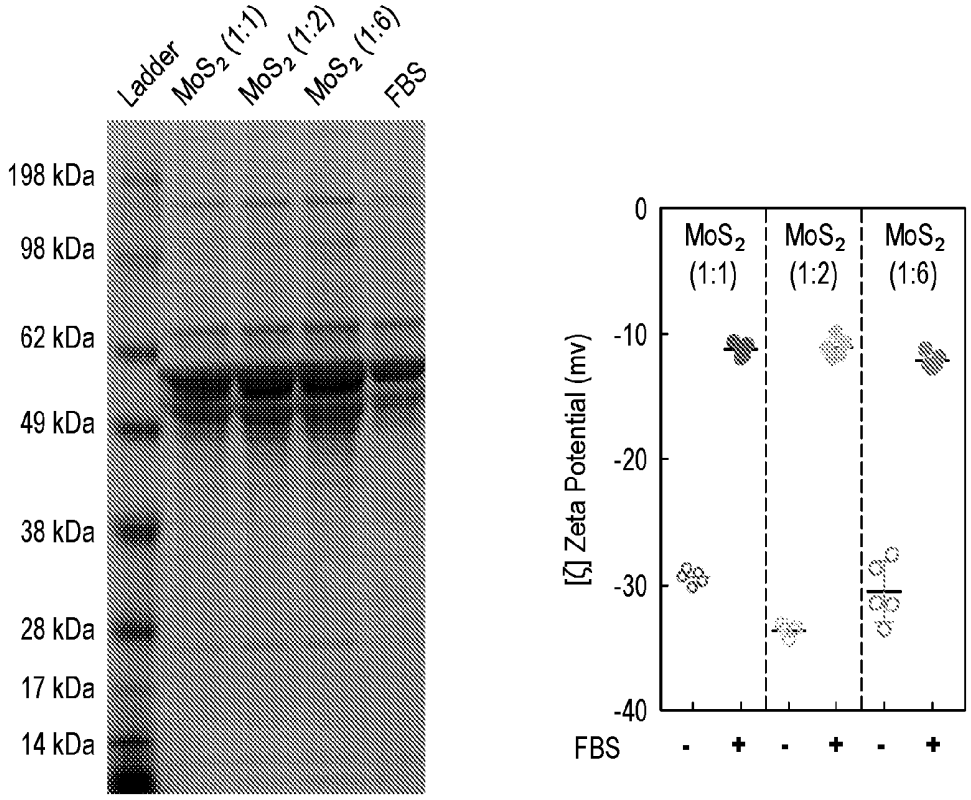
Ladder
MoS2 (1:1)
MoS2 (1:2)
MoS2 (1:6)
FBS
198 kDa
98 kDa
62 kDa
49 kDa
38 kDa
28 kDa
17 kDa
14 kDa
[ζ] Zeta Potential (mv)
0
-10
-20
-30
-40
MoS2 (1:1)
MoS2 (1:2)
MoS2 (1:6)
FBS
- + - + - +

FIG. 4

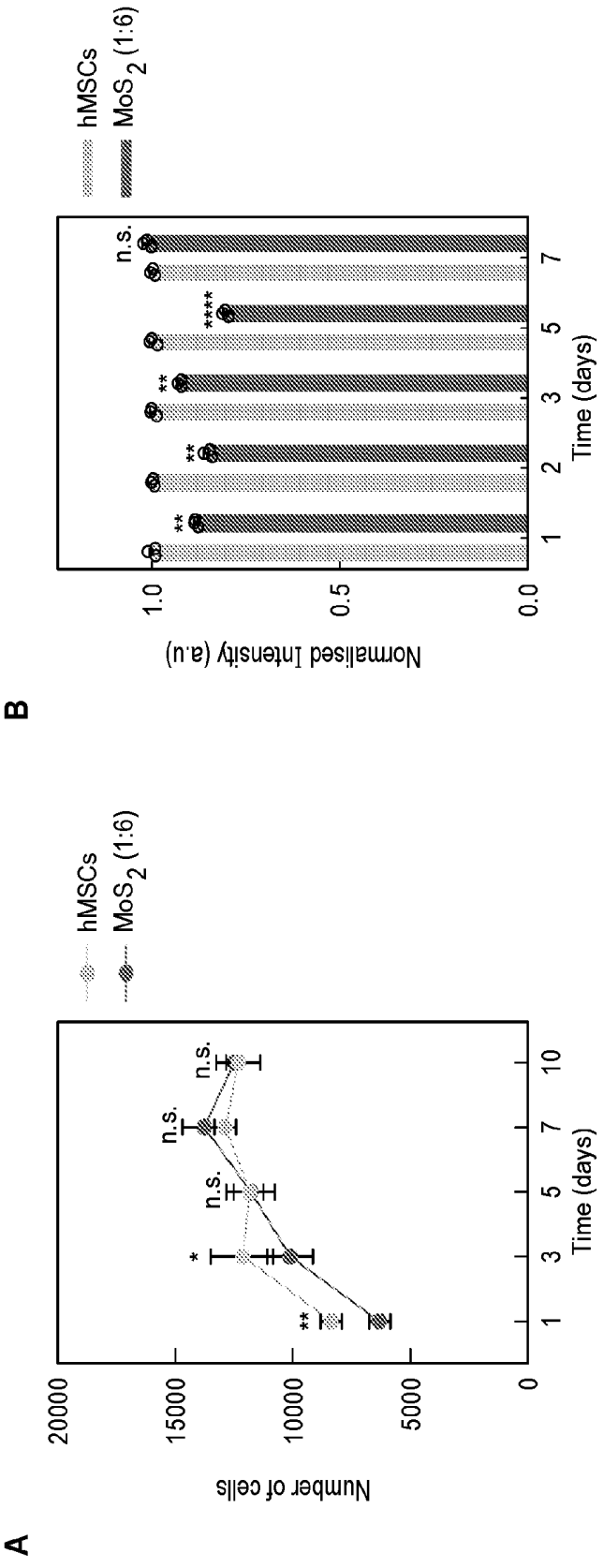
A
hMSCs
MoS2 (1:6)
Number of cells
20000
15000
10000
5000
0
1
3
5
7
10
Time (days)
**
*
n.s.
n.s.
n.s.
B
hMSCs
MoS2 (1:6)
Normalised Intensity (a.u)
1.0
0.5
0.0
1
2
3
5
7
Time (days)
**
**
**
****
n.s.

FIG. 5

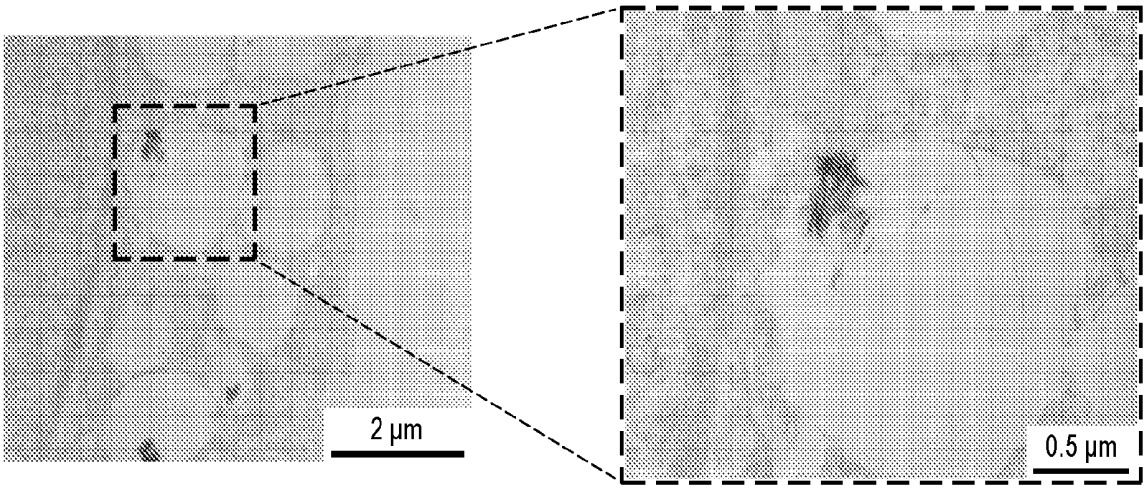

FIG. 6

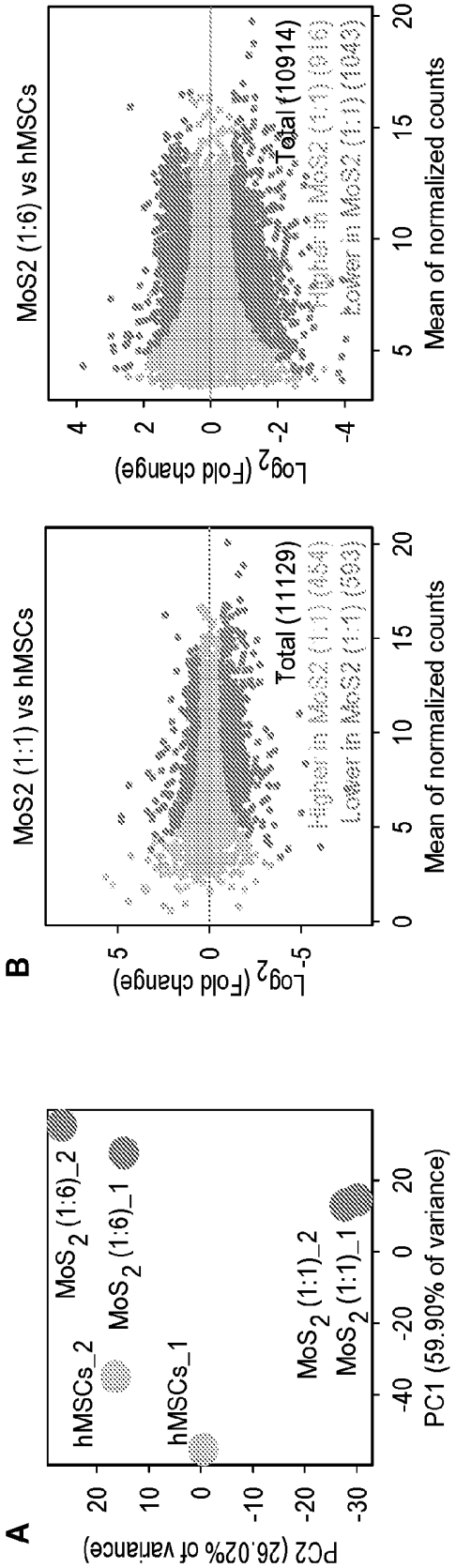
A
PC2 (26.02% of variance)
PC1 (59.90% of variance)
hMSCs_2
MoS2 (1:6)_2
MoS2 (1:6)_1
hMSCs_1
MoS2 (1:1)_2
MoS2 (1:1)_1
B
MoS2 (1:1) vs hMSCs
Log2 (Fold change)
Mean of normalized counts
Total (11129)
Higher in MoS2 (1:1) (664)
Lower in MoS2 (1:1) (593)
MoS2 (1:6) vs hMSCs
Total (10914)
Higher in MoS2 (1:6) (616)
Lower in MoS2 (1:6) (1043)

FIG. 6
(CONTINUED)

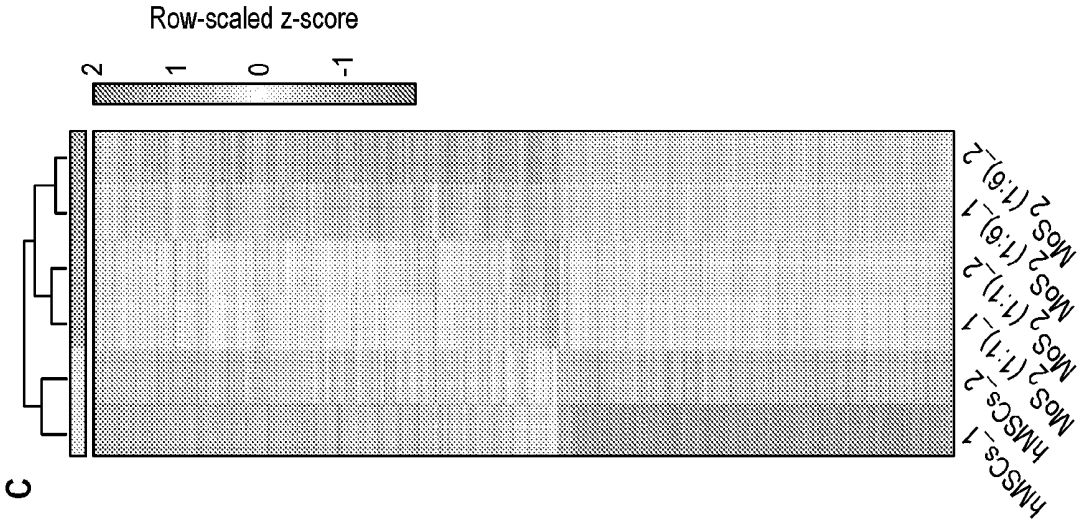

D

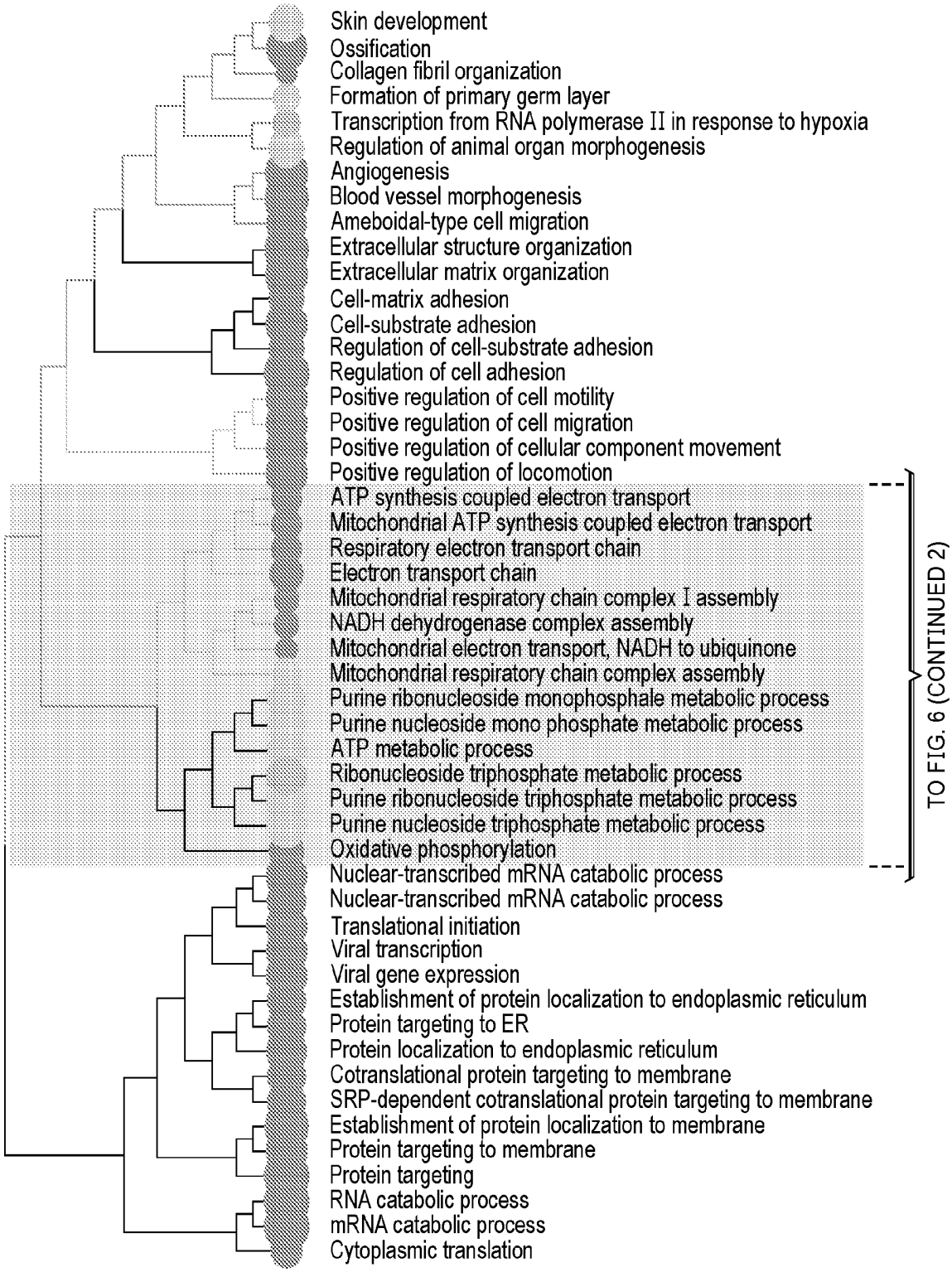

FIG. 6
(CONTINUED)

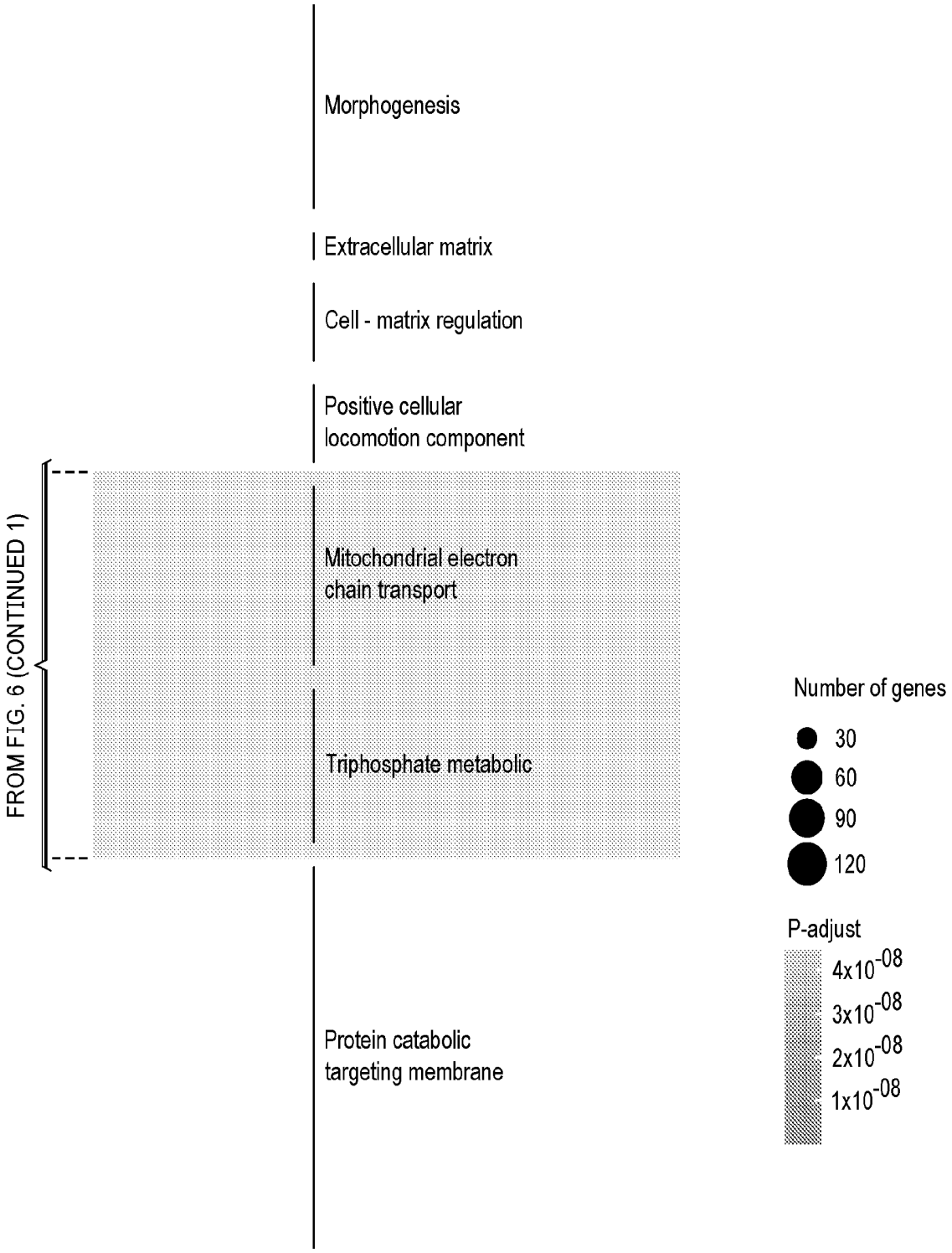

FIG. 6
(CONTINUED)

FIG. 7

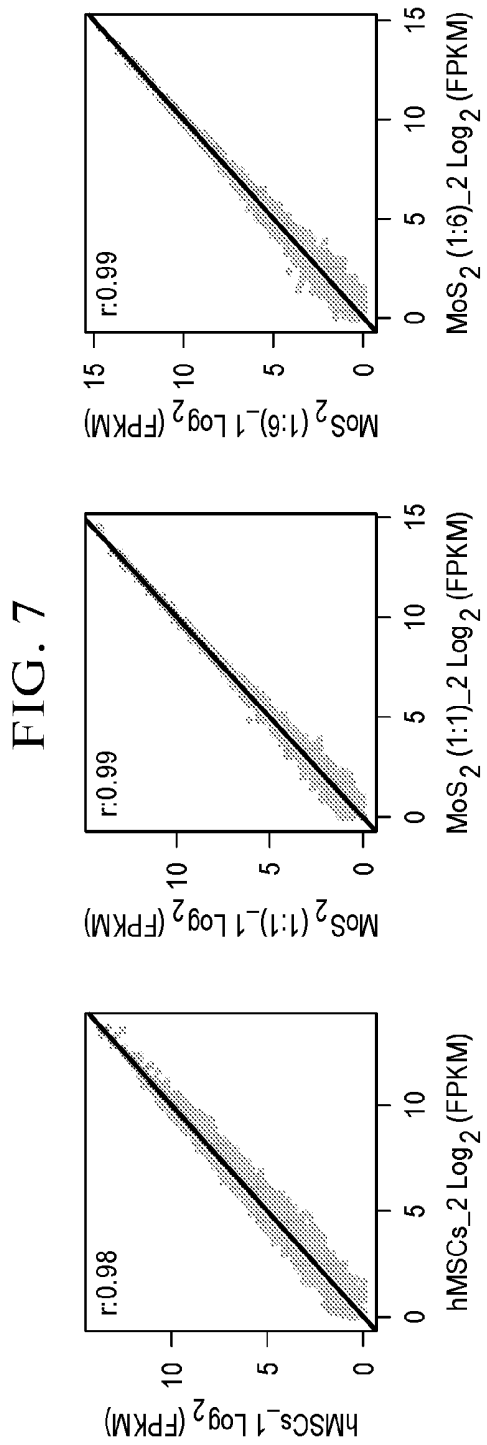
r:0.98
hMSCs_1 Log2 (FPKM)
hMSCs_2 Log2 (FPKM)
r:0.99
MoS2 (1:1)_1 Log2 (FPKM)
MoS2 (1:1)_2 Log2 (FPKM)
r:0.99
MoS2 (1:6)_1 Log2 (FPKM)
MoS2 (1:6)_2 Log2 (FPKM)
0
5
10
15

FIG. 8

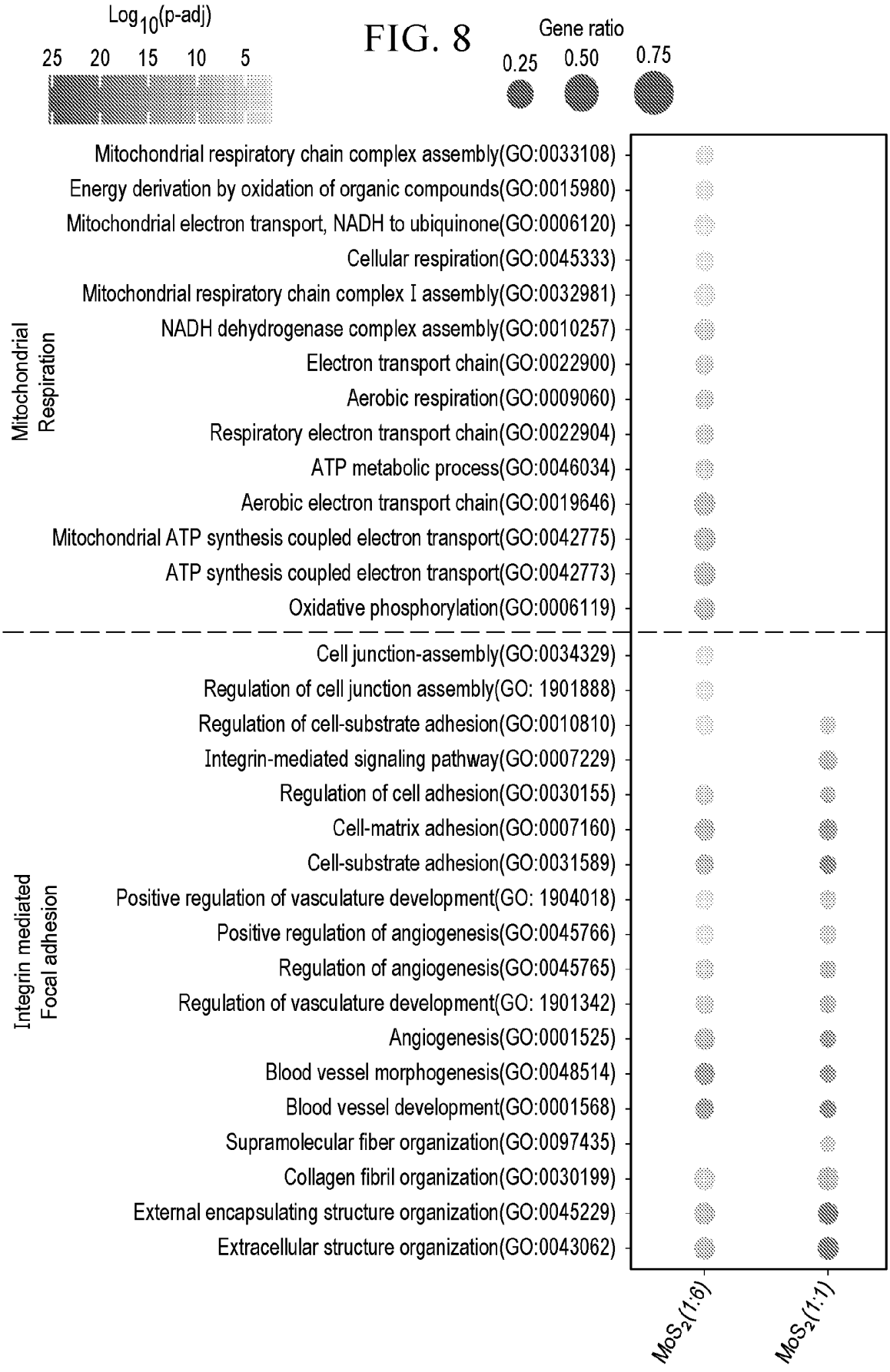
Log10(p-adj)
25 20 15 10 5
Gene ratio
0.25 0.50 0.75
Mitochondrial Respiration
Mitochondrial respiratory chain complex assembly(GO:0033108)
Energy derivation by oxidation of organic compounds(GO:0015980)
Mitochondrial electron transport, NADH to ubiquinone(GO:0006120)
Cellular respiration(GO:0045333)
Mitochondrial respiratory chain complex I assembly(GO:0032981)
NADH dehydrogenase complex assembly(GO:0010257)
Electron transport chain(GO:0022900)
Aerobic respiration(GO:0009060)
Respiratory electron transport chain(GO:0022904)
ATP metabolic process(GO:0046034)
Aerobic electron transport chain(GO:0019646)
Mitochondrial ATP synthesis coupled electron transport(GO:0042775)
ATP synthesis coupled electron transport(GO:0042773)
Oxidative phosphorylation(GO:0006119)
Integrin mediated Focal adhesion
Cell junction-assembly(GO:0034329)
Regulation of cell junction assembly(GO: 1901888)
Regulation of cell-substrate adhesion(GO:0010810)
Integrin-mediated signaling pathway(GO:0007229)
Regulation of cell adhesion(GO:0030155)
Cell-matrix adhesion(GO:0007160)
Cell-substrate adhesion(GO:0031589)
Positive regulation of vasculature development(GO: 1904018)
Positive regulation of angiogenesis(GO:0045766)
Regulation of angiogenesis(GO:0045765)
Regulation of vasculature development(GO: 1901342)
Angiogenesis(GO:0001525)
Blood vessel morphogenesis(GO:0048514)
Blood vessel development(GO:0001568)
Supramolecular fiber organization(GO:0097435)
Collagen fibril organization(GO:0030199)
External encapsulating structure organization(GO:0045229)
Extracellular structure organization(GO:0043062)
MoS2(1:6)
MoS2(1:1)

FIG. 9

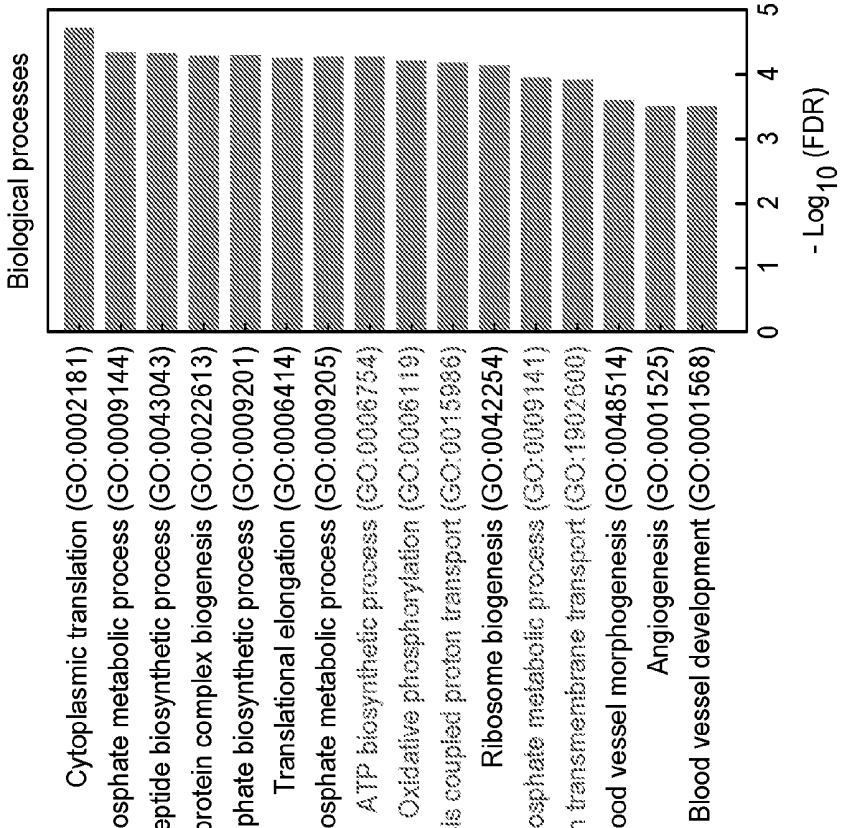
Biological processes
Cytoplasmic translation (GO:0002181)
Purine nucleoside triphosphate metabolic process (GO:0009144)
Peptide biosynthetic process (GO:0043043)
Ribonucleoprotein complex biogenesis (GO:0022613)
Ribonucleoside triphosphate biosynthetic process (GO:0009201)
Translational elongation (GO:0006414)
Purine ribonucleoside triphosphate metabolic process (GO:0009205)
ATP biosynthetic process (GO:0006754)
Oxidative phosphorylation (GO:0006119)
ATP synthesis coupled proton transport (GO:0015986)
Ribosome biogenesis (GO:0042254)
Nucleoside triphosphate metabolic process (GO:0009141)
Proton transmembrane transport (GO:1902600)
Blood vessel morphogenesis (GO:0048514)
Angiogenesis (GO:0001525)
Blood vessel development (GO:0001568)
0
1
2
3
4
5
- Log10 (FDR)

FIG. 9
(CONTINUED)

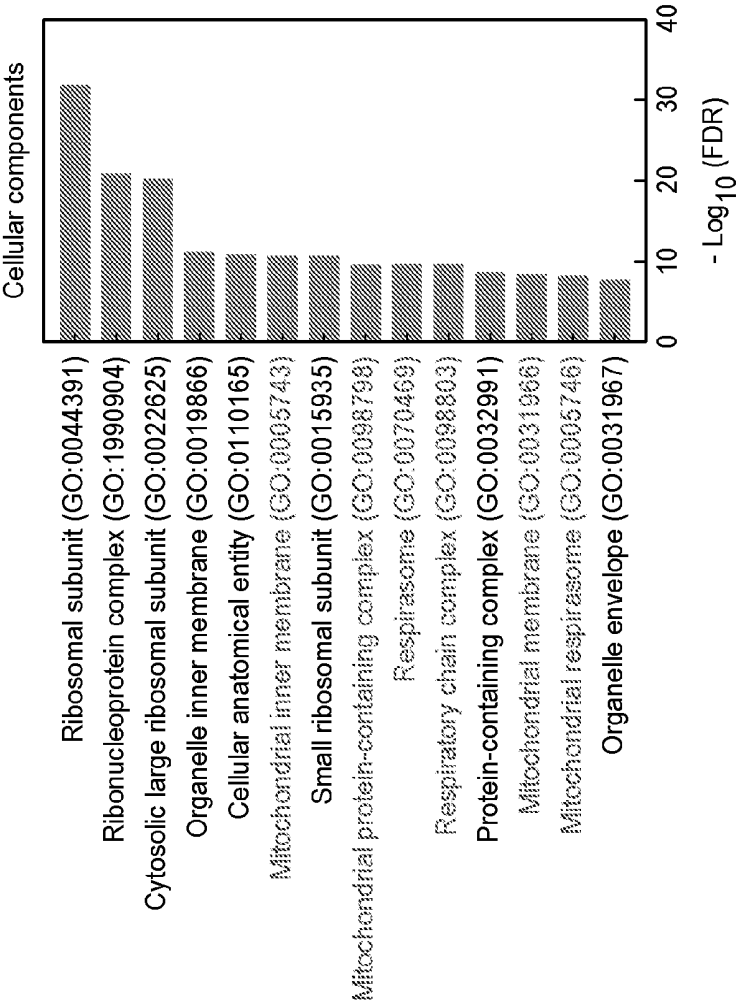

FIG. 10

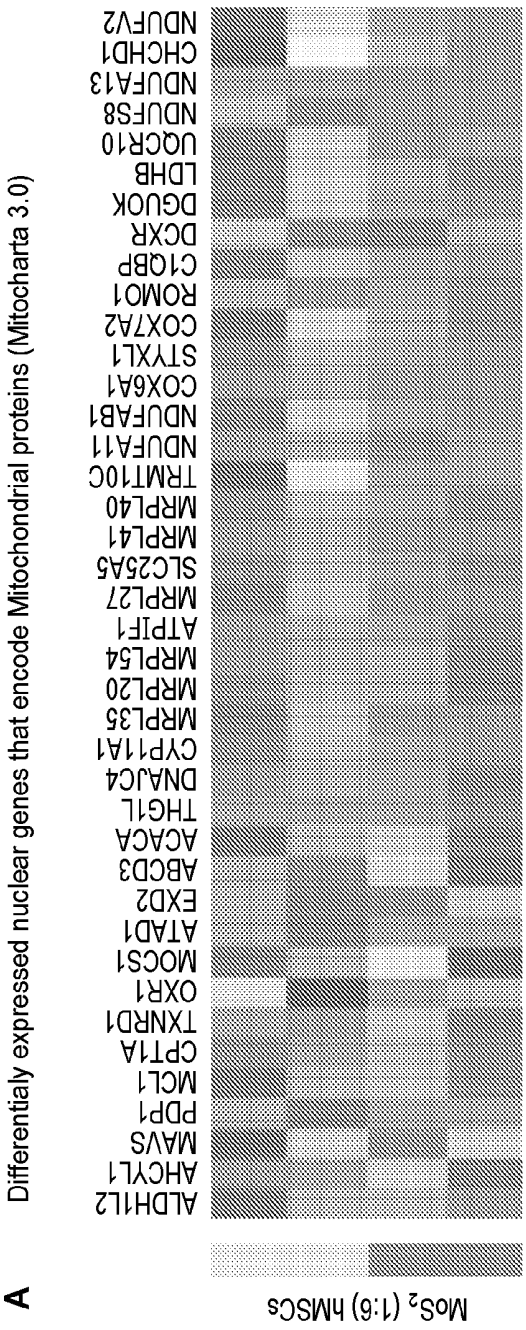
A
Differentialy expressed nuclear genes that encode Mitochondrial proteins (Mitocharta 3.0)
MoS2 (1:6) hMSCs
ALDH1L2
AHCYL1
MAVS
PDP1
MCL1
CPT1A
TXNRD1
OXR1
MOCS1
ATAD1
EXD2
ABCD3
ACACA
THG1L
DNAJC4
CYP11A1
MRPL35
MRPL20
MRPL54
ATPIF1
MRPL27
SLC25A5
MRPL41
MRPL40
TRMT10C
NDUFA11
NDUFAB1
COX6A1
STYXL1
COX7A2
ROMO1
C1QBP
DCXR
DGUOK
LDHB
UQCR10
NDUFS8
NDUFA13
CHCHD1
NDUFV2

FIG. 10
(CONTINUED)

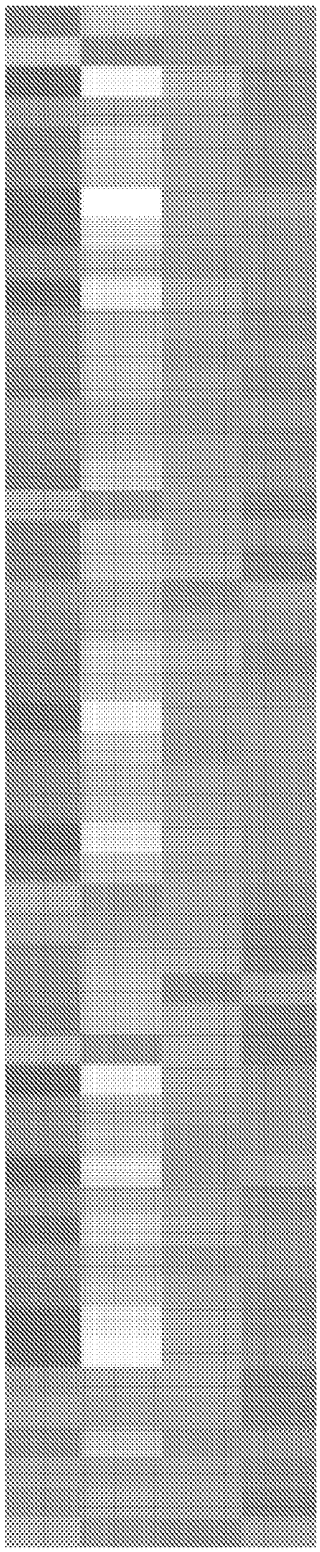

FIG. 10
(CONTINUED)

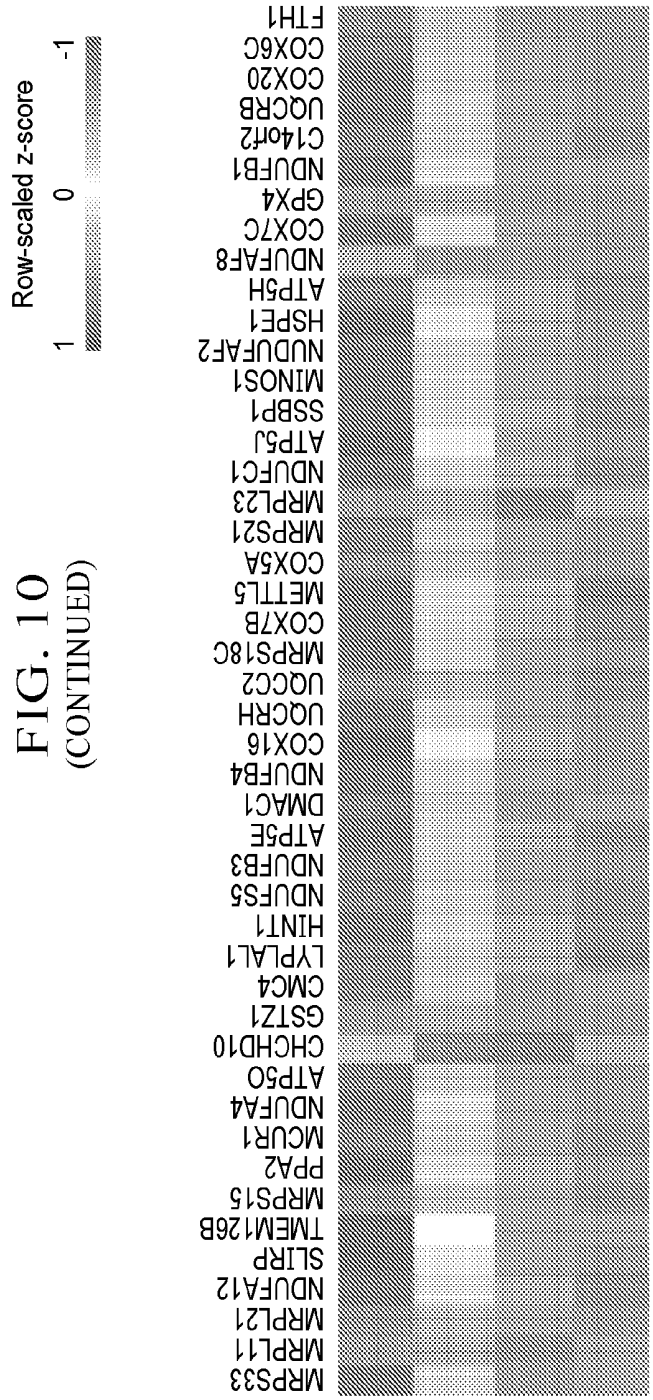

FIG. 10
(CONTINUED)

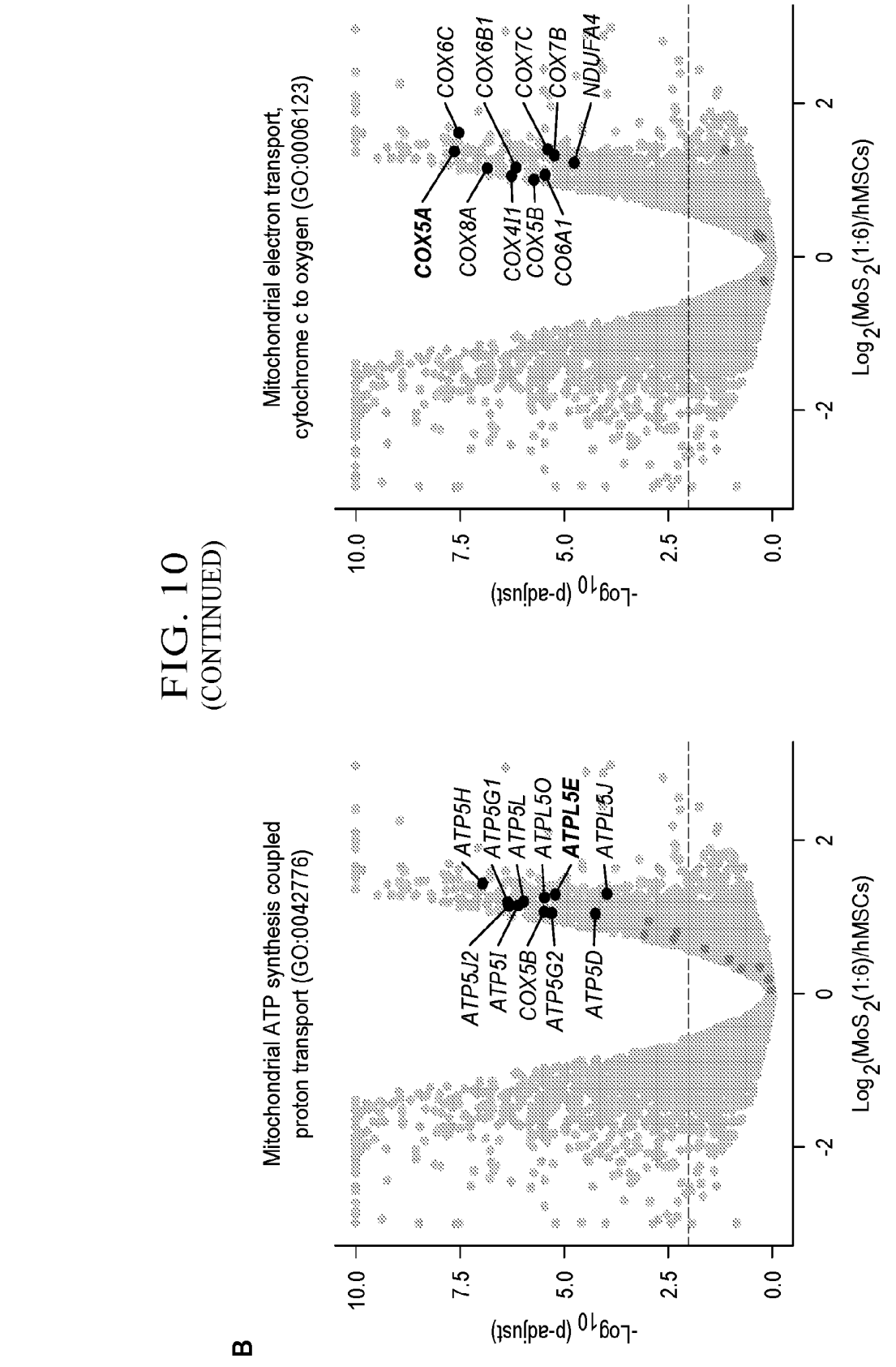

FIG. 10
(CONTINUED)

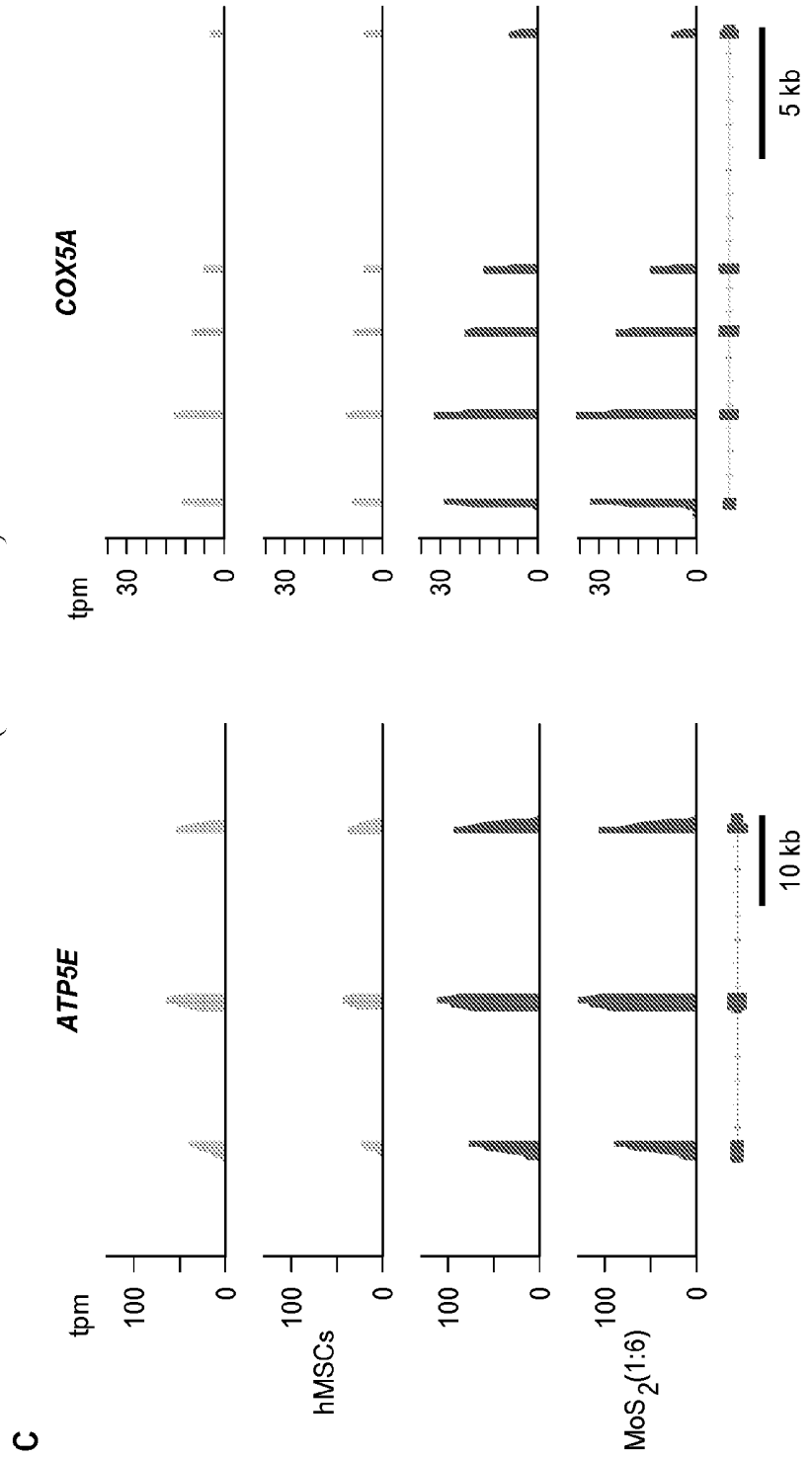

FIG. 10
(CONTINUED)

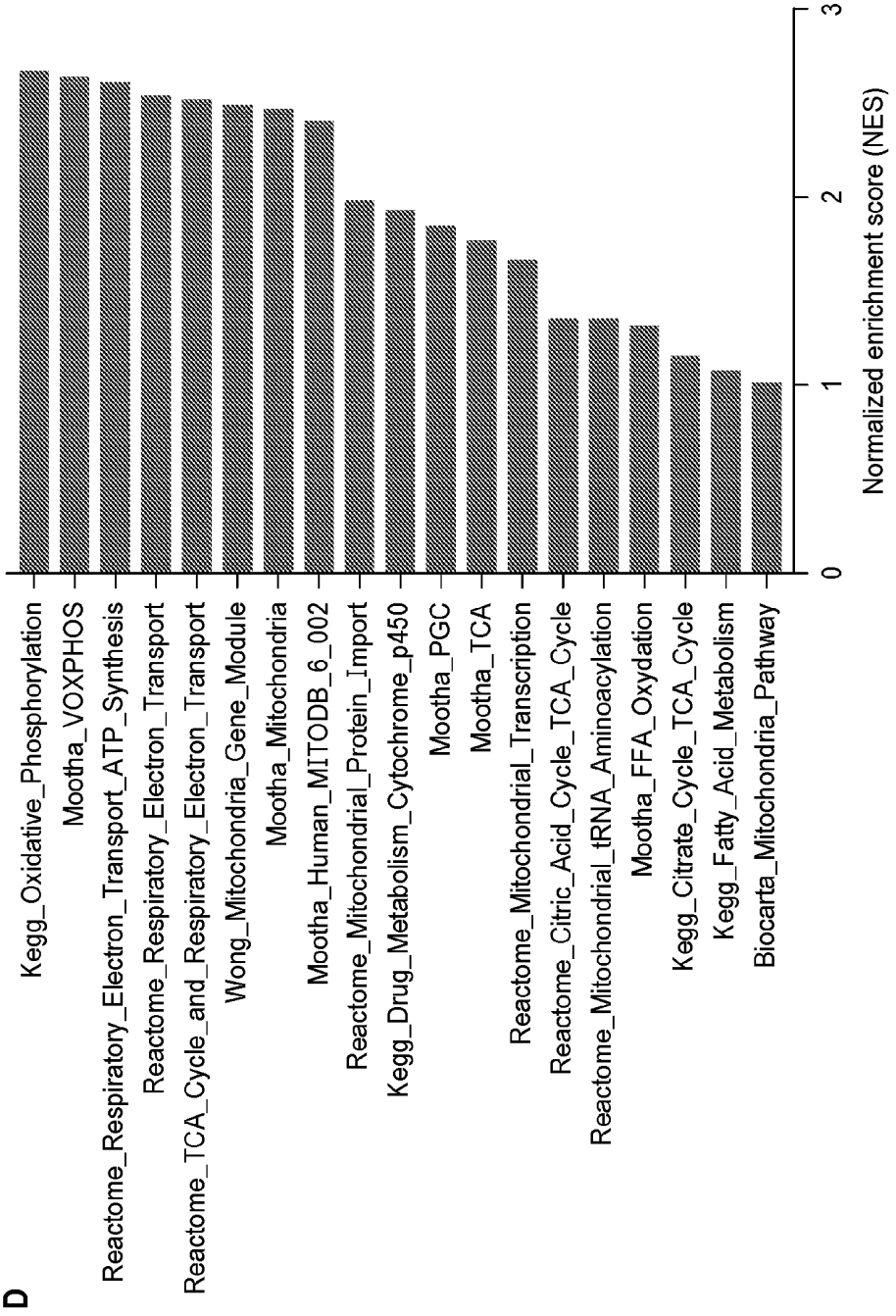

FIG. 10
(CONTINUED)

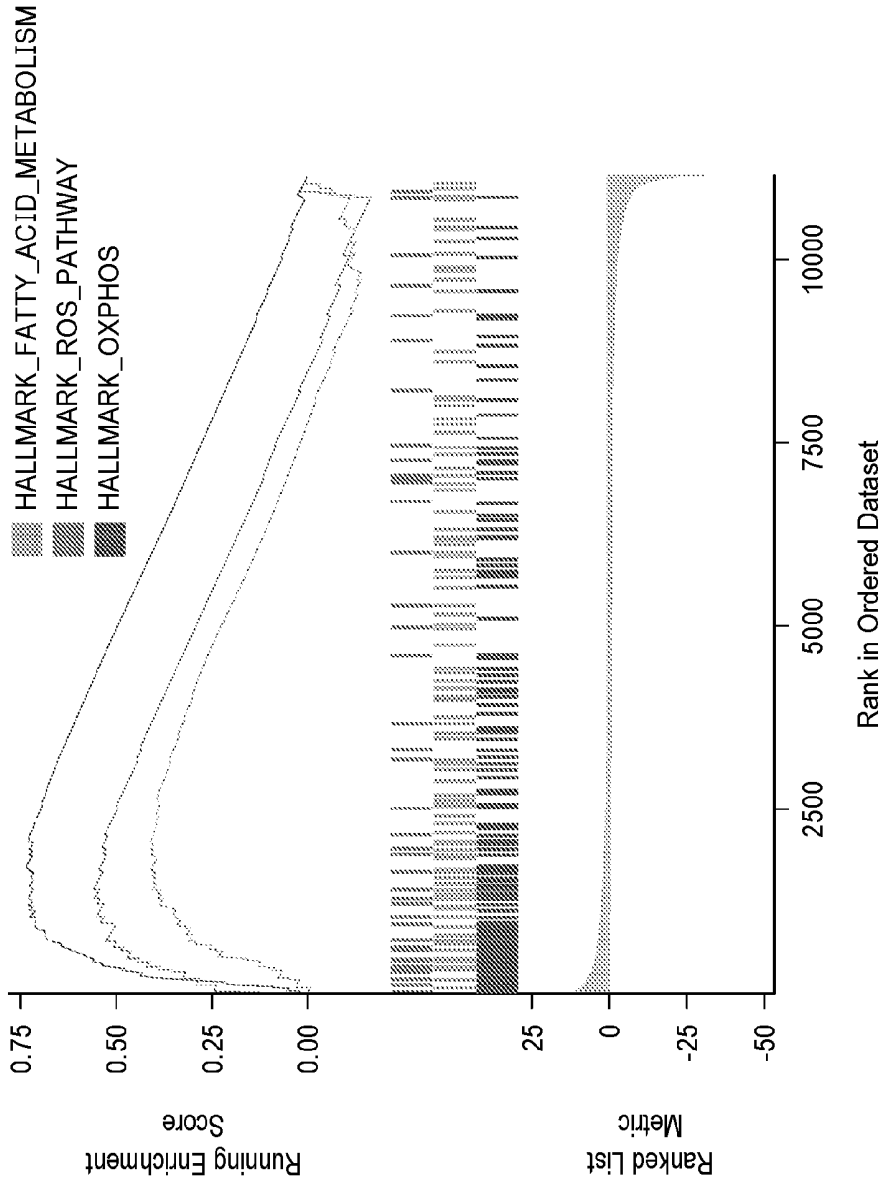

E

FIG. 10
(CONTINUED)

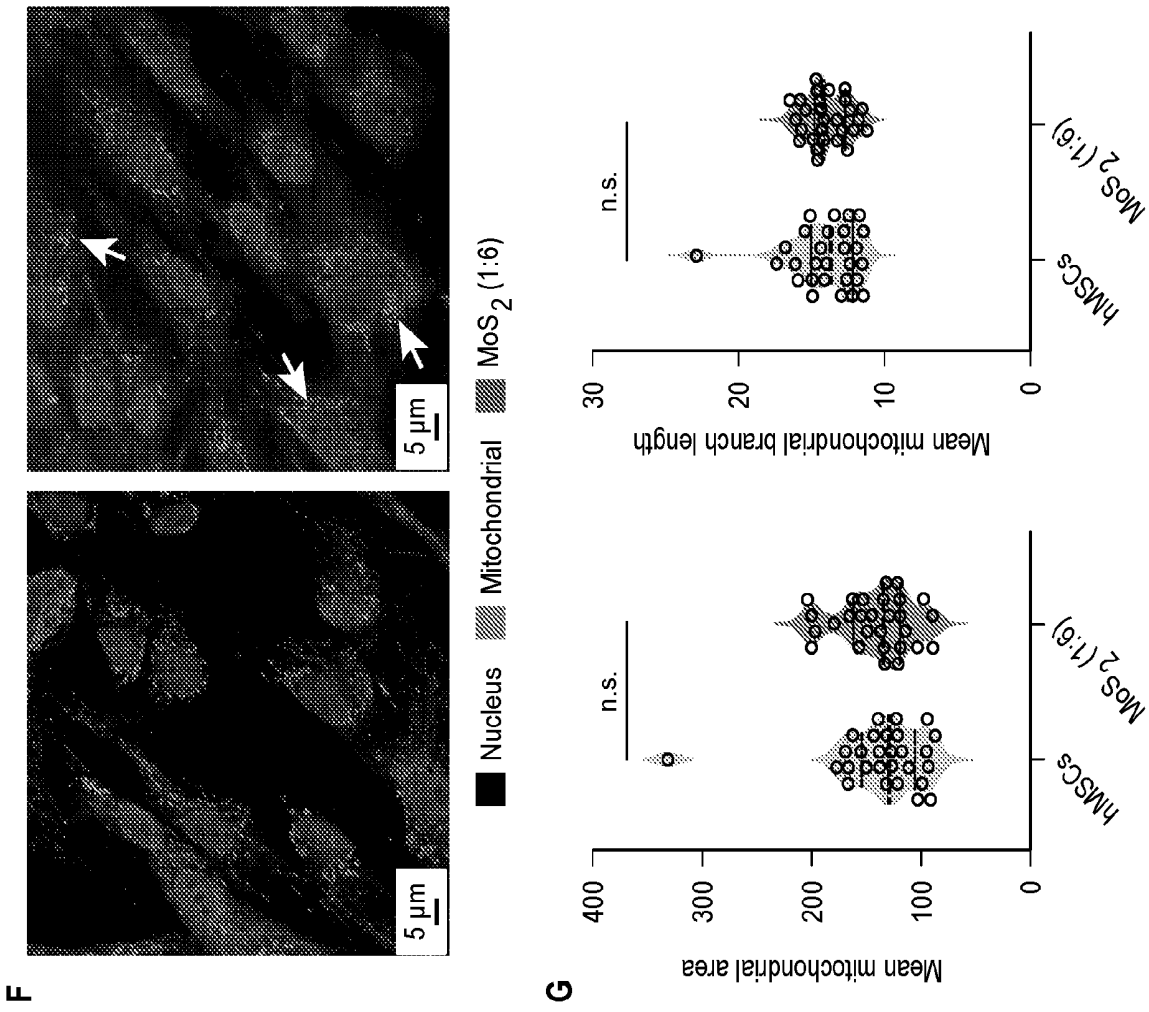

FIG. 11

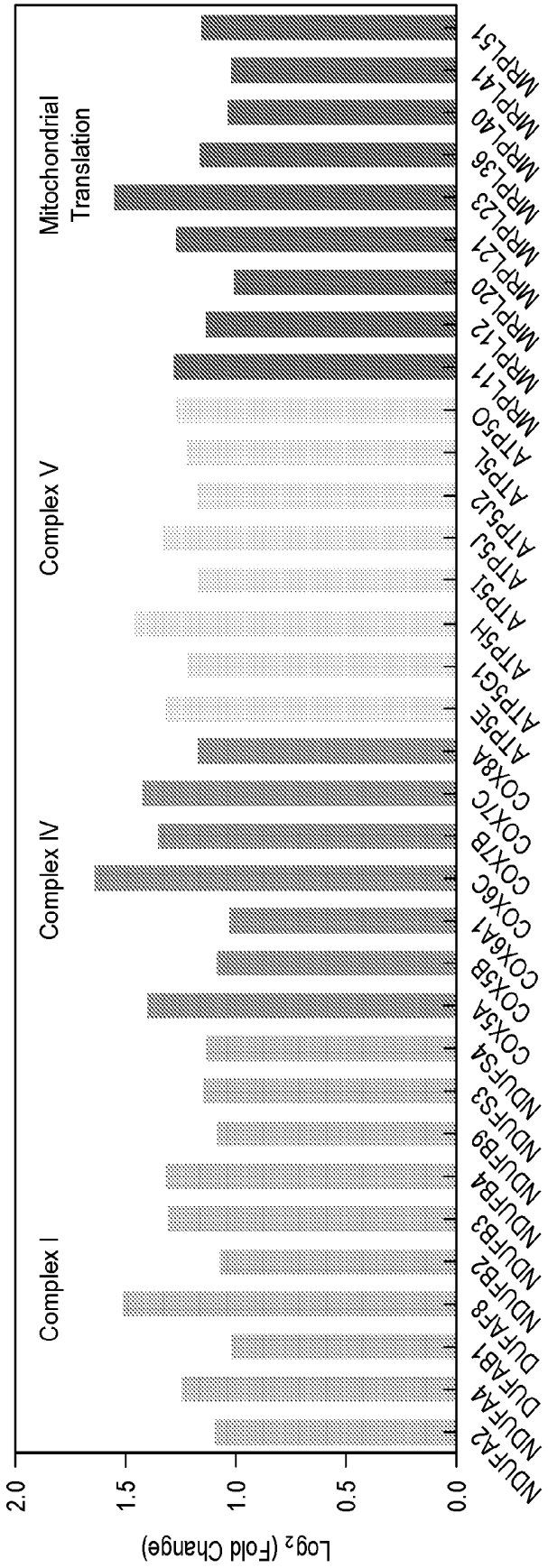
Log2 (Fold Change)
2.0
1.5
1.0
0.5
0.0
Complex I
Complex IV
Complex V
Mitochondrial Translation
NDUFA2
NDUFA4
DUFAB1
DUFAF8
NDUFB2
NDUFB3
NDUFB4
NDUFB9
NDUFS3
NDUFS4
COX5A
COX5B
COX6A1
COX6C
COX7B
COX7C
COX8A
ATP5E
ATP5G1
ATP5H
ATP5I
ATP5J
ATP5J2
ATP5L
ATP5O
MRPL11
MRPL12
MRPL20
MRPL21
MRPL23
MRPL36
MRPL40
MRPL41
MRPL51

FIG. 12

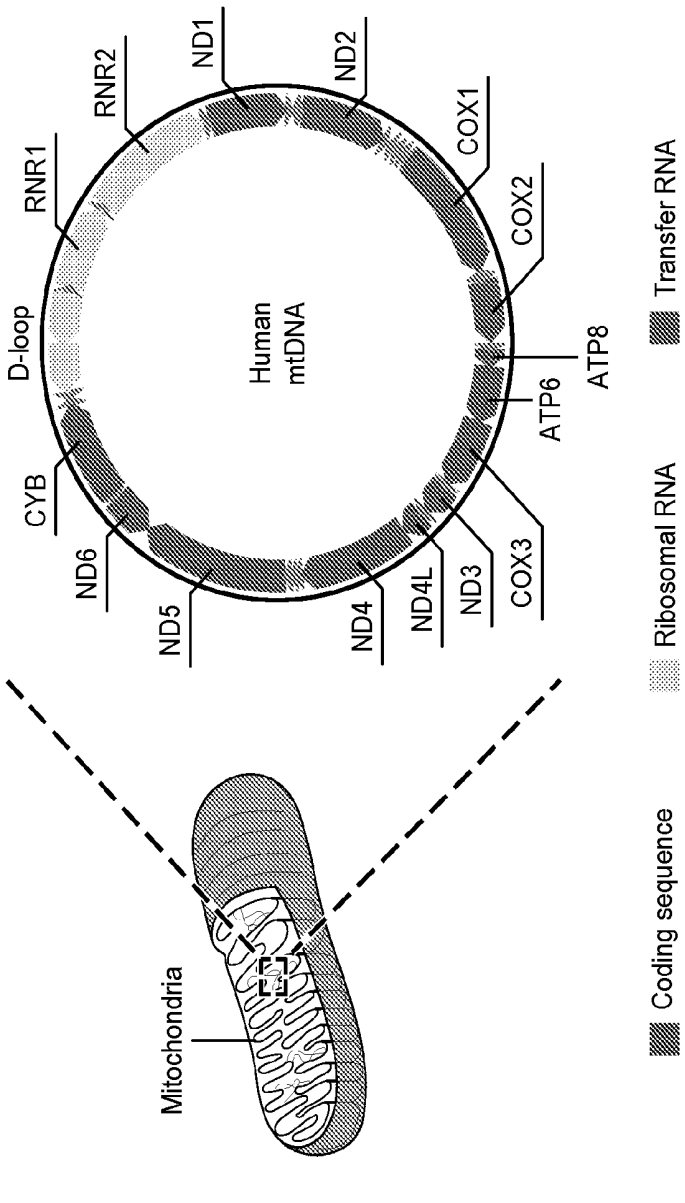
A
Mitochondria
Human mtDNA
D-loop
RNR1
RNR2
ND1
ND2
COX1
COX2
ATP8
ATP6
COX3
ND3
ND4L
ND4
ND5
ND6
CYB
Coding sequence
Ribosomal RNA
Transfer RNA

FIG. 12
(CONTINUED)

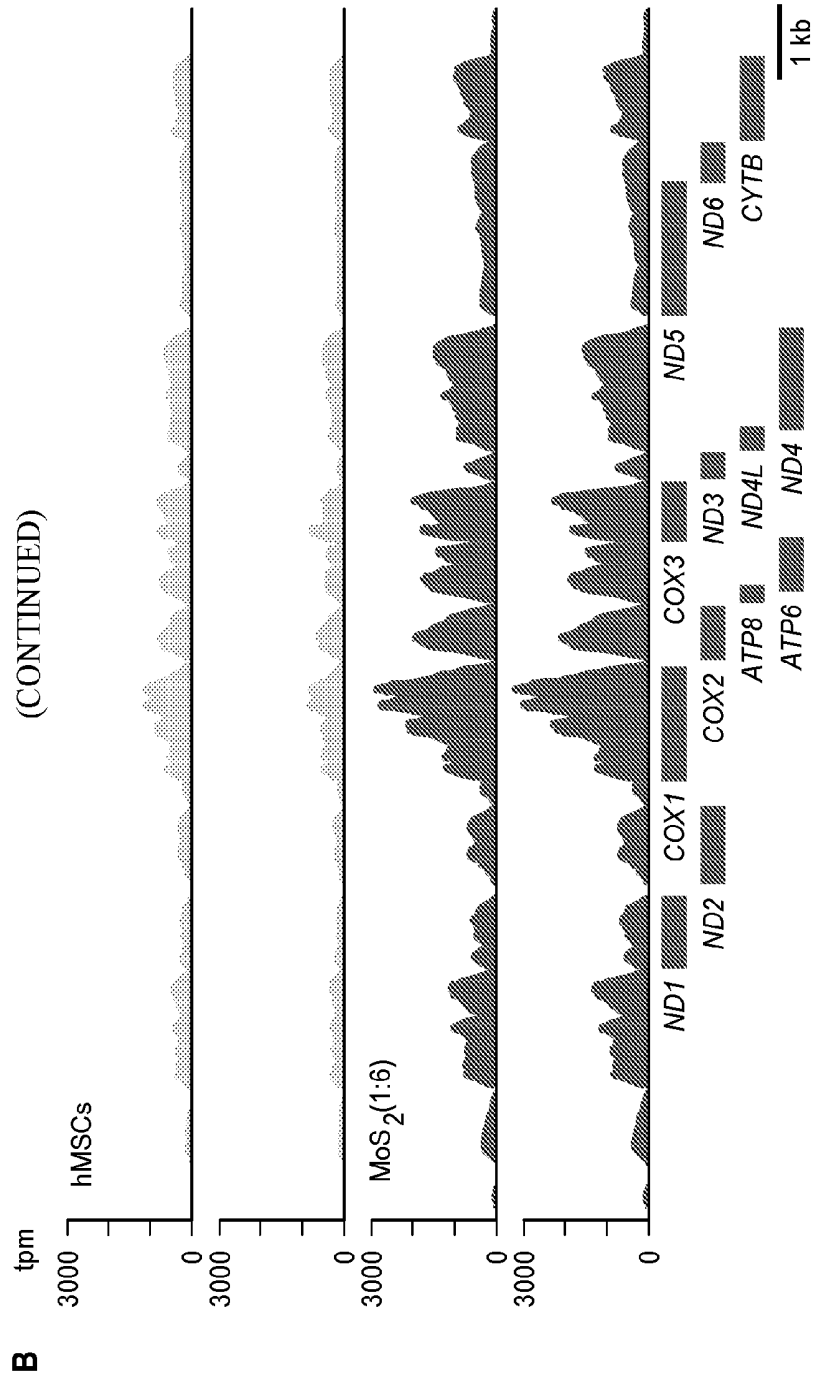

FIG. 12
(CONTINUED)

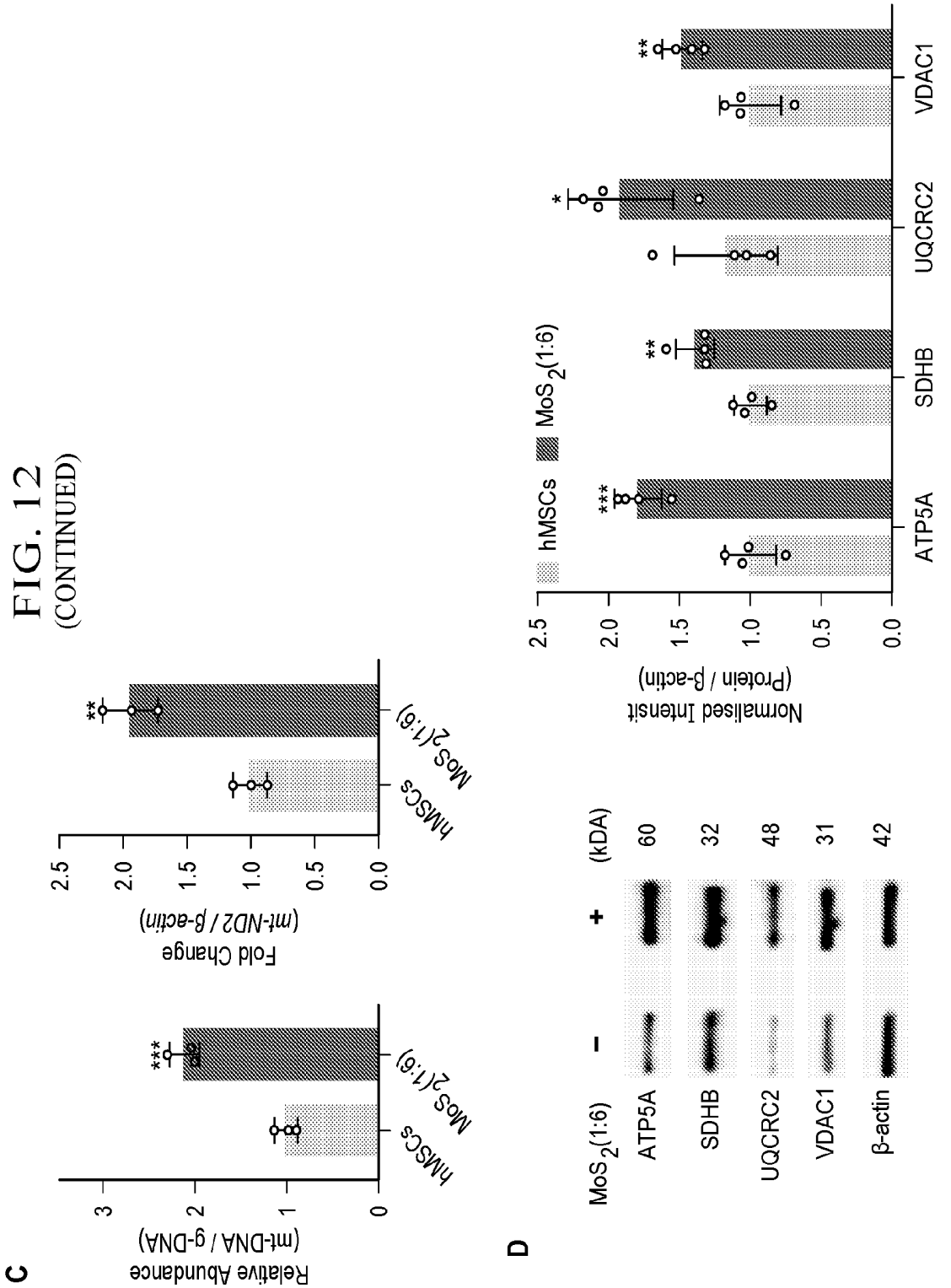

FIG. 12
(CONTINUED)

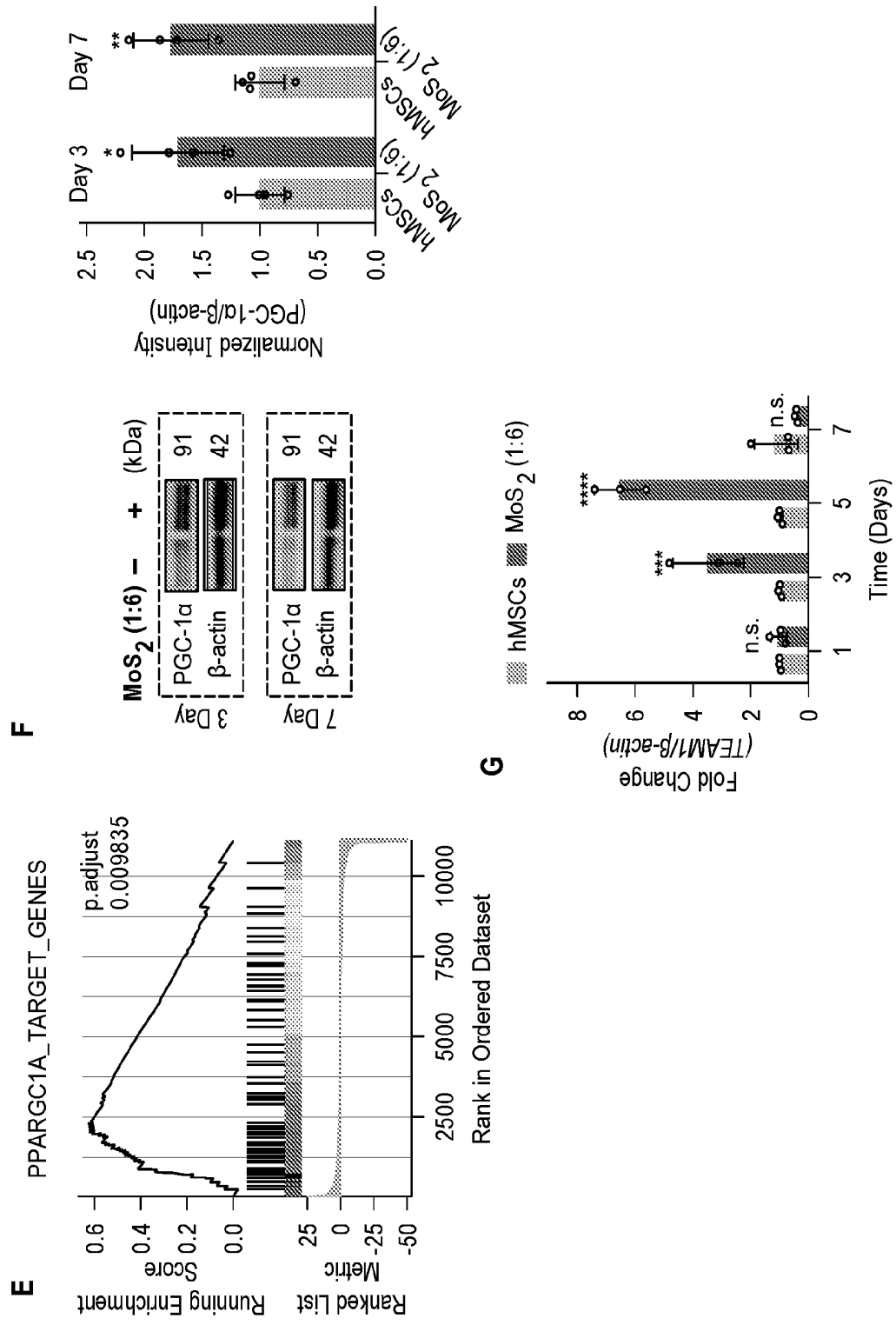

FIG. 13

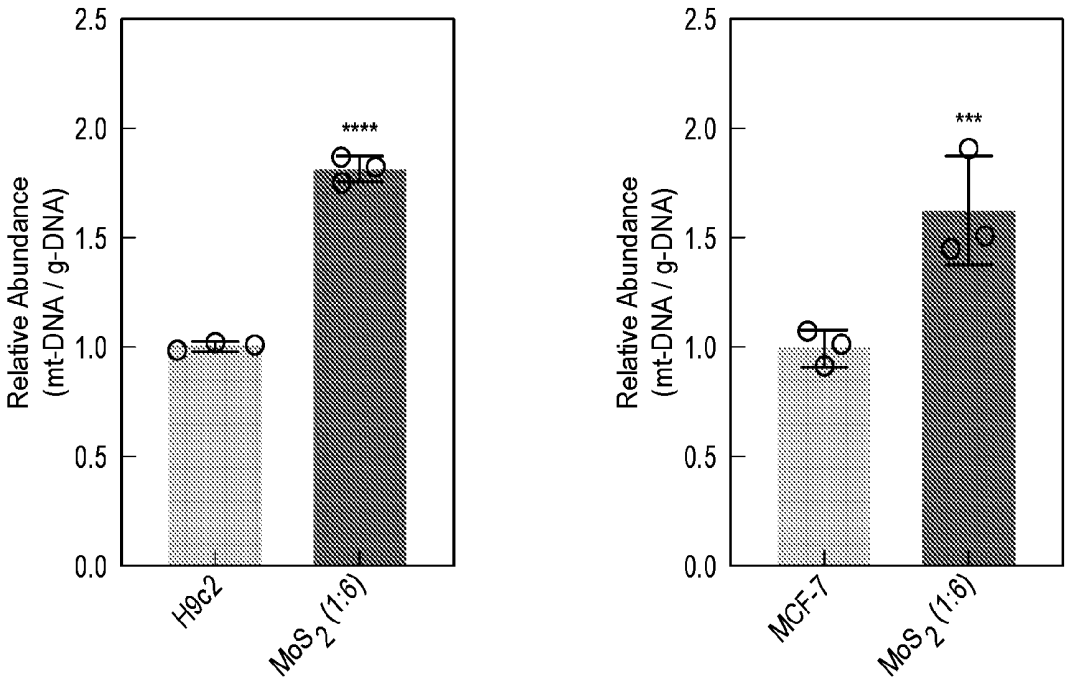
Relative Abundance
(mt-DNA / g-DNA)
2.5
2.0
1.5
1.0
0.5
0.0
****
H9c2
MoS2 (1:6)
Relative Abundance
(mt-DNA / g-DNA)
2.5
2.0
1.5
1.0
0.5
0.0
***
MCF-7
MoS2 (1:6)

FIG. 14

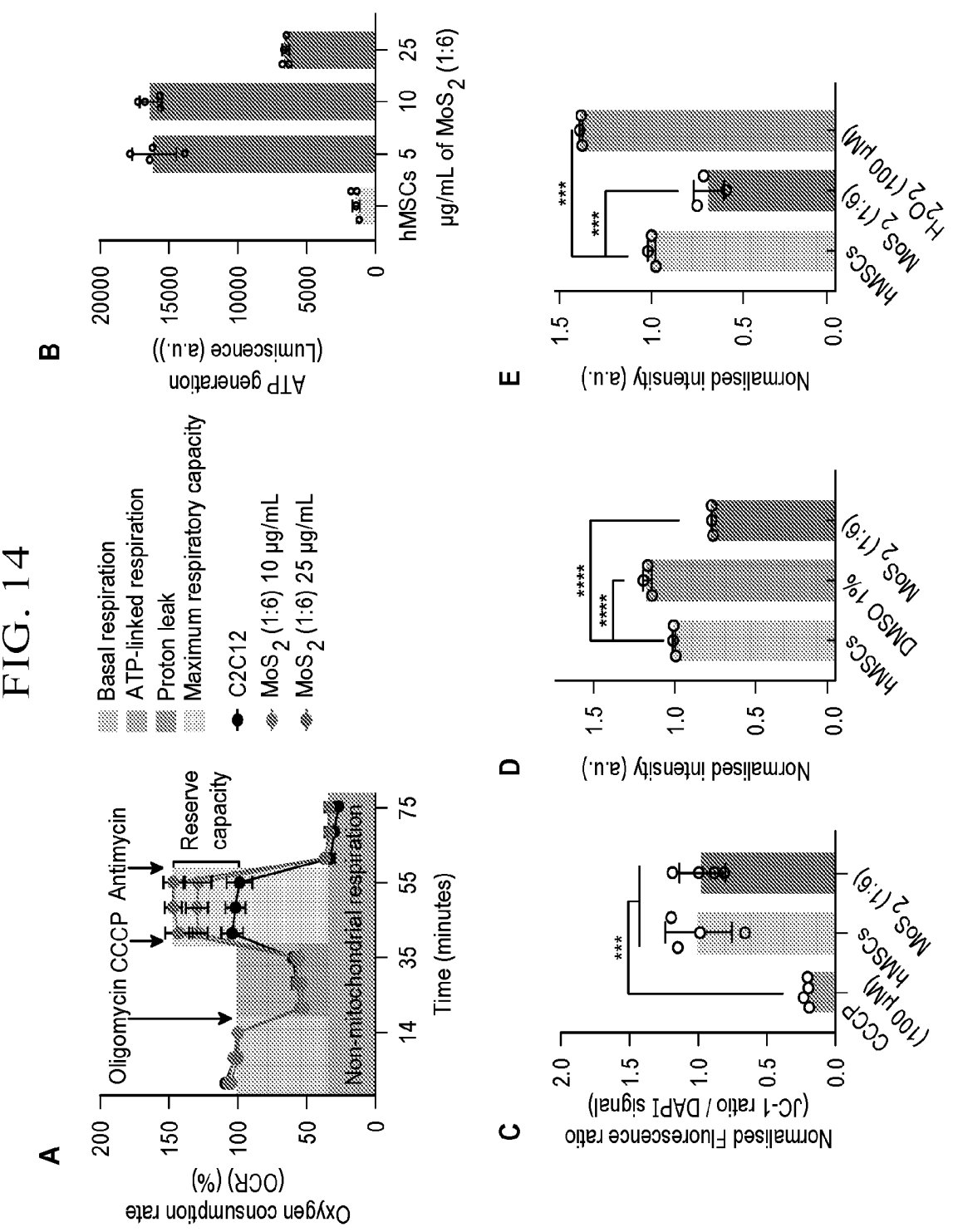
A
Oxygen consumption rate (OCR) (%)
Oligomycin
CCCP
Antimycin
Reserve capacity
Non-mitochondrial respiration
Time (minutes)
Basal respiration
ATP-linked respiration
Proton leak
Maximum respiratory capacity
C2C12
MoS2 (1:6) 10 µg/mL
MoS2 (1:6) 25 µg/mL
B
ATP generation (Lumiscence (a.u.))
hMSCs
µg/mL of MoS2 (1:6)
C
Normalised Fluorescence ratio (JC-1 ratio / DAPI signal)
CCCP (100 µM)
hMSCs
MoS2 (1:6)
D
Normalised intensity (a.u.)
hMSCs
DMSO 1%
MoS2 (1:6)
E
Normalised intensity (a.u.)
hMSCs
MoS2 (1:6)
H2O2 (100 µM)

FIG. 14
(CONTINUED)

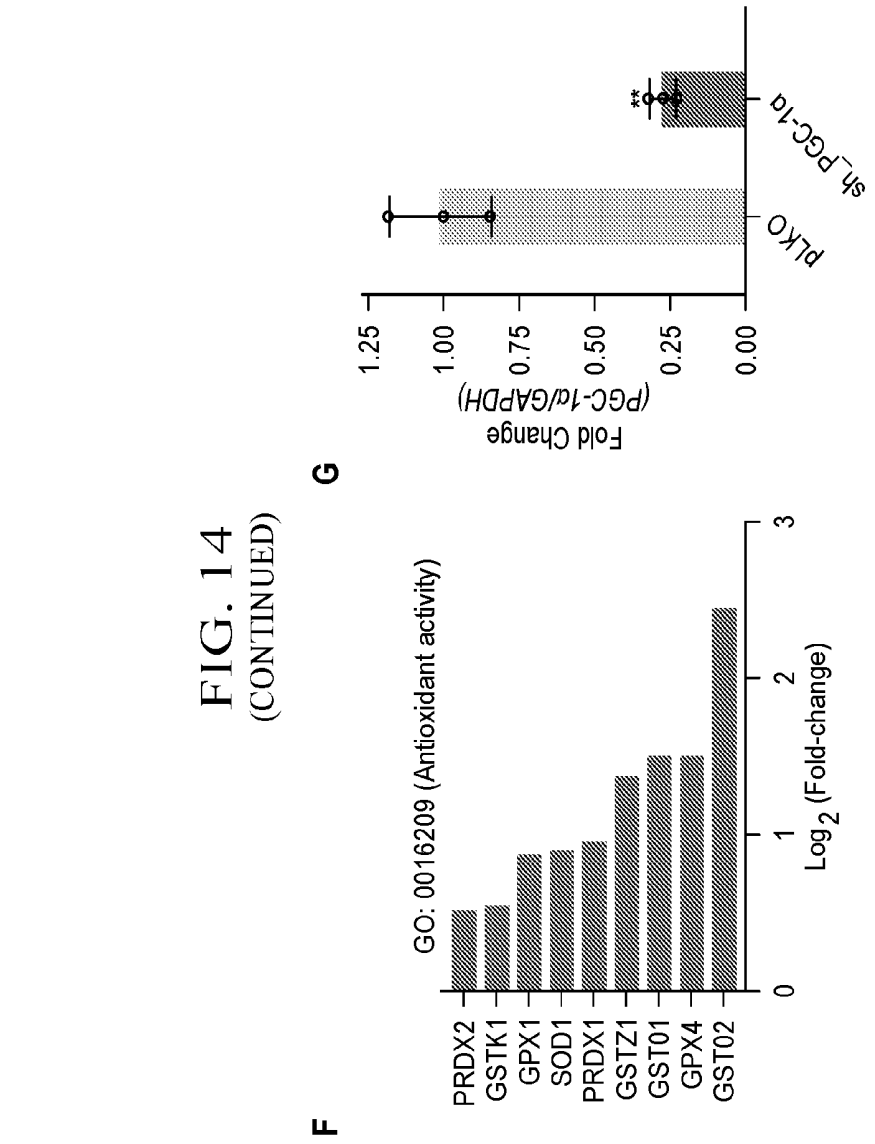

FIG. 14
(CONTINUED)

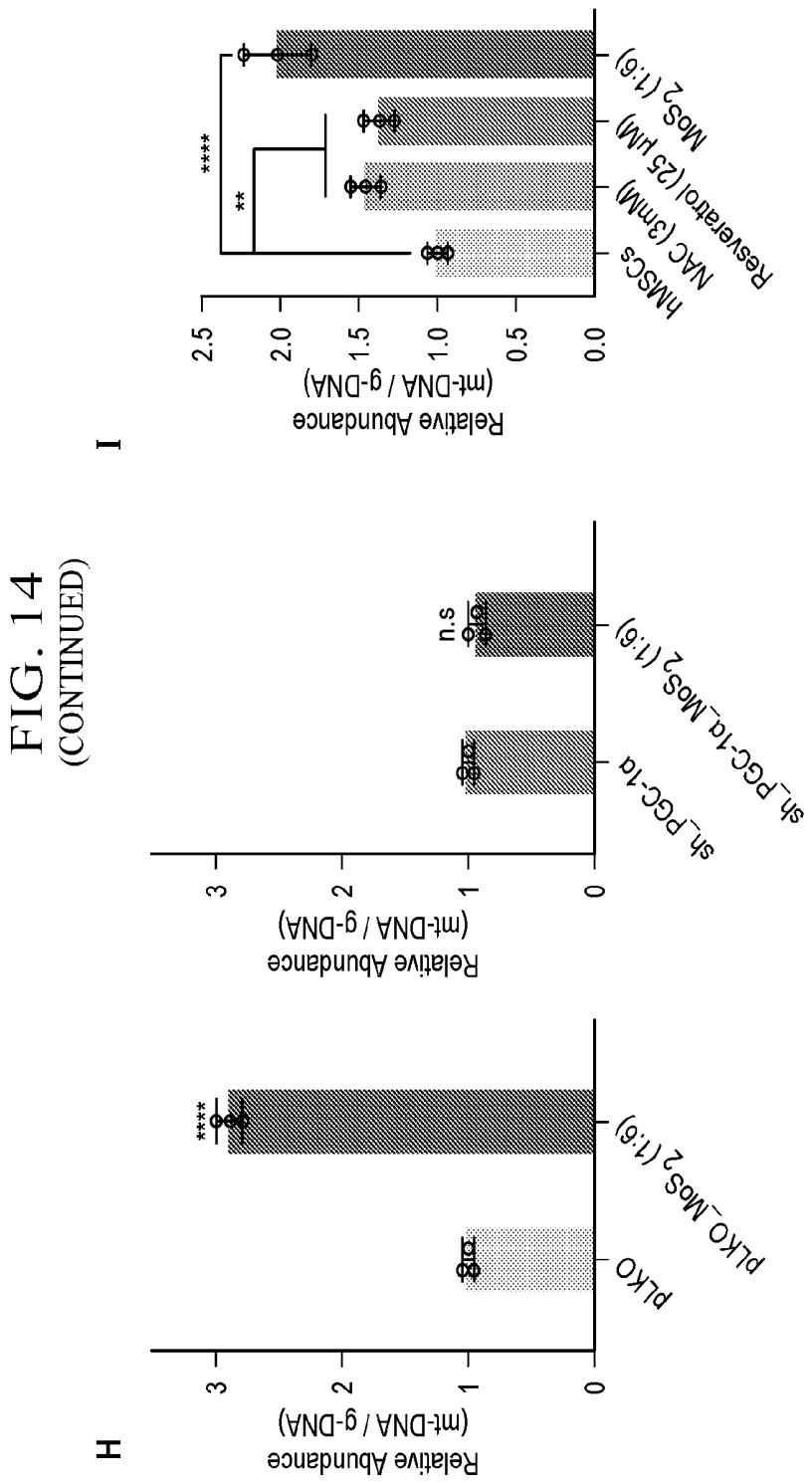

FIG. 14
(CONTINUED)

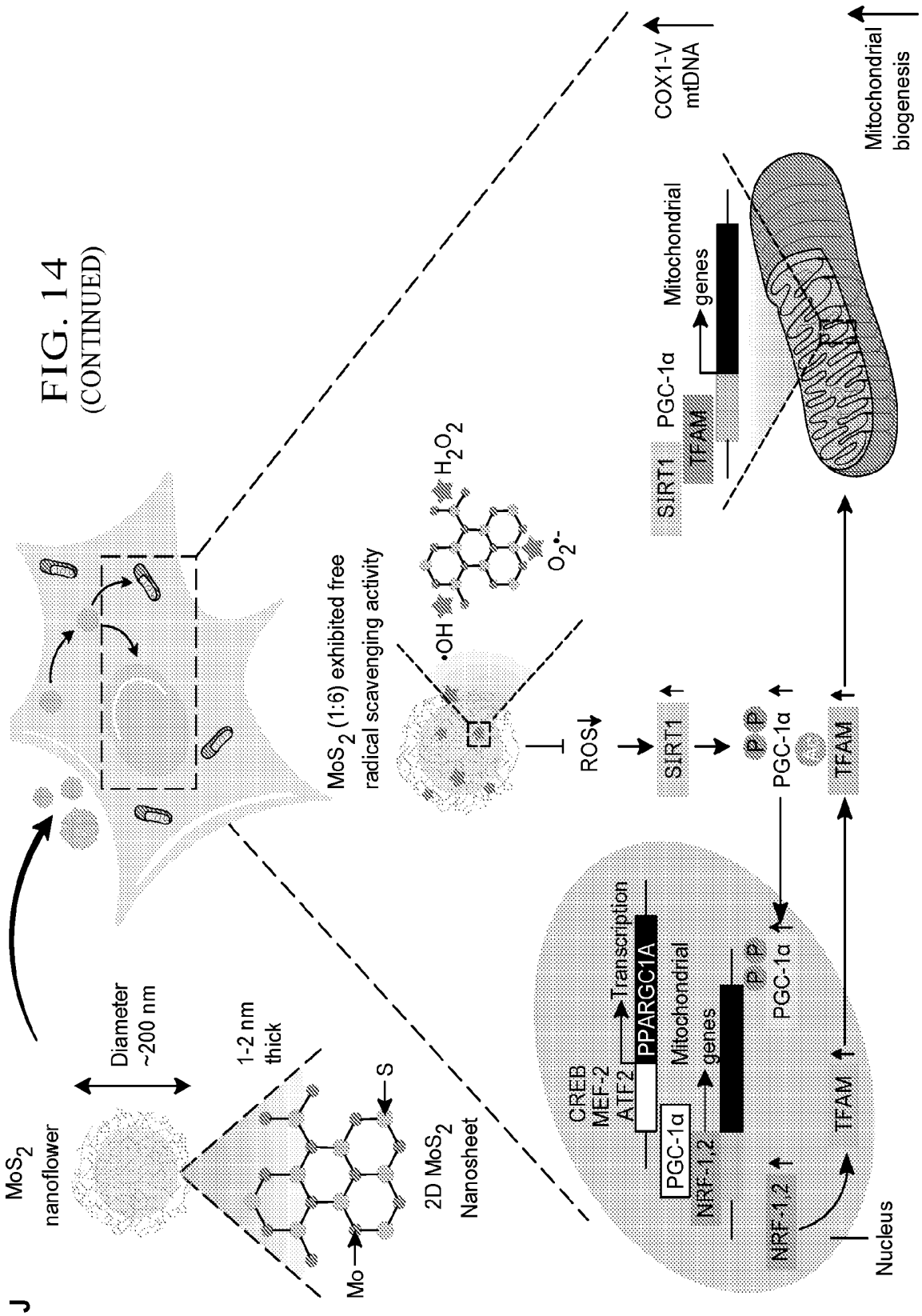

FIG. 15

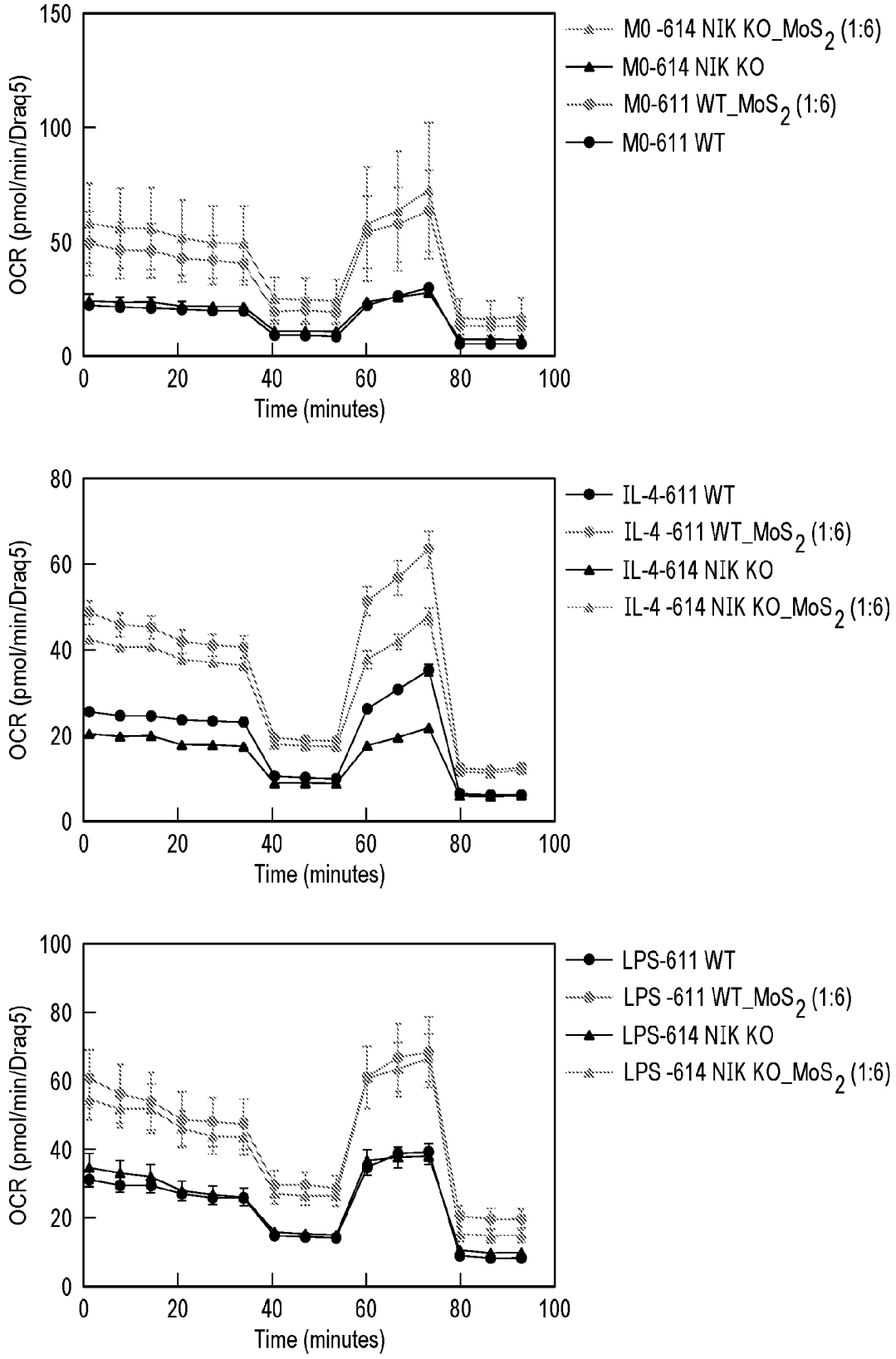
150
100
50
0
OCR (pmol/min/Draq5)
0
20
40
60
80
100
Time (minutes)
M0 -614 NIK KO_MoS2 (1:6)
M0-614 NIK KO
M0-611 WT_MoS2 (1:6)
M0-611 WT
80
60
40
20
0
OCR (pmol/min/Draq5)
0
20
40
60
80
100
Time (minutes)
IL-4-611 WT
IL-4 -611 WT_MoS2 (1:6)
IL-4-614 NIK KO
IL-4 -614 NIK KO_MoS2 (1:6)
100
80
60
40
20
0
OCR (pmol/min/Draq5)
0
20
40
60
80
100
Time (minutes)
LPS-611 WT
LPS -611 WT_MoS2 (1:6)
LPS-614 NIK KO
LPS -614 NIK KO_MoS2 (1:6)

FIG. 16

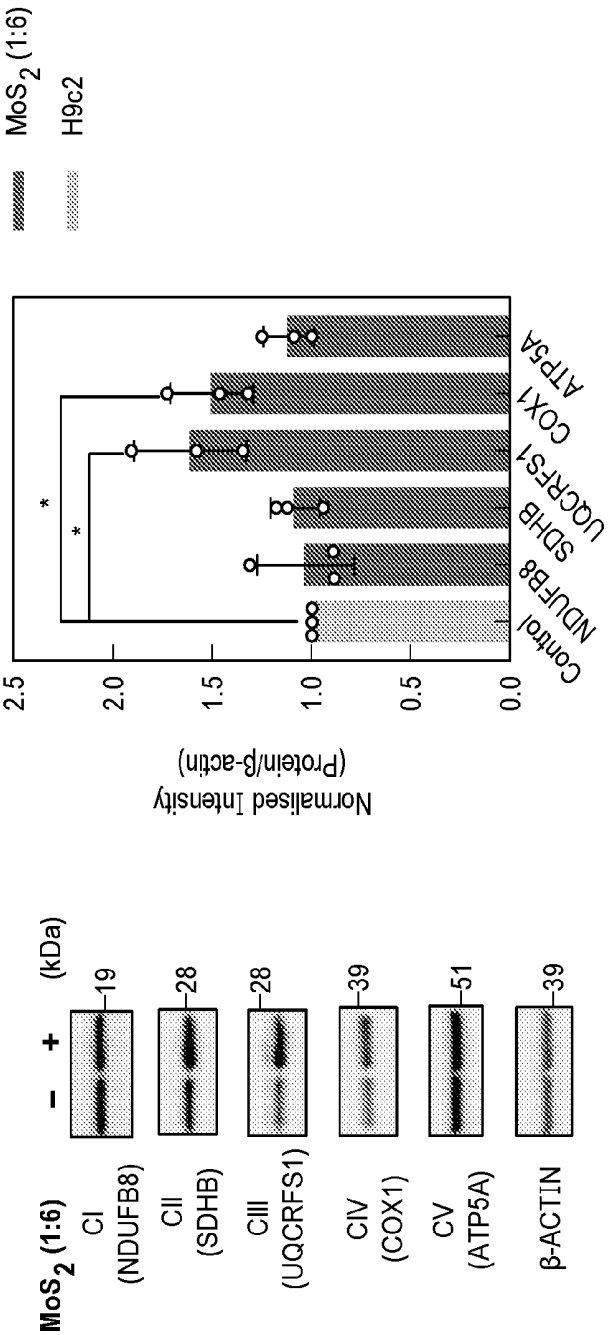
MoS2 (1:6)
H9c2
Normalised Intensity
(Protein/β-actin)
2.5
2.0
1.5
1.0
0.5
0.0
Control
NDUFB8
SDHB
UQCRFS1
COX1
ATP5A
*
*
MoS2 (1:6)
–
+
(kDa)
CI
(NDUFB8)
CII
(SDHB)
CIII
(UQCRFS1)
CIV
(COX1)
CV
(ATP5A)
β-ACTIN
19
28
28
39
51
39

FIG. 17

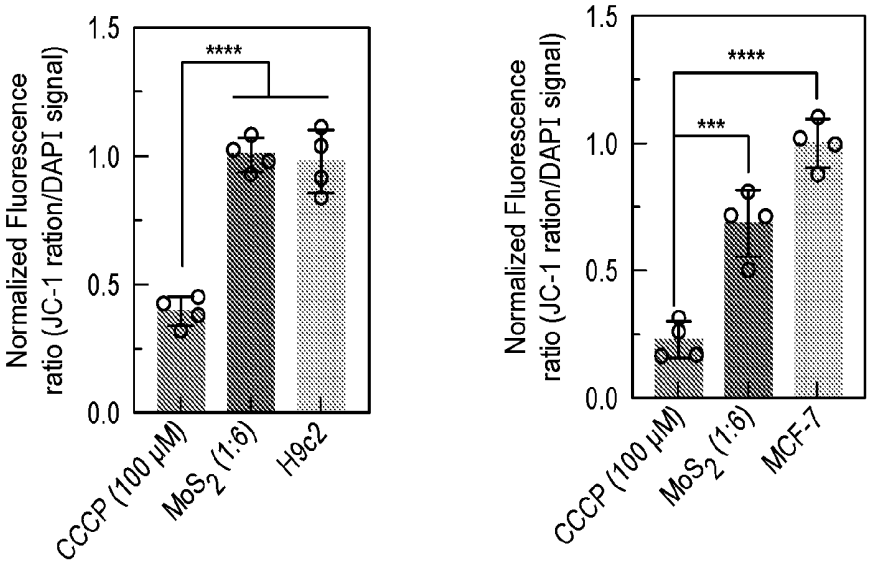
Normalized Fluorescence ratio (JC-1 ration/DAPI signal)
1.5
1.0
0.5
0.0
****
CCCP (100 μM)
MoS2 (1:6)
H9c2
Normalized Fluorescence ratio (JC-1 ration/DAPI signal)
1.5
1.0
0.5
0.0
****
***
CCCP (100 μM)
MoS2 (1:6)
MCF-7

FIG. 18

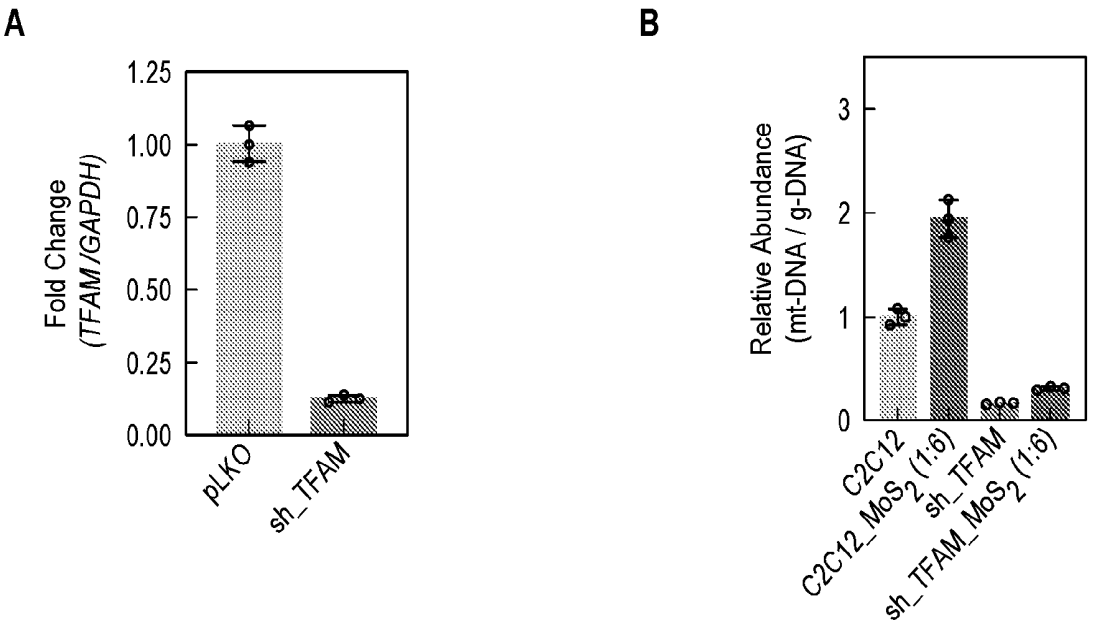
A
Fold Change
(TFAM/GAPDH)
1.25
1.00
0.75
0.50
0.25
0.00
pLKO
sh_TFAM
B
Relative Abundance
(mt-DNA / g-DNA)
3
2
1
0
C2C12
C2C12_MoS2 (1:6)
sh_TFAM
sh_TFAM_MoS2 (1:6)

INTERNATIONAL SEARCH REPORT

International application No.
PCT/US2024/050330

A. CLASSIFICATION OF SUBJECT MATTER

IPC: ***A61K 33/00*** (2024.01); ***A61K 33/04*** (2024.01); ***A61K 47/52*** (2024.01); ***A61K 9/70*** (2024.01); ***A61P 3/00*** (2024.01); ***A61P 31/00*** (2024.01); ***A61P 39/06*** (2024.01); ***B82Y 5/00*** (2024.01); ***A61K 31/765*** (2024.01)

CPC: ***A61K 33/00; A61K 33/04; A61K 9/70; A61P 31/00; A61P 39/06; A61K 47/52; A61P 3/00; A61K 31/765; B82Y 5/00;*** *A61K 2121/00*

According to International Patent Classification (IPC) or to both national classification and IPC

B. FIELDS SEARCHED

Minimum documentation searched (classification system followed by classification symbols)

See Search History Document

Documentation searched other than minimum documentation to the extent that such documents are included in the fields searched

See Search History Document

Electronic data base consulted during the international search (name of data base and, where practicable, search terms used)

See Search History Document

C. DOCUMENTS CONSIDERED TO BE RELEVANT

Category*	Citation of document, with indication, where appropriate, of the relevant passages	Relevant to claim No.
Y	KR 2020095671 A (KOREA ADVANCED INSTITUTE OF SCIENCE & TECHNOLOGY) 11 August 2020 (11.08.2020) entire document	1-19
Y	CN 114177291 A (ANHUI POLYTECHNIC UNIVERSITY) 15 March 2022 (15.03.2022) entire document	9, 10, 17, 18
Y	WO 2022/025499 A1 (STANDIGM INC.) 03 February 2022 (03.02.2022) entire document	13
A	US 2023/0256003 A1 (INDUSTRY-UNIVERSITY COOPERATION FOUNDATION HANYANG UNIVERSITY ERICA CAMPUS) 17 August 2023 (17.08.2023) entire document	1-19

☑ Further documents are listed in the continuation of Box C. ☐ See patent family annex.

* Special categories of cited documents:
"A" document defining the general state of the art which is not considered to be of particular relevance
"D" document cited by the applicant in the international application
"E" earlier application or patent but published on or after the international filing date
"L" document which may throw doubts on priority claim(s) or which is cited to establish the publication date of another citation or other special reason (as specified)
"O" document referring to an oral disclosure, use, exhibition or other means
"P" document published prior to the international filing date but later than the priority date claimed
"T" later document published after the international filing date or priority date and not in conflict with the application but cited to understand the principle or theory underlying the invention
"X" document of particular relevance; the claimed invention cannot be considered novel or cannot be considered to involve an inventive step when the document is taken alone
"Y" document of particular relevance; the claimed invention cannot be considered to involve an inventive step when the document is combined with one or more other such documents, such combination being obvious to a person skilled in the art
"&" document member of the same patent family

Date of the actual completion of the international search	Date of mailing of the international search report
05 November 2024 (05.11.2024)	**02 January 2025 (02.01.2025)**

Name and mailing address of the ISA/US	Authorized officer
COMMISSIONER FOR PATENTS **MAIL STOP PCT, ATTN: ISA/US** **P.O. Box 1450** **Alexandria, VA 22313-1450** **UNITED STATES OF AMERICA**	**TAINA MATOS**
Facsimile No. **571-273-8300**	Telephone No. **571-272-4300**

INTERNATIONAL SEARCH REPORT

International application No.
PCT/US2024/050330

Box No. III Observations where unity of invention is lacking (Continuation of item 3 of first sheet)

The inventions listed in Groups I-III therefore lack unity under Rule 13 because they do not share a same or corresponding special technical feature.

1. ☐ As all required additional search fees were timely paid by the applicant, this international search report covers all searchable claims.

2. ☐ As all searchable claims could be searched without effort justifying additional fees, this Authority did not invite payment of additional fees.

3. ☐ As only some of the required additional search fees were timely paid by the applicant, this international search report covers only those claims for which fees were paid, specifically claims Nos.:

4. ☑ No required additional search fees were timely paid by the applicant. Consequently, this international search report is restricted to the invention first mentioned in the claims; it is covered by claims Nos.: **1-19**

Remark on Protest

☐ The additional search fees were accompanied by the applicant's protest and, where applicable, the payment of a protest fee.

☐ The additional search fees were accompanied by the applicant's protest but the applicable protest fee was not paid within the time limit specified in the invitation.

☐ No protest accompanied the payment of additional search fees.

INTERNATIONAL SEARCH REPORT

International application No.
PCT/US2024/050330

Box No. III Observations where unity of invention is lacking (Continuation of item 3 of first sheet)

This International Searching Authority found multiple inventions in this international application, as follows:

This application contains the following inventions or groups of inventions which are not so linked as to form a single general inventive concept under PCT Rule 13.1. In order for all inventions to be examined, the appropriate additional examination fees need to be paid.

Group I: claims 1-19 are drawn to methods of increasing mitochondrial function in a subject in need thereof.

Group II: claims 20-31 and 50-60 are drawn to pharmaceutical compositions.

Group III: claims 32-49 are drawn to methods of decreasing cellular oxidative stress in a subject in need thereof.

The inventions listed in Groups I-III do not relate to a single general inventive concept under PCT Rule 13.1, because under PCT Rule 13.2 they lack the same or corresponding special technical features for the following reasons:

The special technical features of Group I, methods of increasing mitochondrial function in a subject in need thereof, are not present in Groups II and III; the special technical features of Group II, pharmaceutical compositions, are not present in Groups I and III; and the special technical features of Group III, methods of decreasing cellular oxidative stress in a subject in need thereof, are not present in Groups I and II.

Additionally, even if Groups I-III were considered to share the technical features of a method comprising administering to the subject an effective amount of a nanomaterial structure comprising a transition metal and a chalcogen, wherein the nanomaterial structure comprises a high atomic vacancy concentration, these shared technical features do not represent a contribution over the prior art as disclosed by the publication entitled "Atomic Vacancy Rich 2D Nanoparticles Drive Mitochondrial Biogenesis and Bioenergetics" to Singh et al. (hereinafter, "Singh") and US 2023/0256003 A1 to Industry-University Cooperation Foundation Hanyang University Erica Campus (hereinafter, "HYU").

Singh teaches a method (RNA-seq analysis indicates enhanced expression of all 13 mitochondrial encoded genes in hMSCs treated with high atomic vacancy MoS2 compared to untreated cells, Pg. 1, left hand column, first partial paragraph from bottom) comprising a nanomaterial structure (MoS2 nanoflower with high atomic vacancies were fabricated by modulating the precursor ratio of Mo (hexaammonium heptamolybdate): sulphur (thiourea) during hydrothermal synthesis, Pg. 1, left hand column, first full paragraph from bottom) comprising a transition metal and a chalcogen (molybdenum disulfide (MoS2) nanoflower, Pg. 1, left hand column, first full paragraph from top, See instant disclosure, Para. [0008], which lists molybdenum as an example of an acceptable transition metal and lists sulfur as an example of an example of an acceptable chalcogen), wherein the nanomaterial structure comprises a high atomic vacancy concentration (molybdenum disulfide (MoS2) nanoflower with predefined atomic vacancies capable of modulating cellular bioenergetics and activating mitochondrial biogenesis, Pg. 1, left hand column, first full paragraph from top; high atomic vacancy MoS2, Pg. 1, left hand column, first partial paragraph from bottom; hMSCs treated with high atomic vacancy MoS2 were shown to have a nearly 2-fold increase in mRNA expression of mitochondrial encoded gene, Pg. 1, right hand column, first partial paragraph from bottom).

Singh fails to explicitly disclose administering an effective amount of a nanomaterial structure.

HYU is in the field of a 2D TMD nanosheet with scavenging activity for intracellular and mitochondrial ROS (Abstract) and teaches administering an effective amount of a nanomaterial structure (a method for preventing or treating sepsis or septic shock, which includes a step of administering the functionalized 2D TMD to a subject, Para. [0019]; A 2D TMD nanosheet of the present disclosure functionalized with an amphiphilic block polymer compound has superior activity of scavenging intracellular ROS and RNS and mitochondrial ROS, Para. [0021]).

It would have been obvious to one of ordinary skill in the art before the priority date to modify the method of Singh by an administration as taught by HYU for the purpose of preventing or treating sepsis (HYU, Title).

INTERNATIONAL SEARCH REPORT

International application No.
PCT/US2024/050330

Box No. I Nucleotide and/or amino acid sequence(s) (Continuation of item 1.c of the first sheet)

1. With regard to any nucleotide and/or amino acid sequence disclosed in the international application, the international search was carried out on the basis of a sequence listing:
   a. ☑ forming part of the international application as filed.
   b. ☐ furnished subsequent to the international filing date for the purposes of international search (Rule 13*ter*.1(a)),
      ☐ accompanied by a statement to the effect that the sequence listing does not go beyond the disclosure in the international application as filed.

2. ☐ With regard to any nucleotide and/or amino acid sequence disclosed in the international application, this report has been established to the extent that a meaningful search could be carried out without a WIPO Standard ST.26 compliant sequence listing.

3. Additional comments:

C. DOCUMENTS CONSIDERED TO BE RELEVANT

Category*	Citation of document, with indication, where appropriate, of the relevant passages	Relevant to claim No.
Y	SINGH et al., Atomic Vacancy Rich 2D Nanoparticles Drive Mitochondrial Biogenesis and Bioenergetics, Society for Biomaterials 2023 Annual Meeting, 21 April 2023, Pgs. 1-4. [retrieved on 30.10.2024]. Retrieved from the internet: <URL:https://abstracts.biomaterials.org/data/2023/toc6.html>. entire document	1-19
P, X	SINGH et al., Atomic vacancies of molybdenum disulfide nanoparticles stimulate mitochondrial biogenesis, Nature Communications, Vol. 15: 8136, 17 September 2024, Pgs. 1-15. [retrieved on 29.10.2024]. Retrieved from the internet: <URL:https://doi.org/10.1038/s41467-024-52276-8>. entire document	1-19